การสังเคราะห์และผลของอัลคิลกลีเซอรอลอีเทอร์ต่อสมบัติการไหลที่อุณหภูมิต่ำของไบโอดีเซลจากน้ำมันปาล์ม

นายจักรพงษ์ แสงอรุณ

วิทยานิพนธ์นี้เป็นส่วนหนึ่งของการศึกษาตามหลักสูตรปริญญาวิทยาศาสตรดุษฎีบัณฑิต
สาขาวิชาปิโตรเคมี
คณะวิทยาศาสตร์ จุฬาลงกรณ์มหาวิทยาลัย
ปีการศึกษา 2554
ลิขสิทธิ์ของจุฬาลงกรณ์มหาวิทยาลัย

SYNTHESIS AND EFFECT OF ALKYL GLYCEROL ETHER ON COLD FLOW PROPERTY OF BIODIESEL FROM PALM OIL

Mr. Chakrapong Saengarun

A Dissertation Submitted in Partial Fulfillment of the Requirements
for the Degree of Doctor of Philosophy Program in Petrochemistry
Faculty of Science
Chulalongkorn University
Academic Year 2011

Thesis Title	SYNTHESIS AND EFFECT OF ALKYL GLYCEROL ETHER ON COLD FLOW PROPERTY OF BIODIESEL FROM PALM OIL
By	Mr. Chakrapong Saengarun
Field of Study	Petrochemistry
Thesis Advisor	Associate Professor Amorn Petsom, Ph.D.
Thesis Co-advisor	Duangamol Tungasmita, Ph.D.

Accepted by the Graduate School, Chulalongkorn University in Partial Fulfillment of the Requirements for the Doctoral Degree

…… Dean of the Faculty of Science
(Professor Supot Hannongbua, Dr.rer.nat.)

THESIS COMMITTEE

…….. Chairman
(Associate Professor Supawan Tantayanon, Ph.D.)

……..……. Thesis Advisor
(Associate Professor Amorn Petsom, Ph.D.)

…….. Thesis Co-advisor
(Duangamol Tungasmita, Ph.D.)

…….. Examiner
(Associate Professor Nuanphun Chantarasiri, Ph.D.)

…….. Examiner
(Associate Professor Wimonrat Trakarnpruk, Ph.D.)

…….. External Examiner
(Damrong Sommit, Ph.D.)

จักรพงษ์ แสงอรุณ : การสังเคราะห์และผลของอัลคิลกลีเซอรอลอีเทอร์ต่อสมบัติการไหลที่อุณหภูมิต่ำของไบโอดีเซลจากน้ำมันปาล์ม. (SYNTHESIS AND EFFECT OF ALKYL GLYCEROL ETHER ON COLD FLOW PROPERTY OF BIODIESEL FROM PALM OIL) อ. ที่ปรึกษาวิทยานิพนธ์หลัก : รศ.ดร. อมร เพชรสม, อ. ที่ปรึกษาวิทยานิพนธ์ร่วม : อ. ดร. ดวงกมล ตุงคะสมิต, 100 หน้า.

ปฏิกิริยาอีเทอริฟิเคชันระหว่างกลีเซอรีนกับแอลคีน ซึ่งประกอบด้วยเอทิลีน โพรพิลีน บิวทีน เพนทีน เฮกซีน เฮปทีน และออกทีน เป็นผลมาจากตัวเร่งปฏิกิริยาวิวิธพันธ์ชนิดกรด ได้แก่ Amberlyst-15, S100, S200, Al-SBA-15, Pr-SO_3H-SBA-15, ซีโอไลต์ เบต้า และซีโอไลต์ วาย ตัวเร่งAmberlyst-15มีความเป็นกรดสูงและมีโพรงขนาดกลาง เกิดปฏิกิริยาโพรพิเลชันและบิวทิเลชันของกลีเซอรีนสูงที่สุด เรซินS200มีความเป็นกรดสูงและไม่มีโพรง เกิดปฏิกิริยาอีเทอริฟิเคชันของกลีเซอรีนกับโพรพิลีนและบิวทีนได้ต่ำ เรซินS100มีความเป็นกรดสูงและไม่มีโพรง เกิดปฏิกิริยากลีเซอรีนโพรพิเลชันต่ำสุดและไม่เกิดปฏิกิริยากลีเซอรีนบิวทิเลชัน ส่วนตัวเร่งAl-SBA-15, Pr-SO_3H-SBA-15, ซีโอไลต์ บีตา และซีโอไลต์ วายมีความเป็นกรดอ่อนและมีโพรงขนาดใหญ่ไม่เกิดปฏิกิริยากลีเซอรีนอีเทอริฟิเคชันกับโพรพิลีนและบิวทีน ปฏิกิริยาโพรพิเลชันของกลีเซอรีนบนตัวเร่งAmberlyst-15ที่อุณหภูมิ 100 องศาเซลเซียส เป็นเวลา 24 ชั่วโมง เกิดโพรพิลกลีเซอรอลอีเทอร์ผสม(PGE)ซึ่งประกอบด้วยโมโนโพรพิลกลีเซอรอลอีเทอร์ (MPGE) 24.99%, ไดโพรพิลกลีเซอรอลอีเทอร์ (DPGE) 20.84% และไตรโพรพิล-กลีเซอรอลอีเทอร์ (TPGE) 54.17% TPGEเป็นผลิตภัณฑ์เดี่ยวที่เกิดผ่านปฏิกิริยาโพรพิลีนอัลคีเลชันของMPGEและDPGEบนตัวเร่งAmberlyst-15 ณ อุณหภูมิ 100 องศาเซลเซียส ใช้เวลา 48 ชั่วโมง ผลิตภัณฑ์จากปฏิกิริยาบิวทิเลชันของกลีเซอรีนบนตัวเร่งAmberlyst-15 ณ อุณหภูมิ 100 องศาเซลเซียส ใช้เวลา 48 ชั่วโมงประกอบด้วยโมโนบิวทิลกลีเซอรอลอีเทอร์(MBGE) 79.40%, อนุพันธ์ของไดออกเซน 9.71% และไดบิวทิลกลีเซอรอลอีเทอร์(DBGE) 10.89% โพรพิลกลีเซอรอลอีเทอร์ผสม(PGE)และไตรโพรพิลกลีเซอรอลอีเทอร์(TPGE) ลดค่าจุดขุ่นและจุดไหลเทของไบโอดีเซลจากน้ำมันปาล์มผสมดีเซล ลดค่าดัชนีซีเทนของน้ำมันดีเซลและB100 และเพิ่มค่า RON และMON ในน้ำมันแก๊สโซลีน เมื่อเติม 10% PGE หรือ TPGE ลงไป

สาขาวิชา ปิโตรเคมี ลายมือชื่อนิสิต.....

ปีการศึกษา 2554 ลายมือชื่อ อ.ที่ปรึกษาวิทยานิพนธ์หลัก.....

ลายมือชื่อ อ.ที่ปรึกษาวิทยานิพนธ์ร่วม.....

5073808223 : MAJOR PETROCHEMISTRY
KEYWORDS : ETHERIFICATION / SBA / AMBERLYST / ION-EXCHANGE RESIN / ZEOLITE

CHAKRAPONG SAENGARUN : SYNTHESIS AND EFFECT OF ALKYL GLYCEROL ETHER ON COLD FLOW PROPERTY OF BIODIESEL FROM PALM OIL. ADVISOR : ASSOC. PROF. AMORN PETSOM, Ph.D., CO-ADVISOR : DUANGAMOL TUNGASMITA, Ph.D., 100 pp.

The etherification reaction between glycerin and alkenes (ethylene, propylene, 1-butene, 1-pentene, 1-hexene, 1-heptene and 1-octene) over acidic heterogeneous catalysts (Amberlyst-15, S100, S200, Al-SBA-15, Pr-SO_3H-SBA-15, Zeolite Beta and Zeolite Y) were carried out. Strong acidity with mesopore size of Amberlyst-15 gave the highest activity in propylation and butylation of glycerin. S200 resin, strong acidity with non porous type, showed low reaction in glycerin etherification with propylene and 1-butene. S100 resin, strong acidity with non porous type, gave the lowest reaction in glycerin propylation and gave no reaction of glycerin butylation. Weak acidity with high pore size of Al-SBA-15, Pr-SO_3H-SBA-15, Z-Beta and Z-Y gave no reaction on glycerin etherification with propylene and 1-butene. The propylation of glycerin over Amberlyst-15 at 100 °C after 24 h showed mixed propyl glycerol ethers (PGE) which composed of mono-propyl glycerol ether (MPGE) 24.99%, di-propyl glycerol ether (DPGE) 20.84% and tri-propyl glycerol ether (TPGE) 54.17%. TPGE was obtained as a sole product through propylene alkylation of MPGE and DPGE, over Amberlyst-15 at 100 °C after 48 h. The butylation product of glycerin over Amberlyst-15 at 100 °C after 48 h composed of mono-butyl glycerol ether (MBGE) 79.40%, dioxan derivative 9.71% and di-butyl glycerol ether (DBGE) 10.89%. The mixed PGE and TPGE reduced cloud point and pour point of blended palm biodiesel with diesel, reduced cetane index of diesel and B100, and increased RON and MON in gasoline when 10% of mixed PGE or TPGE was added.

Field of Study : Petrochemistry Student's Signature .....
Academic Year : 2011 Advisor's Signature .....
Co-advisor's Signature .....

ACKNOWLEDGEMENTS

The author would like to express his deep gratitude to his advisor, Associate Professor Dr. Amorn Petsom for his encouraging guidance, supervision and helpful suggestions throughout the course of this research. He is sincerely grateful to his co-advisor, Dr. Duangamol Tungasmita for her useful guidance and understanding.

He also wishes to heartfully thank the thesis committee for their valuable suggestions and comments and all who has contributed suggestions and support during this research.

He is sincerely grateful to Miss Phatchari Phengphit, Mr. Egawit Sangprasertsuk, Mr. Woraphong Khawprapan and Mr. Prakit Piya-asawajinda for their useful support and guidance during this research.

Finally, the author would like to express sincere appreciation to Miss Puangpaka Charuenwongtrakool for her unfailing support, tolerance, and intuition in preparing of this thesis, without her the works could not have been completed.

CONTENTS

PAGE

ABSTRACT (IN THAI)……...……. iv

ABSTRACT (IN ENGLISH)……..... v

ACKNOWLEDGEMENTS…….. vi

CONTENTS…….. vii

LIST OF TABLES…… x

LIST OF FIGURES……... xii

LIST OF ABBREVIATIONS AND SYMBOLS…….. xvii

CHAPTER

I INTRODUCTION ……..... 1

Objectives and scope of the research...……..... 1

II THEORETICAL REVIEW…….. 3

2.1 Biodiesel…...……..... 3

2.1.1 Quality of biodiesel.……..... 5

2.1.2 Cold flow properties of biodiesel.……..…….…..... 7

2.1.3 Glycerol……..…….…..... 8

2.2 Glycerol-based fuel additives……..... 12

2.3 Acidic catalysts……..... 13

2.3.1 Ion-exchange resin.……..... 13

2.3.2 Mesoporous silica.……..…….…..... 14

2.3.2.1 Aluminium-containing SBA-15 mesoporous silica 14

2.3.2.2 Organosulfonic functionalized mesoporous silica 16

2.3.3 Zeolite ……..…….…..... 19

2.3.3.1 Zeolite beta ……..…….…..... 19

2.3.3.2 Zeolite Y ……..…….…..... 20

2.4 Adsorption isotherms……..... 21

2.4.1 BET surface area ……..…….…..... 21

2.4.2 t-plot method……..... 21

2.4.3 BJH method.……..…….…..... 22

2.5 Literature review……...……..……..... 22

CHAPTER PAGE

III EXPERIMENTAL..... 26

3.1 Apparatus and instruments..... 26

3.2 Materials..... 28

3.3 Catalyst preparation..... 29

3.3.1 Pr-SO_3H-SBA-15..... 29

3.3.2 Al-SBA-15..... 29

3.3.3 Zeolite beta and zeolite Y..... 29

3.3.4 Ion-exchange resins S100 and S200..... 30

3.4 Catalyst characterization..... 30

3.4.1 X-ray powder diffraction (XRD)..... 30

3.4.2 Nitrogen adsorption isotherms..... 30

3.4.3 Acid capacity of catalysts..... 31

3.5 Etherification of glycerin with olefin gases and C_5 to C_8 alkenes..... 31

3.6 Characterization of glycerin and alkyl glycerol ethers by FTIR..... 32

3.7 Characterization of glycerin and alkyl glycerol ethers by GCMS..... 32

3.7.1 Operating condition of GC..... 32

3.7.2 Operating condition of MSD..... 33

3.8 Pour point procedure..... 33

3.9 Cloud point procedure..... 34

3.10 Cetane index procedure..... 34

3.11 Density, relative density, or API gravity procedure..... 35

3.12 Distillation of petroleum products procedure..... 35

3.13 Octane number procedure..... 36

IV RESULTS AND DISCUSSION..... 37

4.1 Characteristics of catalysts..... 37

4.1.1 X-ray powder diffraction (XRD)..... 38

4.1.2 Nitrogen adsorption..... 40

4.2 Performance of catalysts..... 42

CHAPTER PAGE

4.2.2 Etherification of glycerin with propylene……..... 44

4.2.3 Etherification of glycerin with 1-butene …….…. 45

4.3 Characterization of etherification products by using FTIR …….. 46

4.4 Characterization of etherification products by using GCMS ……..... 49

4.5 Reaction pathways ……. 53

4.6 Influence of mixed-propyl glycerol ethers and tri-propyl glycerol ether on cold flow performance of palm biodiesels ……..….. 64

4.7 Influence of mixed-propyl glycerol ethers and tri-propyl glycerol ether on cetane index and octane number of palm biodiesels……...… 69

V CONCLUSION ……...……. 72

Suggestions for Future Works …….. 73

REFERENCES…….. 74

APPENDICES……... 79

APPENDIX A……..... 80

APPENDIX B……..... 94

VITAE……..... 100

LIST OF TABLES

		PAGE
2.1	Composition of various biodiesel feed stocks …….....	4
2.2	Selected properties of typical no. 2 diesel and soybean-biodiesel…..	6
2.3	Fatty acids in feed stocks of biodiesels …….....	8
2.4	Physical and chemical properties of glycerol …….....	9
2.5	Chemical transformations of glycerol...……..	11
3.1	Quality of materials…….	28
4.1	Properties of catalysts …….	38
4.2	Glycerin conversion (%) of etherification between glycerin and propylene on acidic catalysts, glycerin/propylene = 1/4, catalyst/glycerin = 10 wt%, temperature 100 °C……...……..	45
4.3	Glycerin conversion (%) of etherification between glycerin and 1-butene on acidic catalysts, glycerin/1-butene = 1/4, catalyst/glycerin = 10 wt%, temperature 100 °C…...……..	46
4.4	Product distribution of etherification between glycerin and propylene on Amberlyst-15, glycerin/propylene = 1/4, catalyst/glycerin = 10 wt %.....	55
4.5	Product distribution of etherification between glycerin and propylene on S200, glycerin/propylene = 1/4, catalyst/glycerin = 10 wt %.....	56
4.6	Product distribution of etherification between glycerin and propylene on S100, glycerin/propylene = 1/4, catalyst/glycerin = 10 wt %.....	56
4.7	Product distribution of etherification between glycerin and 1-butene on Amberlyst 15, glycerin/1-butene = 1/4, catalyst/glycerin = 10 wt %.....	57
4.8	Product distribution of etherification between glycerin and 1-butene on S200, glycerin/1-butene = 1/4, catalyst/glycerin = 10 wt %.....	57
4.9	Cold flow properties of propyl glycerol ethers in blended palm biodiesels…….	68

TABLE PAGE

4.10 Cetane index of diesel and palm biodiesel by adding 10% of oxygenated-compound additives……..……... 70

4.11 Octane number of gasoline by adding 10% of oxygenated-compound additives……. 71

B1 Analysis result of pure glycerin...……... 94

B2 Analysis result of palm biodiesel (B100)……...…. 94

B3 Analysis result of diesel …..…… 95

B4 Properties of catalysts ……. 95

B5 Product distribution of etherification between glycerin and propylene over Amberlyst-15…….……. 95

B6 Product distribution of etherification between glycerin and propylene over S200 resin…….. 95

B7 Product distribution of etherification between glycerin and propylene over S100 resin……... 96

B8 Product distribution of etherification between glycerin and 1-butene over Amberlyst-15……... 96

B9 Product distribution of etherification between glycerin and 1-butene over S200 resin……..... 97

B10 Could point of mixed-propyl glycerol ethers in blended palm biodiesels……. 97

B11 Could point of mixed-propyl glycerol ethers in blended palm biodiesels……. 97

B12 Could point of tri-propyl glycerol ethers in blended palm biodiesels. 98

B13 Pour point of tri-propyl glycerol ethers in blended palm biodiesels... 98

B14 Cetane index of diesel by adding 10% of oxygenated-compound additives……... 98

B15 Cetane index of biodiesel by adding 10% of oxygenated-compound additives……... 98

B16 Octane number of gasoline by adding 10% of oxygenated-compound additives…**……** 99

LIST OF FIGURES

		PAGE
2.1	Transesterification of palm oil.……...	5
2.2	Molecular structure of glycerol …….…….	8
2.3	Etherification between glycerol with isobutylene …….....	13
2.4	XRD pattern of SBA-15……..	15
2.5	TEM Images of SBA-15 (a) in the direction of the pore axis and (b) in the direction perpendicular to the pore axis.…….....	15
2.6	Adsorption-desorption isotherm of nitrogen on SBA-15 at 77 K the insert shows the BJH pore size distribution calculated from the desorption branch of the isotherm……...	16
2.7	Propylsulfonic-acid and arenesulfonic-acid modified on the pore surface of SBA-15……...	18
2.8	XRD pattern of organosulfonic functionalized SBA-15…….……	18
2.9	TEM images (a) in the direction of the pore axis and (b) in the direction perpendicular to the pore axis of an organosulfonic modified SBA-15 material…..……..	18
2.10	Nitrogen adsorption isotherm of organosulfonic-acid-modified SBA-15……	18
2.11	Framework of zeolite beta……..….	19
2.12	XRD powder pattern of zeolite beta……..……..	20
2.13	Framework of zeolite Y…….…….	20
2.14	XRD powder pattern of zeolite Y…….…….….	21
3.1	Micro reactor ……..	27
3.2	FTIR spectrum of standard glycerin……..…….	32
3.3	Mass spectrum of standard glycerin ……..…….	33
4.1	XRD pattern of Pr-SO_3H-SBA-15…….……..	39
4.2	XRD pattern of Al-SBA-15 ……...	39
4.3	XRD pattern of zeolite beta …….....	40
4.4	XRD pattern of zeolite Y…….....	40
4.5	BJH plot of Amberlyst-15 ……..	41

FIGURE		PAGE
4.6	BJH plot of resins (a) S100 and (b) S200.……..……...…	41
4.7	BJH plot of zeolites (a) zeolite beta and (b) zeolite Y……	42
4.8	BJH plot of mesopores (a) Pr-SO_3H-SBA-15 and (b) Al-SBA-15…	42
4.9	Glycerin conversion of etherification between glycerin and alkenes on acidic catalysts, glycerin/alkene = 1/4, catalyst/glycerin = 10 wt %, temperature 90 °C, reaction time 8 h..……	43
4.10	Glycerin conversion of etherification between glycerin and alkenes on acidic catalysts, glycerin/alkene = 1/4, catalyst/glycerin = 10 wt %, temperature 100 °C, reaction time 8 h.……...…	44
4.11	FTIR spectrum of tri-propyl glycerol ether…….	47
4.12	FTIR spectrum of propyl glycerol ethers……...….	48
4.13	FTIR spectrum of butyl glycerol ethers…….....	48
4.14	Mass spectrum of propyl glycerol ethers……..……..……..	50
4.15	Mass spectrum of butyl glycerol ethers…….…….	52
4.16	Chromatogram of propyl glycerol ethers……...……..…..	54
4.17	Chromatogram of butyl glycerol ethers……..……	54
4.18	Reaction pathway of etherification between glycerin and propylene on Amberlyst-15……..	61
4.19	Reaction pathway of etherification between glycerin and 1-butene on Amberlyst-15 to form 3-MBGE and 2-MBGE……..	62
4.20	Reaction pathway of etherification between glycerin and 1-butene on Amberlyst-15 to form dioxan derivative……	63
4.21	Reaction pathway of etherification between 3-MBGE and 2-MBGE with 1-butene on Amberlyst-15 to form 1,3-DBGE and 2,3-DBGE...	64
4.22	Could point of mixed-propyl glycerol ethers in blended palm biodiesels…….	66
4.23	Pour point of mixed-propyl glycerol ethers in blended palm biodiesels…….	66
4.24	Could point of tri-propyl glycerol ether in blended palm biodiesels...	67
4.25	Pour point of tri-propyl glycerol ether in blended palm biodiesels….	67

FIGURE PAGE

A1 GC chromatogram of pure glycerin……. 80
A2 GC chromatogram of etherification between glycerin and propylene over Amberlyst-15, temperature 90 °C and time 8 h…….. 80
A3 GC chromatogram of etherification between glycerin and propylene over Amberlyst-15, temperature 100 °C and time 8 h…… 80
A4 GC chromatogram of etherification between glycerin and propylene over Amberlyst-15, temperature 100 °C and time 16 h….. 81
A5 GC chromatogram of etherification between glycerin and propylene over Amberlyst-15, temperature 100 °C and time 24 h…. 81
A6 GC chromatogram of etherification between glycerin and propylene over Amberlyst-15, temperature 100 °C and time 32 h….. 81
A7 GC chromatogram of etherification between glycerin and propylene over Amberlyst-15, temperature 100 °C and time 40 h…. 82
A8 GC chromatogram of etherification between glycerin and propylene over Amberlyst-15, temperature 100 °C and time 48 h….. 82
A9 GC chromatogram of etherification between glycerin and propylene over S100 resin, temperature 100 °C and time 16 h……... 82
A10 GC chromatogram of etherification between glycerin and propylene over S100 resin, temperature 100 °C and time 24 h……... 83
A11 GC chromatogram of etherification between glycerin and propylene over S100 resin, temperature 100 °C and time 32 h…….. 83
A12 GC chromatogram of etherification between glycerin and propylene over S100 resin, temperature 100 °C and time 40 h…….. 83
A13 GC chromatogram of etherification between glycerin and propylene over S100 resin, temperature 100 °C, and time 48 h…….. 84
A14 GC chromatogram of etherification between glycerin and propylene over S100 resin, temperature 100 °C and time 56 h…….. 84
A15 GC chromatogram of etherification between glycerin and propylene over S100 resin, temperature 100 °C and time 64 h…….. 84

FIGURE PAGE

A16 GC chromatogram of etherification between glycerin and propylene over S100 resin, temperature 100 °C and time 72 h…….. 85
A17 GC chromatogram of etherification between glycerin and propylene over S200 resin, temperature 100 °C and time 16 h……. 85
A18 GC chromatogram of etherification between glycerin and propylene over S200 resin, temperature 100 °C and time 24 h……. 85
A19 GC chromatogram of etherification between glycerin and propylene over S200 resin, temperature 100 °C and time 32 h……. 86
A20 GC chromatogram of etherification between glycerin and propylene over S200 resin, temperature 100 °C and time 40 h…….. 86
A21 GC chromatogram of etherification between glycerin and propylene over S200 resin, temperature 100 °C and time 48 h……. 86
A22 GC chromatogram of etherification between glycerin and propylene over S200 resin, temperature 100 °C and time 56 h…….. 87
A23 GC chromatogram of etherification between glycerin and propylene over S200 resin, temperature 100 °C and time 64 h…….. 87
A24 GC chromatogram of etherification between glycerin and propylene over S200 resin, temperature 100 °C and time 72…….. 87
A25 GC chromatogram of etherification between glycerin and 1-butene over Amberlyst-15, temperature 100 °C and time 8 h……. 88
A26 GC chromatogram of etherification between glycerin and 1-butene over Amberlyst-15, temperature 100 °C and time 16 h……... 88
A27 GC chromatogram of etherification between glycerin and 1-butene over Amberlyst-15, temperature 100 °C and time 24 h……... 88
A28 GC chromatogram of etherification between glycerin and 1-butene over Amberlyst-15, temperature 100 °C and time 32 h……... 89
A29 GC chromatogram of etherification between glycerin and 1-butene over Amberlyst-15, temperature 100 °C and time 40 h……... 89
A30 GC chromatogram of etherification between glycerin and 1-butene over Amberlyst-15, temperature 100 °C and time 48 h……... 89

FIGURE PAGE

A31 GC chromatogram of etherification between glycerin and 1-butene over Amberlyst-15, temperature 100 °C and time 56 h……... 90
A32 GC chromatogram of etherification between glycerin and 1-butene over Amberlyst-15, temperature 100 °C and time 64 h……... 90
A33 GC chromatogram of etherification between glycerin and 1-butene over Amberlyst-15, temperature 100 °C and time 72 h……... 90
A34 GC chromatogram of etherification between glycerin and 1-butene over S200 resin, temperature 100 °C and time 16 h…… 91
A35 GC chromatogram of etherification between glycerin and 1-butene over S200 resin, temperature 100 °C and time 24 h…… 91
A36 GC chromatogram of etherification between glycerin and 1-butene over S200 resin, temperature 100 °C and time 32 h…… 91
A37 GC chromatogram of etherification between glycerin and 1-butene over S200 resin, temperature 100 °C and time 40 h…… 92
A38 GC chromatogram of etherification between glycerin and 1-butene over S200 resin, temperature 100 °C and time 48 h…… 92
A39 GC chromatogram of etherification between glycerin and 1-butene over S200 resin, temperature 100 °C and time 56 h…… 92
A40 GC chromatogram of etherification between glycerin and 1-butene over S200 resin, temperature 100 °C and time 64 h…… 93
A41 GC chromatogram of etherification between glycerin and 1-butene over S200 resin, temperature 100 °C and time 72 h…… 93

LIST OF ABBREVIATIONS AND SYMBOLS

Å	Angstrom
a_0	unit cell parameter
A_{BET}	Brunauer Emmett Teller surface area
A_{BJH}	Barrett-Joyner-Halenda surface area
^{27}Al	Aluminium
Al-SBA-15	Aluminum Santa Barbara amorphous material
API	American petroleum institute
Ar-SO_3H	Aryl sulfonic acid group
ASTM	American society for testing and materials
B100	Pure biodiesel
BET	Brunauer Emmett Teller
BGE	Butyl glycerol ether
BJH	Barrett-Joyner-Halenda
Btu/gal	British thermal unit per gallon
°C	Degree Celsius
cal/g	calorie per gram
CFPP	Cold filtration plugging point
CI	Cetane index
cm^{-1}	per centimeter
cm^3/g	cubic centimeter per gram
C/O	Carbon per oxygen
Conv	Conversion
cP	centi Point
CSPTMS	2-(4-Chlorosulfonylphenyl)-ethyltrimethoxy silane
cSt	centi Stoke
DBGE	di-Butyl glycerol ether
DCP	di-Chloropropanol
der	derivative
DHA	Docosahexaenoic acid
dif.	difference

DIN EN	Deutsches institut fur normung of European standard
DPGE	di-Propyl glycerol ether
DSC	Differential scanning calorimetry
DTBG	di-tert-Butyl glycerol ether
EN	European standard
EO	Ethylene oxide
ESR	Electron spin resonance
ETBE	Ethyl tert-butyl ether
°F	Degree Fahrenheit
FAME	Fatty acid methyl ester
FAU	Faujasite
FID	Flame ionization detector
FTIR	Fourier transform infrared spectroscopy
g	gram
GCMS	Gas chromatography mass spectrometry
Gly	Glycerin
h	hour
^{1}H-NMR	Proton nuclear magnetic resonance
ISO	International organization for standardization
IUPAC	International union of pure and applied chemistry
IZA-SC	International zeolite association-structure commission
K	Kelvin
kg/l	kilogram per liter
lb/gal	pound per gallon
m	meter
MAS NMR	Magic-angle-spinning nuclear magnetic resonance spectroscopy
max	maximum
MBGE	mono-Butyl glycerol ether
MCM-41	Mobil crystalline materials
meq H^{+}/g	milli equivalent proton per gram
mg	milligram

m^2/g	square meter per gram
MIBK	Methyl isobutyl ketone
min	minimum
ml	milliliter
mm	millimeter
mmHg	millimeter mercury
mmol/g	milli mole per gram
MON	Motor octane number
mp	melting point
MPGE	mono Propyl glycerol ether
MPTMS	3-Mercaptopropyltrimethoxysilane
MSD	Mass spectrometry detector
MTBE	Methyl tert-butyl ether
MTBG	mono-tert-Butyl glycerol ether
m/z	mass per charge
MW	Molecular weight
Ni–Sn	Nickel-Tin
No.	Number
^{31}P	Phosphorus
PET	Polyethylene terephthalate
PGE	Butyl glycerol ether
Ph Eur	European pharmacopoeia
PO	Propylene oxide
P/P_0	relative pressure
ppm	part per million
Pr-SO_3H	Propylsulfonic acid group
psig	pounds per square inch
PTT	Polytrimethylene terephthalate
RI	Reflective index
r_c (x_k)	current relative pressure
RON	Research octane number
rpm	round per minute

SBA-15	Santa Barbara amorphous material
SD	Standard deviation
Si/Al	Silicon per Aluminium
SLBOCLE	Scuffing load ball on cylinder lubricity evaluator
Sp Gr	Specific gravity
Spec	Specification
sq cm/s	square centimeter per second
STP	Standard conditions for temperature and pressure
TAME	tert-Amyl methyl ether
TBE	Ethyl tert-butyl ether
TBU	tertiary building unit
TEM	Transmission electron microscopy
TEOS	Tetraethyl orthosilicate
TMOS	Tetramethyl orthosilicate
TPGE	tri-Propyl glycerol ether
TTBG	tri-tert-Butyl glycerol ether
USP	United states pharmacopoeia
V_a	amount of adsorbed-gas at an arbitrary pressure
V_{ads} (X_k)	volume of liquid adsorbate at relative pressure
V_m	monolayer adsorbed-gas quantity
vol %	volume percentage
wt %	weight percentage
XRD	X-ray diffraction
ZSM-5	Zeolite
β	Beta
Δ	Delta
θ	Theta
Σ	Summation
μm	micrometer

CHAPTER I
INTRODUCTION

Biodiesel is a diesel replacement fuel that is manufactured from renewable natural materials. The manufacturing process of biodiesel converts vegetable oils, recycled cooking greases or oils and animal fats into chemicals called fatty acid methyl esters or FAME and glycerin as co-product. Some typical uses of glycerin are food additives, pharmaceuticals, cosmetics, detergents, personal care and paper manufacture. Particularly, glycerin can be converted to glycerol-based additives by using acetylation or esterification reaction of glycerin with acetic acid, etherification reaction of sole glycerin and etherification reaction of glycerin with alkenes. The glycerol-based additives are recognized as alternative oxygenate additives to diesel, biodiesel and their mixtures. A considerable reduction in pour point and cloud point of biodiesel has been noticed by using glycerol-based additive as cold flow improvers. That is one of the possibilities of glycerin utilization.

Previous studies demonstrated that the transformation of glycerin into glycerol-based additives through acetylation or esterification and etherification reactions have been developed by using different types of heterogeneous solid catalysts. Those catalysts were alkaline earth metal, carbonate based, polysaccharide derived mesoporous material, zeolite, ion exchange resin and mesoporous silica. The reactions were studied in preparation technique of catalyst, acidity, basicity, porosity, catalyst loading and especially catalyst activity.

Objectives and scope of the research

The scope of this work is to study the etherification of glycerin with olefins; i.e. ethylene, propylene, 1-butene, and higher alkene; i.e. 1-pentene, 1-hexene, 1-heptene and 1-octene over heterogeneous solid catalysts. Three types of catalysts were selected in this research, namely mesostructured silicas, ion-exchange resins and large-pore zeolites. This study examined the influence of catalysts, alkenes, temperatures and reaction times towards the reaction conversion and the selectivity. The products from this reaction, alkyl glycerol ethers, were characterized by using GCMS for structure identification and FTIR for functional group identification. In

addition, these products were used for investigation of their potential use as cold flow property improver of palm biodiesel and palm biodiesel blended with diesel at various concentrations.

CHAPTER II
THEORETICAL REVIEW

2.1 Biodiesel

On August 31, 1937, G. Chavanne of the University of Brussels in Belgium was granted a patent for a "Procedure for the transformation of vegetable oils for their uses as fuels" Belgian Patent 422,877. This patent described the transesterification or alcoholysis of vegetable oils using methanol or ethanol in order to separate the fatty acid methyl ester or biodiesel from the glycerol [1]. Biodiesel is also manufactured from recycled cooking greases or oils, or animal fats. In the manufacturing process, 100 pounds of oils or fats are reacted with 10 pounds of a short chain alcohol (usually methanol) in the presence of a catalyst (usually sodium hydroxide or sulfuric acid) to form 100 pounds of biodiesel and 10 pounds of a co-product glycerin.

Biodiesel can be produced commercially from a variety of oils and fats:

1) Animal fats: edible tallow, inedible tallow, and all the other variations of tallow, lard, choice white grease, yellow grease, poultry fats and fish oils.
2) Vegetable oils: soy, corn, canola, sunflower, rapeseed and cottonseed.
3) Recycled greases: used cooking oils and restaurant frying oils.

It is also possible to make biodiesel from other oils, fats and recycled oils such as mustard, palm, coconut, peanut, olive, sesame, and safflower oils, trap greases, and even oils produced from algae, fungi, bacteria, molds, and yeast. The chemistry of different fats and oils typically used for biodiesel are very similar. Each fat or oil molecule is made up of a glycerin backbone of three carbons, and on each of these carbons is attached a long chain fatty acid. These long chain fatty acids are what react with methanol to make the fatty acid methyl ester (FAME), or biodiesel. The glycerin backbone is turned into glycerin as a byproduct. The fats and oils listed above contain 10 common types of fatty acids which have between 12 and 22 carbons, with over 90% of them being between 16 and 18 carbons [2]. Some of these fatty acid chains are saturated, while others are unsaturated. These different feed stocks are made of different proportions of saturated and unsaturated fatty acids, as shown in Table 2.1.

Table 2.1 Composition of various biodiesel feed stocks [3].

Fat or oil	Saturated fatty acids			Unsaturated fatty acids	
	Lauric (12:0)*	**Palmitic (16:0)**	**Stearic (18:0)**	**Oleic (18:1)**	**Linoleic (18:2)**
Butter fat	2.5	29.0	9.2	26.7	3.6
Coconut oil	45.4	10.5	2.3	7.5	Trace
Corn oil	-	10.2	3.0	49.6	34.3
Olive oil	-	6.9	2.3	84.4	4.6
Palm oil	-	40.1	5.5	42.7	10.3
Peanut oil	-	8.3	3.1	56.0	26.0
Soybean oil	0.2	9.8	2.4	28.9	50.7

***Note** The first number shows the number of carbons in the fatty acid chain and the second number is the level of saturation or unsaturation (0 for saturated, 1 for monounsaturated, and 2 or 3 for polyunsaturated).

The physical properties of a triglyceride depend on its fatty acid components. In general, the melting point of a triglyceride increase as the number of carbons in its hydrocarbon chains increases and as the number of carbon-carbon double bonds decreases. Triglycerides rich in oleic acid, linoleic acid, and other unsaturated fatty acids are generally liquid at room temperature and are called oils. Triglycerides rich in palmitic acid, stearic acid, and other saturated fatty acids are generally semisolids or solids at room temperature and are called fats. Most plant oils contain 20% or less saturated fatty acids and 80% or more unsaturated fatty acids. The notable exception to this generalization about plant oils are the tropical oils, e.g. coconut and palm oils, which are considerably richer in the lower-molecular-weight saturated fatty acids [3]. A perfect biodiesel would be made only from unsaturated fatty acids. Generally, the biodiesel from palm oil contains 50% of saturated fatty acids (palmitic and stearic acids), 40% of monounsaturated fatty acid (oleic acid) and 10% of polyunsaturated fatty acid (linoleic acid). Transesterification of biodiesel from palm oil is shown in Figure 2.1.

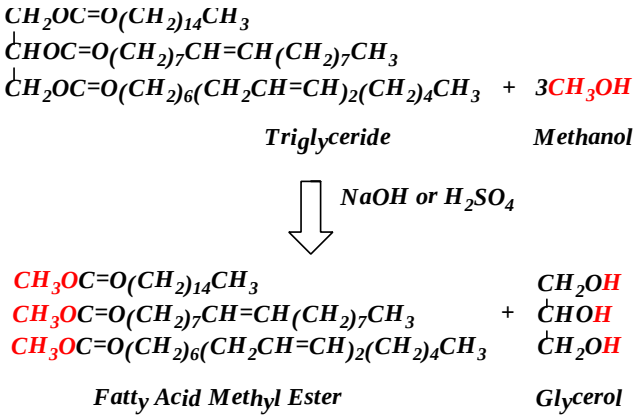

Figure 2.1 Transesterification of palm oil.

Raw or refined vegetable oils contain three ester linkages. Biodiesel can be made from methyl, ethyl, isopropyl and other alcohols. But, all commercial-production of biodiesel is fatty acid methyl esters. Productions of fatty acid ethyl esters have hampered in the commercial market due to higher ethanol prices relative to methanol, lower ethyl ester conversions and the difficulty of recycling excess ethanol internally in the process.

2.1.1 Quality of biodiesel

Biodiesel is a diesel replacement fuel. It is produced from either agricultural or recycled resources. Biodiesel is nontoxic and biodegradable fuel. Any biodiesel used for fuel and diesel blending should meet American Society for Testing and Materials (ASTM) D6751 standards. The definition of biodiesel within this standard describes mono-alkyl esters of long chain fatty acids that derived from vegetable oils and animal fats [4]. There are physical and chemical properties that biodiesel is different from petroleum diesel. These differences provide significant benefits for biodiesel quality. Biodiesel has lower sulfur than petroleum diesel that can be generated low SO_2. Biodiesel contains 11% oxygen by weight, which provides for more complete combustion. A slightly high cetane number of biodiesel provides for more reduction in white smoke emissions. Cetane number is a measure of the ignition quality of the fuel and influences white smoke and combustion roughness. The cetane number requirements depend on engine design, size, nature of speed and load variations, and on starting and atmospheric conditions [5]. The flash point is important in safety

precautions that involved in fuel handling and storage. It is normally specified to meet insurance and fire regulations. The flash point specification for biodiesel is intended to be 100 °C minimum [6]. Biodiesel's flash point is higher than diesel's flash point. Fuel lubricity is evaluated the lubricity (load carrying ability) of fuel using a scuffing load ball-on-cylinder lubricity evaluator (SLBOCLE). Diesel fuel injection equipment has some reliance on lubricating properties of the diesel fuel. Shortened life of engine components, such as diesel fuel injection pumps and injectors, sometimes has been ascribed to lack of lubricity in a diesel fuel. The trend of SLBOCLE test results to diesel injection system pump component distress due to wear has been demonstrated in pump rig tests for some fuel/hardware combinations where boundary lubrication is believed to be a factor in the operation of the component [7]. The selected properties of typical No. 2 diesel and soybean-biodiesel fuels are shown in Table 2.2.

Table 2.2 Selected properties of typical no. 2 diesel and soybean-biodiesel [2].

Fuel property	Diesel	Biodiesel
Fuel standard	ASTM D975	ASTM D6751
Lower heating value, btu/gal	~129,050	~118,170
Kinematic viscosity, 40 °C	1.3 to 4.1	4.0 to 6.0
Specific gravity, kg/l 60 °F	0.85	0.88
Density, lb/gal 15 °C	7.079	7.328
Water and sediment, vol %	0.05 max	0.05 max
Carbon, wt %	87	77
Hydrogen, wt %	13	12
Oxygen, by dif. wt %	0	11
Sulfur, wt %	0.05 max	0.0 to 0.0024
Boiling point, °C	180 to 340	315 to 350
Flash point, °C	60 to 80	100 to 170
Cloud point, °C	-15 to 5	-3 to 12
Pour point, °C	-35 to -15	-15 to 10
Cetane number	40 to 55	48 to 65
Lubricity SLBOCLE, grams	2,000-5,000	>7,000

2.1.2 Cold flow properties of biodiesel

The cold flow properties of conventional diesel and biodiesel are extremely important. Unlike gasoline, both diesel and biodiesel can start to freeze or gel as the temperature gets colder. If the fuel begins to gel, it can clog filters or can eventually become too thick to pump from the fuel tank to the engine. There are three tests used to measure the cold flow properties of fuels for diesel engines, i.e. cloud point, cold filter plug point, and pour point.

Cloud point is the temperature at which a cloud or haze of crystals appears in the fuel under prescribed test conditions. It generally relates to the temperature at which crystals begin to precipitate from the fuel in use. Biodiesel generally has a higher cloud point than petroleum based diesel fuel. The cloud point of biodiesel and its impact on the cold flow properties of the resulting blend should be monitored by the user to ensure trouble-free operation in cold climates [8]. The ASTM D2500 is test method for cloud point determination.

Cold filter plug point (CFPP) is the temperature at which fuel crystals have agglomerated in sufficient amounts to cause a test filter to plug. The CFPP is less conservative than the cloud point, and is considered by some to be a better indication of low temperature operability [9]. CFPP temperature is measured by following the ASTM D4539.

Pour point is the lowest temperature at which the fuel with many agglomerated crystals is essentially a gel and will no longer flow. The low-temperature flow properties of a waxy fuel oil depend on handling and storage conditions. Thus, they may not be truly indicated by pour point. The pour point test does not indicate what happens when oil has a considerable head of pressure behind it, such as when gravitating from storage tank or being pumped along a pipeline. Failure to flow at the pour point is normally attributed to the separation of wax from the fuel. However, it can also be the effect of viscosity in the case of very viscous fuel oils. In addition pour points of residual fuels are influenced by the previous thermal history of the specimens. A loosely knit wax structure built up on cooling of the oil can be normally broken by the application of relatively little pressure. The ASTM D97 is test method for pour point measurement [10].

The differing levels of saturation in fatty acid methyl esters can affect the cold flow properties of biodiesels. The different proportions of saturated, monounsaturated and polyunsaturated in fatty acid methyl esters are produced from different types of feed-stocks, as shown in Table 2.3.

Table 2.3 Fatty acids in feed stocks of biodiesels [3].

C atoms : double bonds	Structure	Name	mp (°C)
Saturated fatty acids			
12:0	$CH_3(CH_2)_{10}CO_2H$	Lauric acid	44
14:0	$CH_3(CH_2)_{12}CO_2H$	Myristic acid	58
16:0	$CH_3(CH_2)_{14}CO_2H$	Palmitic acid	63
18:0	$CH_3(CH_2)_{16}CO_2H$	Stearic acid	70
20:0	$CH_3(CH_2)_{18}CO_2H$	Arachidic acid	77
Unsaturated fatty acids			
16:1	$CH_3(CH_2)_5CH{=}CH(CH_2)_7CO_2H$	Palmitoleic acid	32
18:1	$CH_3(CH_2)_7CH{=}CH(CH_2)_7CO_2H$	Oleic acid	16
18:2	$CH_3(CH_2)_4(CH{=}CHCH_2)_2(CH_2)_6CO_2H$	Linoleic acid	-5
18:3	$CH_3CH_2(CH{=}CHCH_2)_3(CH_2)_6CO_2H$	Linolenic acid	-11
20:4	$CH_3(CH_2)_4(CH{=}CHCH_2)_4(CH_2)_2CO_2H$	Arachidonic acid	-49

2.1.3 Glycerol

Glycerol is the tri-hydroxyl alcohol which has IUPAC name of propane-1,2,3-triol. It has other names as glycerin, 1,2,3-propanetriol, 1,2,3-trihydroxypropane, glyceritol or glycyl alcohol. The molecular structure of glycerol is shown in Figure 2.2. Pure glycerol is colorless, odorless, viscous liquid with syrupy and sweet taste. It has three hydrophilic hydroxyl groups that are responsible for its solubility in water. Table 2.4 lists physical and chemical properties of glycerol.

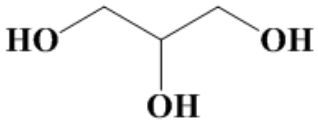

Figure 2.2 Molecular structure of glycerol.

Table 2.4 Physical and chemical properties of glycerol [11].

Properties	Values	Properties	Values
Chemical formula	$CH_2OH–CHOH–CH_2OH$	Vapor pressure in 760mmHg	290 °C
Formula weight	92.09	Heat of fusion at 18.07 °C	47.49 cal/g
Form and color	Colorless and liquid	Viscosity liquid glycerol	
Specific gravity	$1.260^{50/4}$	100%	10 cP
Melting point	17.9 °C	50%	25 cP
Boiling point	290 °C	Diffusivity in	($DL*10^5$ sq cm/s)
Solubility in 100 parts		i-Amyl alcohol	0.12
Water	Infinitely	Ethanol	0.56
Alcohol	Infinitely	Water	0.94
Ether	Insoluble		

Glycerol was first discovered by Swedish researcher, K.W. Scheele in 1779 who obtained substances with sweet taste from heated reaction of olive oil with lead oxide. In 1811, M.E. Chevrel a French chemist called the sweet liquid as glycerin. He defined fatty acids ethereous chemical formulas as well as glycerin formulas in vegetable oils and animal fats. Glycerol form the backbone of triglycerides is produced by saponification of fatty materials with alkali as a byproduct of soap-making**.** Glycerol has been widely used in food and beverages, pharmaceutical and personal care applications, surface science, botanical extracts, antifreeze, nitroglycerin, feedstock for raw chemicals and research and laboratory usage.

Food industry, in foods and beverages, glycerol serves as a solvent, sweetener and food preservation. It is also used as filler in commercially prepared low-fat foods and as a thickening agent in liqueurs. It is used to produce mono- and di-glycerides for use as emulsifiers and poly-glycerol esters for use as margarine.

Pharmaceutical and personal care applications, glycerol is found in allergen immunotherapies, cough syrups, toothpaste, mouthwashes, skin care products, shaving cream, hair care products, soaps and water-based personal lubricants. Glycerol does not feed the bacteria that form plaques and cause dental cavities. It is used as a tablet holding agent. Glycerol is also used as a laxative when introduced into the rectum. Nearly pure glycerol is an effective treatment for psoriasis, burns, bites,

cuts, rashes, bedsores, and calluses. It can be used orally to eliminate halitosis. The same property makes it very helpful with periodontal disease, due to it penetrates biofilm quickly and eliminates bacterial colonies.

Antifreeze, like ethylene glycol and propylene glycol, glycerol forms strong hydrogen bonds with water molecules, competing with water-water hydrogen bonds. This disrupts the crystal lattice formation of ice unless the temperature is significantly lowered. The minimum freezing point temperature is at about -37.8 °C corresponding to 60-70% glycerol in water. Glycerol was historically used as an anti-freeze for automotive applications before being replaced by ethylene glycol, which has a lower freezing point. While the minimum freezing point of a glycerol-water mixture is higher than an ethylene-glycol mixture. Glycerol is not toxic and is being reexamined for use in automotive applications. In the laboratory, glycerol is a common component of solvents for enzymatic reagents stored at temperatures below 0 °C due to the depression of the freezing temperature of solutions with high concentrations of glycerol. It is also used as a cryo-protectant where the glycerol is dissolved in water to reduce damage by ice crystals to laboratory organisms that are stored in frozen solutions, such as bacteria, nematodes, and mammalian embryos.

Nitroglycerin, glycerol is used to produce nitroglycerin, which is an essential ingredient of smokeless gunpowder and various explosives such as dynamite [12].

Chemical transformation is another application to convert glycerol into more valuable products, which includes selective oxidation, hydrogenolysis, dehydration, acetylation, carboxylation, decomposition, dehydroxylation, selective oligomerization, reforming towards syngas, esterification and etherification. The transformation of glycerol into fuel oxygenates by etherification and esterification reactions that draw interest of many researches since there have economically benefited to the glycerol by-product from biodiesel process.

Chemical transformations of glycerol are reported in Table 2.5.

Table 2.5 Chemical transformations of glycerol [13].

Product	Reaction	Usage
Acrolein	-Reaction glycerol/water by zeolite -Glycerol dehydration by ZSM-5 -Glycerol dehydration over silica-supported heteropoly acids -Glycerol dehydration over activated carbon-supported silicotungstic acids	Raw materials of acrylic acid, acrylic acid esters, super absorber polymers, and detergents
Butanol	Glycerol fermentation by *Clostridium pasteuriunum*	-Use as biofuel -Use as solvent for chemical and textile process, organic synthesis -Use as chemical intermediate in coating applications -Use as paint thinner -Use as hydraulic and brake fluids -Use as perfume base
Dichloropropanol (DCP)	-Glycerol with heteropoly acid -Glycerol with hydrochloric acid catalyzed by acetic acid	Chemical feedstock for organic compounds, monomers and reactants for plastics
Dihydroxyacetone	-Glycerol oxidation over carbon-supported gold catalyst	Use as tanning agent in cosmetics industries
Docosahexaenoic acid (DHA)	Crude glycerol with micro-algal culture	Omega-3 polyunsaturated fatty acid an essential nutrient
Ethanol	Glycerol fermentation by *E. coli*	-Use as fuel and fuel additive -Main constituent in alcoholic beverages -Chemical feedstock for organic compounds such as ethyl halides, ethyl ester, acetic acid, butadiene, ethyl amines, diethyl ether -Use in medical application as antiseptic
Glycerol carbonate	Glycerol with CO_2	Monomer for the synthesis of new functionalized polymers
Hydrogen	-Reforming of glycerol aqueous phase by Ni–Sn or ceria-supported metal catalysts	Production of electrical power
1,3-Propanedieol	-Glycerol fermentation by *Klepsiella Pneumoniae* -Glycerol selective dehydroxylation	Use as a monomer in the synthesis of polytrimethylene terephthalate (PTT) and polyethylene terephthalate (PET)
Propylene glycol	Glycerol hydrogenolysis	Applied to unsaturated polyester, antifreeze liquid, and additives for liquid detergent
Succinic acids	Glycerol fermentation by *Anaerobiospirillum succiniciproducens*	Use as an intermediate for chemical synthesis, the manufacture of synthetic resins and biodegradable polymers

2.2 Glycerol-based fuel additives

Glycerol is obtained as by-product of biodiesel production in approximate 10 % wt. The alternatives transformation of glycerol into oxygenated additive of diesel and biodiesel is performed by means of etherification reactions. It increases the yield to biodiesel fuel in the overall production of biodiesel. The preparation of alkyl glycerol ethers is focused on the etherification between glycerol with isobutylene. Glycerol reacts with isobutylene over heterogeneous acid catalysts to obtain a mixture of mono-tert-butyl glycerol ether (MTBG), di-tert-butyl glycerol ether (DTBG), and tri-tert-butyl glycerol ether (TTBG). DTBG and TTBG are used as additives for diesel, biodiesel and their mixtures. These ethers, when blend with diesel can reduce the emissions of particulate matters, hydrocarbons and carbon monoxide. These oxygenated compounds can improve the cold flow property of biodiesel and can reduce viscosity of biodiesel. These tert-butyl glycerol ethers can be used as anti-knock agent for gasoline, as alternative to alkylethers such as methyl tert-butyl ether (MTBE), ethyl tert-butyl ether (ETBE) and tert-amyl methyl ether (TAME). This reaction has been performed over p-toluenesulfonic for homogenous acid catalysts and over sulfonic resins for heterogeneous acid catalysts. The organosulfonic mesostructured silicas have improved catalytic performances for this etherification reaction, when compared with p-toluenesulfonic and sulfonic resins. The sulfonic resins have low surface areas and low of thermal stability. The sulfonic acid modified mesoporous silicas have high surface area with high strong Bronsted acid sites [14]. The reaction of etherification between glycerol with isobutylene (glycerol tert-butylation) is shown in Figure 2.3. The main products from glycerol tert-butylation are MTBG, DTBG and TTBG. There are 2 isomers of MTBG, i.e. 3-(tert-butoxy)propane-1,2-diol and 2-(tert-butoxy)propane-1,3-diol. The isomers of DTBG are 1,3-di-tert-butoxypropan-2-ol and 2,3-di-tert-butoxypropan-1-ol. The isomers of MTBG and DTBG depended upon the etherification position within the glycerol molecule. The final product TTBG (1,2,3-tri-tert-butoxypropane) can be obtained by using appropriate reaction condition.

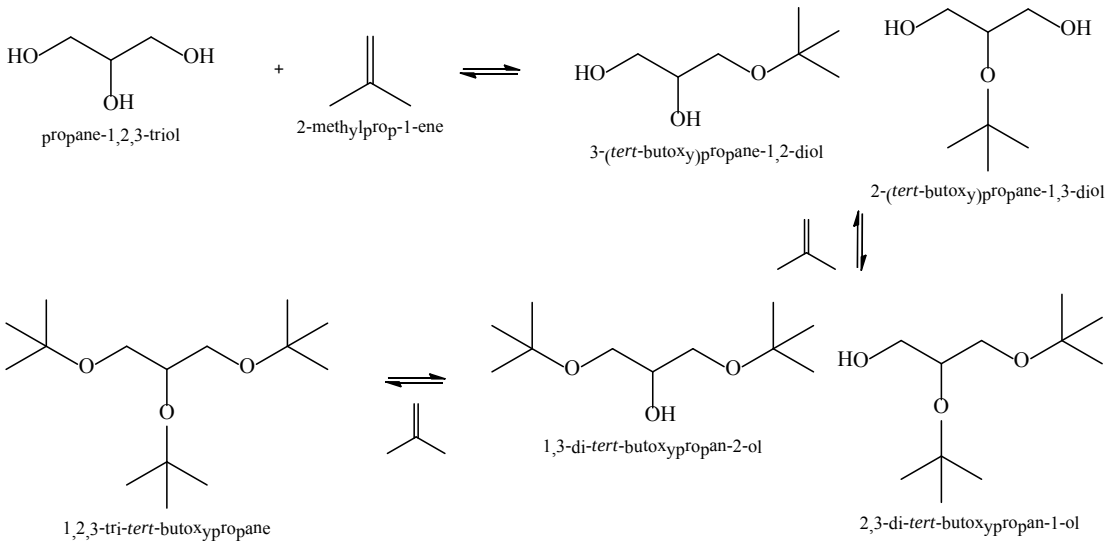

Figure 2.3 Etherification between glycerol with isobutylene [14].

2.3 Acidic catalysts

2.3.1 Ion-exchange resin

An ion-exchange resin or ion-exchange polymer is an insoluble support structure of 1-2 mm uniform mean bead size diameter. It usually has white, yellowish or brown color. The ion-exchange resin beads were produced from an organic polymer substrate. The structure of pores on the surface has been developed for easily trap and ions release. The trapping of ions takes place with simultaneous releasing of other ions, thus this process is called ion-exchange. There are different types of resin, which are produced to selectively trap one or different types of ions. The ion-exchange resins are widely used in processes for separation and purification. The example process is water purification. The ion-exchange resins were used as alternative natural zeolites. The resins are made from crosslinked polystyrene. The active groups are introduced after polymerization. The crosslink is achieved by adding 0.5-25% of divinylbenzene to styrene. Non-crosslinked polymers are low stability. Small particle size of the resin gives high surface area. The ion-exchange resins have four functional groups. There are strongly acid group, e.g. sulfonic acid, strongly basic group, e.g. trimethylammonium, weakly acid group, e.g. carboxylic acid, and weakly basic group, e.g. polyethylene amine [15].

2.3.2 Mesoporous silica

Mesoporous silica is a form of amorphous silica with appearant fine white powder. A procedure for preparation of mesoporous silica was patented in 1970. It was reproduced in 1997. Researchers in Japan synthesized mesoporous silica in 1990. It was later produced at Mobil Corporation laboratories and called Mobil Crystalline Materials or MCM-41. Six years later, mesoporous silicas with pore size 4.6 to 30 nm were produced at the University of California, Santa Barbara. The material was named Santa Barbara Amorphous material, or SBA-15. These particles have hexagonal pores. Nanoparticles of mesoporous silica are synthesized by reacting of micellar rod template with silica source. The silica nanoparticles are filled with a regular arrangement of pores. The template can be removed by washing with a solvent [16].

2.3.2.1 Aluminum-containing SBA-15 mesoporous silica

Mesoporous silica SBA-15 is synthesized and incorporated with aluminum to produce Al-SBA-15 via post-synthesis procedure by reacting SBA-15 with an aqueous solution of sodium aluminate. The amphiphilic tri-block copolymer, poly(ethylene glycol)-block-poly(propylene glycol)-block-poly(ethylene glycol) average molecular weight 5,800, is selected for the template. The silica source of SBA-15 is tetraethyl orthosilicate or TEOS. The template and silica source are crystallized and calcined to decompose the template. A white powder SBA-15 is obtained. This powder is used as the material to produce aluminum-containing SBA-15. Alumination of SBA-15 is prepared by stirring of SBA-15 in water containing sodium aluminate. The solid is filtered, washed with water, and dried in air. Then, this solid powder is calcined in air [17].

The aluminum is incorporated into siliceous SBA-15 in a range of Si/Al = 40/10. The Si/Al ratios are calculated by double integration of the electron spin resonance (ESR) spectra and are plotted against the framework Si/Al ratio based on Al MAS NMR (Al magic-angle-spinning nuclear magnetic resonance spectroscopy). Small-angle x-ray diffraction, XRD, of siliceous SBA-15 shows a well pattern with a prominent peak at 0.8°, and two weak peaks at 1.6° and 1.7° 2θ. The XRD pattern of siliceous SBA-15 is shown in Figure 2.4. The XRD peaks can be indexed to a

hexagonal lattice with a $d(100)$ spacing of 105 Å. That is correspond to a large unit cell parameter a_0 = 122 Å ($a_0 = 2d(100)/\sqrt{3}$).

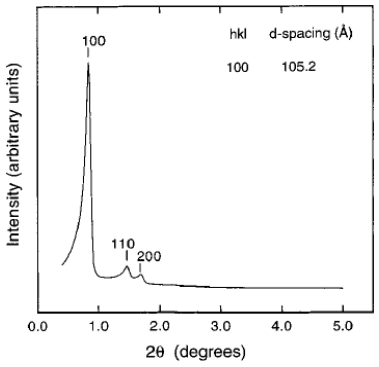

Figure 2.4 XRD pattern of SBA-15 [18].

Transmission electron microscopy (TEM) gives the image of SBA-15. The hexagonal array 60 Å diameter is visible in uniform channels. TEM images from SBA-15 show thick walls of 40 Å, as shown in Figure 2.5.

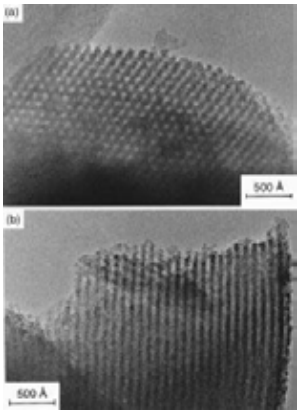

Figure 2.5 TEM images of SBA-15 (a) in the direction of the pore axis and (b) in the direction perpendicular to the pore axis [18].

N_2 adsorption isotherm for SBA-15 has an irreversible type IV with a H1 hysteresis loop. The isotherm exhibits a sharp inflection in P/P_0 range from 0.60 to 0.80 uniform pores with characteristic of capillary condensation. N_2 adsorption isotherms from Al-SBA-15 materials are similar to that from SBA-15. The inflection points of P/P_0 position is related to a mesopore diameter and the sharpness of the step indicates the mesopore size distribution. The pore size distribution can be calculated

from the Kelvin equation and is presented as a Barrett-Joyner-Halenda (BJH) plot in Figure 2.6. It shows a narrow pore size distribution with an average mesopore size of 62 Å and a high surface area, A_{BJH}, 927 m^2/g. The N_2 adsorption amounts decrease depending on the specific post-synthesis procedure and the aluminum loading [18].

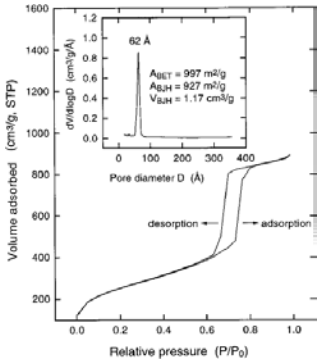

Figure 2.6 Adsorption-desorption isotherm of nitrogen on SBA-15 at 77 K the insert shows the BJH pore size distribution calculated from the desorption branch of the isotherm [18].

2.3.2.2 Organosulfonic functionalized mesoporous silica

Heterogeneous catalysts in chemical reactions are dramatically influenced by the strength of acid sites and the morphology of the support (such as surface area and pore size). Mesoporous materials containing sulfonic groups, which combine a relatively high acid strength with a large surface area and reactant accessibility, are promising for acidic catalysts. The organic functionalized mesoporous silica-based materials have been achieved by grafting of organic functional groups into the internal surface of mesoporous silica-based materials. Direct synthesis involves co-condensation of siloxane and organosiloxane species in the different templates (surfactants). The attachment of sulfonic acid groups to the silica surface increased the acidity of catalyst. The preparation of organo-sulfonic acid groups to the silica-based materials has been used direct synthesis and silylation procedures. There is an single-step procedure for direct synthesis to create periodic ordered of alkane-sulfonic functionalized mesostructures by using poly(ethylene oxide)–poly(propylene oxide)–poly-(ethylene oxide) block copolymer species (Pluronic 123) as the templating surfactant with co-condensation of siloxane (tetraethyl orthosilicate, TEOS, or

tetramethyl orthosilicate, TMOS) and organosiloxane precursors, under acidic condition. 3-Mercaptopropyltrimethoxysilane (MPTMS) and 2-(4-chlorosulfonylphenyl)-ethyltrimethoxy silane (CSPTMS) are used as organosiloxane precursors for synthesis of propyl-SO_3H SBA-15 and aryl-SO_3H SBA-15, respectively.

Propylsulfonic-acid-modified SBA-15 material synthesized by means of an in-situ oxidation procedure. This procedure involved a single-step synthesis based on the co-condensation of TEOS and MPTMS in the presence of Pluronic 123 species ($EO_{20}/PO_{70}/EO_{20}$) and H_2O_2 in HCl aqueous solutions. The in-situ oxidation of thiol groups is exchanged to the sulfonic-acid groups. This acidic catalyst has pore sizes up to 60 Å, high acid-exchange capacities (1-2 meq H^+/g SiO_2) and high surface areas up to 800 m^2/g [19].

Arenesulfonic-acid SBA-15 mesoporous silica has been functionalized by means of a single-step simple synthesis. The preparation involves co-condensation of tetraethoxysilane (TEOS) and 2-(4-chlorosulfonylphenyl)ethyltrimethoxysilane (CSPTMS) in the presence of a poly-($EO_{20}/PO_{70}/EO_{20}$) block copolymer (Pluronic 123) under acid silica-based catalysis. Hydrolysis of the chlorosulfonyl groups (-SO_2Cl) to the sulfonic-acid groups is achieved under acidic condensation conditions. The direct synthesis procedure allowed the effective anchor of arenesulfonic groups on the pore surface of SBA-15 mesoporous silica. The presence of a phenyl group close to the sulfonic group significantly increases the acid strength in acid-catalyzed reactions. The acidic material shows hexagonal mesoscopic order and pore sizes up to 60 Å, with acid exchange capacities 1.3 meq H^+/g SiO_2 and surface areas up to 600 m^2/g [20].

The organic functional groups on the pore surface of SBA-15 mesoporous silica are shown in Figure 2.7. The XRD pattern of organosulfonic functionalized SBA-15 shows the same pattern of SBA-15, which is shown in Figure 2.8. TEM images of Pr-SO_3H SBA-15 and Ar-SO_3H SBA-15 give the hexagonal array, as shown in Figure 2.9. N_2 adsorption isotherms for propylsulfonic and arenesulfonic SBA-15 materials are similar to isotherm from SBA-15. Figure 2.10 showed the nitrogen adsorption isotherm of organosulfonic-acid-modified SBA-15.

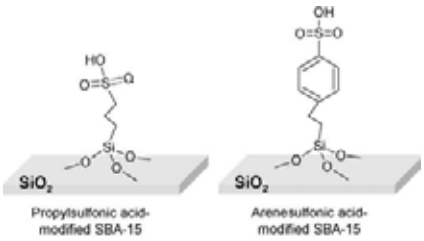

Figure 2.7 Propylsulfonic-acid and arenesulfonic-acid modified on the pore surface of SBA-15 [21].

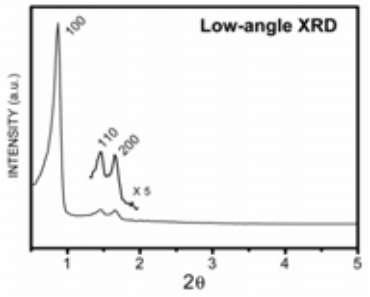

Figure 2.8 XRD pattern of organosulfonic functionalized SBA-15 [22].

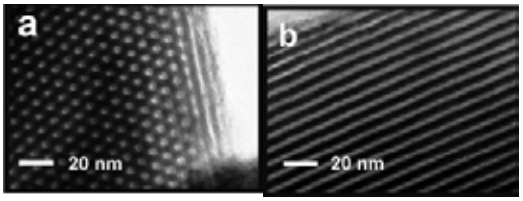

Figure 2.9 TEM images (a) in the direction of the pore axis and (b) in the direction perpendicular to the pore axis of an organosulfonic modified SBA-15 material [20].

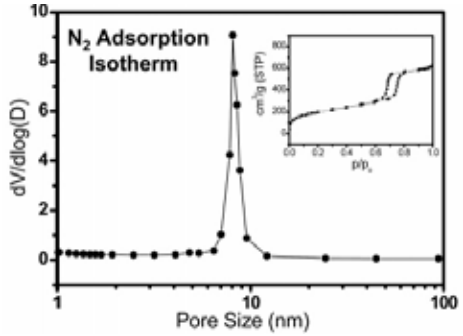

Figure 2.10 Nitrogen adsorption isotherm of organosulfonic-acid-modified SBA-15 [22].

2.3.3 Zeolite

Zeolites are the aluminosilicate, which have cations such as Na^{+}, K^{+}, Ca^{2+}, Mg^{2+} and others in microporous solids. Some of common mineral zeolites are analcime, chabazite, heulandite, natrolite, phillipsite, and stilbite. The molecular or ionic species in the pores of zeolite are controlled by the dimensions of the pores. Natural zeolites are contaminated by other minerals, metals, quartz, or other zeolites. There are several types of synthetic zeolites, which crystallized from a silica and alumina gel in the presence of alkalis and organic templates. The properties of zeolite depend on composition of mixture, pH, temperature, seeding time, reaction time and type of the template.

2.3.3.1 Zeolite beta

In 1967, zeolite beta, a large pore with high-silica zeolite was first reported. Crystal chemical data of zeolite beta is $[Na_7]$ $[Al_7Si_{57}O_{128}]$. Zeolite beta consists of an intergrowth of two distinct structures that are Polymorphs A and B. They grow as two-dimensional sheets. The sheets alternate between the two by randomly. Both polymorphs have a three-dimensional network of 12-ring pores. The intergrowth of the polymorphs does not affect two of the dimensions in the pores. The direction of the faulting, the pore becomes tortuous, but not blocked. Polymorph A, one end member, forms an enantiomorphic pair, space group symmetries $P4_122$ and $P4_322$, with a = 1.25 nm and c = 2.66 nm. Polymorph B is achiral, space group C2/c with a = 1.76 nm, b = 1.78 nm, c = 1.44 nm, β = 114.5°. Both structures are constructed from the same centrosymmetric tertiary building unit (TBU), and arranged in layers [23]. Framework and XRD powder pattern of zeolite beta are shown in Figure 2.11 and 2.12, respectively.

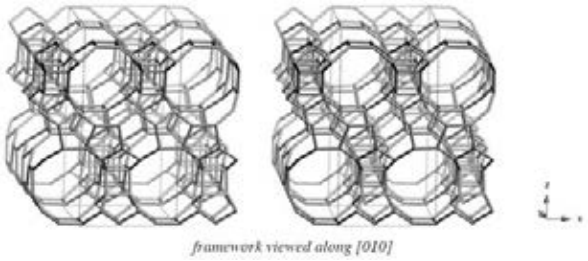

Figure 2.11 Framework of zeolite beta [24].

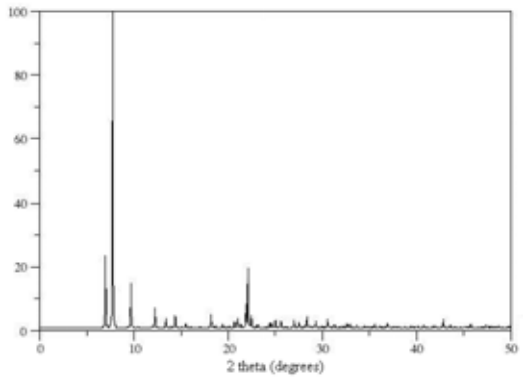

Figure 2.12 XRD powder pattern of zeolite beta [25].

2.3.3.2 Zeolite Y

Zeolite Y exhibits the faujasite (FAU) structure. Crystal chemical data of zeolite Y is $[(Ca, Mg, Na_2)_{29}\ (H_2O)_{240}]\ [Al_{58}\ Si_{134}\ O_{384}]$ [26]. A 3-dimensional structure has perpendicular pore to each other in the x, y, and z planes. The secondary building units are 4, 6, and 6-6. The pore diameter is 7.4 Å. The aperture is defined by a ring of 12 oxygens and a large cavity of diameter 12 Å. The cavity is surrounded by ten sodalite cages that connected on their hexagonal faces. The unit cell is cubic (a = 24.7 Å) with Fd-3m symmetry. Zeolite Y has Si/Al ratio of 2.43. It decomposes at 793 ºC. Zeolite Y is synthesized in a gel of alumina (sodium aluminate) and silica (sodium silicate). They are mixed in NaOH aqueous solution to give a gel. The gel is crystallized at temperature from 70-300 °C. The zeolite is present in Na^+ form and converted to acidic form. The NH_4^+ form of zeolite is converted at first for prevention of structure disintegration from acid attack [27]. Framework and XRD powder pattern of zeolite Y are shown in Figure 2.13 and 2.14, respectively.

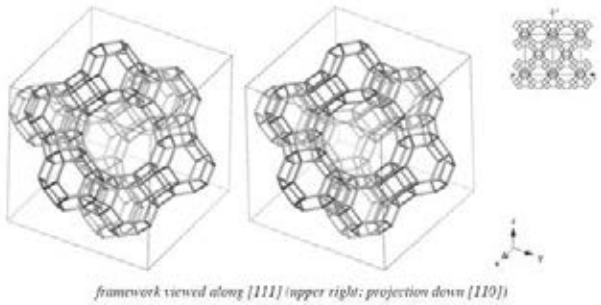

Figure 2.13 Framework of zeolite Y [28].

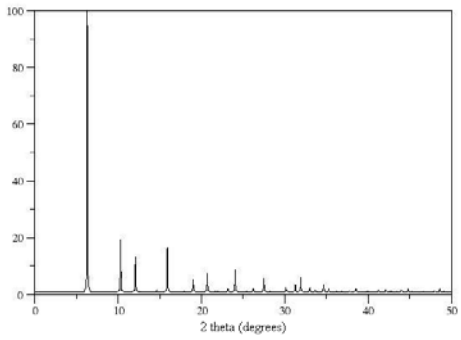

Figure 2.14 XRD powder pattern of zeolite Y [29].

2.4 Adsorption isotherms

2.4.1 BET surface area

In 1938, Stephen Brunauer, Paul Hugh Emmett, and Edward Teller published the BET theory. They described the physical adsorption of gas molecules on a solid surface. The theory is an extension of the Langmuir theory, which are monolayer to multilayer adsorptions. The hypotheses are : (a) gas molecules physically adsorb on a solid in layers infinitely, (b) there is no interaction between each adsorption layer, and (c) the Langmuir theory can be applied to each layer. The BET theory is an important analysis technique for the measurement of the specific surface area of a material. The BET equation is shown in Equation 2.1.

$1/[V((P_0/P)-1)] = [1/(V_mC)] + [(C-1)/(V_mC)][P/P_0]$ ---------- Equation 2.1 [30]

Where : P is equilibrium pressure of adsorbates.

P_0 is the saturated vapor pressure of the gas over the solid.

P/P_0 is the relative pressure.

V is adsorbed-gas quantity, in volume units.

V_m is the monolayer adsorbed-gas quantity

and C is the BET constant which is related to the net heat of adsorption.

2.4.2 t-plot method

The t-plot method is the multi-layer adsorption curve for nitrogen at different pressures and constant temperature. This curve is multi-molecular adsorption. The t-plot equation is shown in Equation 2.2.

$t = [V_a/V_m]\ [0.354\ nm]$ ---------- Equation 2.2 [31]

Where : t is adsorption layer thickness.

V_a is the amount of adsorbed-gas at an arbitrary pressure.

V_m is the monolayer adsorbed-gas quantity

0.354 is the thickness of monomolecular layer that based on N_2 molecule.

2.4.3 BJH method

In 1955, Barret, Joyner, and Halenda reported the BJH method. The BJH theory is the measurement of the specific surface area of a mesoporous material. The BJH equation is shown in Equation 2.3.

$$v_{ads}(x_k) = \Sigma_{(i = 1\ to\ k)}\Delta V_i(r_i \leq r_c(x_k)) + \Sigma_{(i = k+1\ to\ n)}\Delta S_i t_i(r_i > r_c(x_k))$$ ------ Equation 2.3 [32]

Where : $v_{ads}(x_k)$ is the volume of liquid adsorbate (cm^3/g) at relative pressure.

x_k is calculated from the value of adsorption expressed in cm^3/g STP.

V is pore volume in cm^3/g.

S is surface area (m^2/g).

t is the thickness of adsorbed layer in appropriate units.

k is the adsorbed amount at k-th point of adsorption isotherm.

$r_c(x_k)$ is current relative pressure. That 1^{st} is a volume in condensate in all pores smaller than some characteristic size depending on current relative pressure, $r_c(x_k)$. The 2^{nd} is a volume of adsorbed film on all larger pores which calculated a sum of terms Σ (pore surface and thickness of film in pore).

2.5 Literature review

Melero, et al., [14] studied acid-catalyzed etherification of glycerol and isobutylene over sulfonic mesostructured silicas. They yield DTBG and TTBG. The molar ratio of isobutylene to glycerol is 4/1 at reaction temperature 75 °C. At reaction condition, after 4 h of reaction time over arenesulfonic-acid-modified SBA-15, the conversion of glycerol and the selectivity of DTBG and TTBG reach 100% and 92%, respectively.

Klepacova, et al., [33] studied etherification of glycerol and ethylene glycol with isobutylene. The influence of catalyst (i.e. strong acid ion-exchange resins, p-toluenesulfonic acid and large-pore zeolites), solvent and temperature on the etherification of glycerol and ethylene glycol with isobutylene was studied. Reactions were carried out in the temperature range from 50 to 90 ºC in solvent (dioxane, dimethyl sulfoxide and sulfolane). The highest glycerol conversion was achieved at 88.7% over zeolite H-Y after 8 h. Reaction over H-Beta zeolite has high selectivity to di-ethers. The highest amount of di- and tri-ethers was formed over Amberlyst 35. The reaction over zeolite H-Y was low due to zeolite H-Y had low acidity. p-Toluenesulfonic acid provided high concentration of DTBG when sulfolane was used as a solvent. The ethers from etherification of glycerol and ethylene glycol by using isobutylene decreased when reaction temperature increased.

Klepacova, et al., [34] studied tert-butylation of glycerol catalysed by ion-exchange resins. The etherification of glycerol with isobutylene or tert-butyl alcohol without solvent in the liquid phase catalyzed by strong acid ion-exchange resins of Amberlyst type and by two large-pore zeolites H-Y and H-Beta was studied. The strong acid resins in dry form are very active catalysts for etherification reaction with isobutylene. The etherification of glycerol with isobutylene or tert-butyl alcohol over Amberlyst achieved 100% of glycerol conversion with 92% selectivity to di- and tri-ethers. Alkylation agent, tert-butyl alcohol, is not suitable because water from reaction deactivates the catalysts. The zeolites are not effective for this etherification reaction because these zeolites have small pore diameter.

Xiao, et al., [35] studied enhanced performance of HY zeolites by acid wash for glycerol etherification with isobutene. The etherification of glycerol with isobutene to synthesize DTBG and TTBG was studied on acid-treated HY zeolites. The glycerol etherification over a citric acid washed HY zeolite with 1 wt% catalyst loading at 70 °C after 7 h, the glycerol conversion and the selectivities to DTBG and TTBG were 85% and 58%, respectively. The zeolite crystalinity was retained although the nitric acid or citric acid was used to treat HY zeolite.

Margolese, et al., [19] studied direct syntheses of ordered SBA-15 mesoporous silica containing sulfonic acid groups. A simple procedure has been developed for the synthesis of functionalized mesoporousmaterial SBA-15 with propyl-sulfonic group.

The preparation involves the co-condensation of tetraethoxysilane and mercaptopropyltrimethoxysilane in the presence of tri-block copolymers and hydrogen peroxide under acidic conditions. The modified propyl-SO_3H-SBA-15 shows hexagonal mesoscopic order and 60 Å of pore size. The acid capacities range from 1 to 2 mequiv of H^+/g of SiO_2 with surface area 800 m^2/g. The formation of the propyl-sulfonic acid groups during co-condensation of the silica species coincides with enhanced meso-structure. The presence of Bronsted acid centers was confirmed by using ^{31}P MAS NMR measurements of chemically adsorbed triethylphosphine oxide.

Luan, et al., [18] studied the alumination and ion exchange of mesoporous SBA-15. The mesoporous silica SBA-15 has been synthesized and incorporated of postsynthesis with aluminum via three different procedures. SBA-15 reacted with $AlCl_3$ in dry ethanol, or SBA-15 reacted with aluminum iso-propoxide in dry hexane, or SBA-15 reacted with an aqueous solution of sodium aluminate. These obtained products were calcined then were characterized to evaluate the efficiency of these alumination methods and their effect on the pore structure and ion exchange capacity of SBA-15 by using transmission electron microscopy, N_2 adsorption, electron probe microanalysis, powder X-ray diffraction, ^{27}Al magic-angle-spinning NMR, and electron spin resonance spectroscopies. The aluminum is mostly incorporated into silica SBA-15. The percentage of aluminum with tetrahedral symmetry in the synthesized materials is about 100% for the first procedure, > 76% for the second procedure and > 71% for the third procedure. It indicates that alumination by aqueous sodium aluminate is the most effective. The BET specific surface areas are 85% for the first procedure, > 60% for the second procedure and > 42% for the third procedure. The alumination by $AlCl_3$ in ethanol gives the best performance in maintaining the mesoporous structure of SBA-15.

Noureddini, [36] studied the process for producing biodiesel fuel with reduced viscosity and a cloud point below 32 °F. Crude glycerol, by-product from biodiesel production, was passed through a strong cationic ion exchanger to remove anions and flashed to remove methanol. Glycerol was reacted with isobutylene in the presence of a strong acid catalyst to produce glycerol ethers. The mole ratio of isobutylene and glycerol was 3:1 to produce higher ethers, i.e. di- and tri-tertiary butyl ethers.

Reaction was operated at 80 °C, 320 psig, 4% of catalyst load with residence time of 2 h. The glycerol ethers were then added back to the fatty acid methyl ester phase to improve viscosity and cloud point of biodiesel fuel. Biodiesel from soybean had a kinematic viscosity of 5.94 cSt at 70 °F and a cloud-point of 23 °F, 0.5 cSt reduction in viscosity and 9 degree cloud-point depression when 12% of glycerol ethers was added into biodiesel.

Kesling, et al., [37] studied a low sulfur diesel which contained di-alkyl and tri-alkyl derivative of glycerol to reduce particulate matter emissions. The glycerol was etherified by reaction with isobutylene or t-butanol in order to produce a product mixture of the 1,2-di-t-alkyl ether, the 1,3-di-t-alkyl glycerol and the 1,2,3-tri-t-alkyl glycerol. This reaction used a highly cross-linked sulfonic acid resin catalyst with an isoalkene to glycerol ratio of 2:1 or higher at temperatures in the range of 55 to 75 °C. The product mixtures were comprised of 60 to 70% by weight of 1,3-di-t-alkyl glycerol, 5 to 15 wt % of 1,2-di-t-alkyl glycerol and 15 to 30 wt % of 1,2,3-tri-t-alkyl glycerol. A 5 volume % blend of this butyl glycerol mixture with diesel fuel (31% aromatic content, 400 ppm sulfur and 43 cetane number) gave cetane number at 44. These additives (glycerol ethers) had good solubility in diesel fuel hydrocarbons and were effective in reducing particulate matter emissions. The butyl glycerol mixtures in amounts from 1 to 5% in diesel were evaluated for emission reduction. The butyl glycerol mixture combined with soybean biodiesel at 20:80 ratio was also blended at the 5 to 30% level with diesel and was evaluated for emission reduction potential. Both blends result in improvements of emissions reduction. The carbon monoxide, hydrocarbons, particulate matter, aldehydes, ketones and benzene are reduced by the additive addition.

CHAPTER III
EXPERIMENTAL

3.1 Apparatus and instruments

1.	Analytical balance	Mettler Toledo, model XS205, readability to 0.1 mg
2.	Autoclave	Teflon-lined
3.	Cooling bath	Heto, model AT 110
4.	FTIR	Perkin Elmer, model Spectrum One
		Software version 5.0.1
5.	Furnace	Vulcan, model 3-550
6.	Gas chromatography	Agilent, model 7890A
		Detector type MSD, model 5975C
		Auto sampler, model G4513A
		Data analysis, ChemStation model 7890GC-Wasson
7.	Gas cylinder	Stainless steel, 300 ml, Whitey 304L-HDF4-300-T
		Outage tube
		Non-rotating stem needle valve, max 3,000 psi
		Pressure gauge, range 0-160 bar
8.	GC column	DB-624, stationary phase: 6% cyanopropylphenyl and 94% dimethyl polysiloxane, 60 m length, 0.25 mm inside diameter, 1.4 μm film thickness
9.	Hot plate with stirrer	IKA, model C-MAG HS7
10.	Micro reactor	Internal volume 4 ml, as showed in Figure 3.1
	Adapter	Stainless steel, female non-parallel thread to male parallel thread
	Cap	Stainless steel 304, 1 inch outside diameter
	Male connector	Stainless steel, tapered thread, 1 inch outside diameter
	Pipe fitting	Stainless steel, 1/4 inch street tees
		Stainless steel, 1/4 inch male non-parallel thread
		Stainless steel, 1/4 inch female non-parallel thread
	Port connector	Stainless steel, tube 6 mm outside diameter

	Pressure gauge	Stainless steel, 1 ½ inch dial size 40 mm Stainless steel, 1/4 inch male non-parallel thread range 0-160 bar
	Quick connector	Stainless steel, 1/4 inch stem tube fitting
	Valve	Stainless steel 316 Non-rotating stem needle, Pressure, max 206 bar (3,000 psi) Temperature, max 232 ^{o}C (450 ^{o}F)
11.	N_2 pressure regulator	Concoa, CGA fitting No. 580 single stage, delivery pressure range 0 to 1000 psi and cylinder pressure range 0 to 4000 psi
12.	Specific-gravity bottle	Pycnometer, capacity 10 ml
13.	Surface area analyzer	Belsorp, mini-II
14.	Thermometer	Temperature range from 0 ^{o}C to 200 ^{o}C

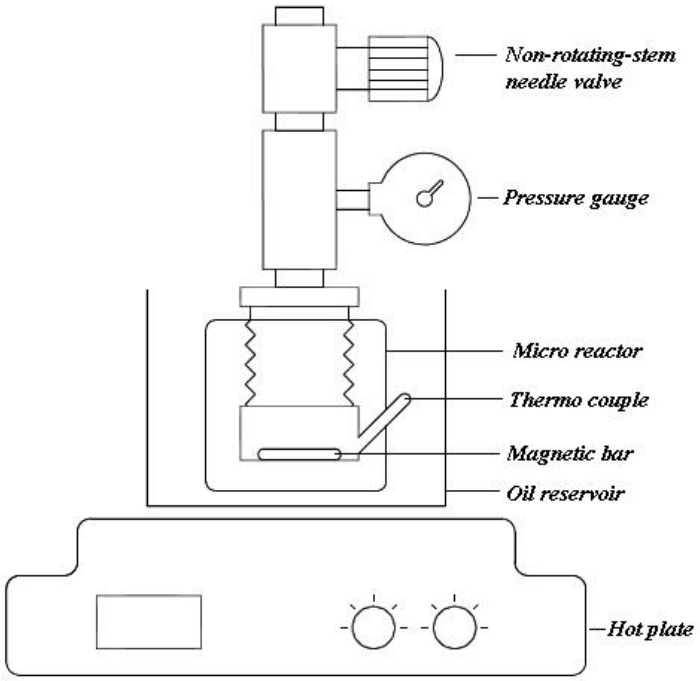

Figure 3.1 Micro reactor.

3.2 Materials

Table 3.1 Quality of materials.

Item	Material	Purity(%)	Supplied by
1	Alkenes :		
	1-Pentene	98.5	Sigma-Aldrich
	1-Hexane	99.0	Sigma-Aldrich
	1-Heptene	99.0	Fluka
	1-Octene	98.0	Sigma-Aldrich
2	Catalysts :		
2.1	Sulfonic acid functionalized styrene-divinyl benzene copolymers		
	-Amberlyst-15		Rohm and Haas
	Bead size 0.60-0.80 mm		
	Pale grey color		
	-S100		Bayer
	Mean bead size 0.58 mm		
	Brown with translucent		
	-S200		Bayer
	Mean bead size 0.60 mm		
	Dark brown with translucent		
2.2	Zeolite		
	-Zeolite beta, trade name CP814E		Zeolyst
	-Zeolite Y, trade name CBV720		Zeolyst
3	Glycerin	99.78	IRPC public co., ltd.
4	Palm biodiesel	97.62	PTTGC public co., ltd.
5	Hydrocarbon gases:		
	-Ethylene	99.95	IRPC public co., ltd.
	-Propylene	99.00	IRPC public co., ltd.
	-Butene-1	99.00	IRPC public co., ltd.
6	Silica base Tetraethoxysilane (TEOS)	95	Sigma-Aldrich
7	Organosiloxane 3-Mercaptopropyltrimethoxysilane (MPTMS)	95	Sigma-Aldrich
8	Template Poly [ethylene oxide]-poly [propylene oxide]-poly [ethylene oxide] (Pluronic 123) M_n 5,800		Sigma-Aldrich
9	HCl	37	Carlo Erba Reagenti
10	H_2O_2	50	Carlo Erba Reagenti
11	$NaAlO_2$		Sigma-Aldrich
12	Ethanol	99.8	Sigma-Aldrich
13	Liquid nitrogen	99.99	IRPC public co., ltd.
14	Silicone oil		Carlo Erba Reagenti
15	Helium gas	99.9995	Chuttrakorn special gases co.,ltd.

3.3 Catalyst preparation

3.3.1 Pr-SO_3H-SBA-15

4 g of Pluronic 123 were dissolved under stirring in 125 ml of 1.9 M HCl at room temperature. This solution was heated to 40 °C and then 7.68 g of TEOS was added. A prehydrolysis time for TEOS was done for 45 min. Then 8.05 g of MPTMS and an aqueous solution of 30% H_2O_2 were added at once into the solution. The mixture was stirred at 40 °C for 24 h and aged at 100 °C for 24 h. The solid products were recovered by filtration and air-dried overnight. Template molecules were removed by washing with ethanol under reflux for 24 h [19].

3.3.2 Al-SBA-15

The Al-SBA-15 was synthesized by using the incorporation of postsynthesis mesoporous siliceous SAB-15 with aluminum. The synthesis procedure for mesoporous siliceous SBA-15 was prepared as following procedure: 2 g of Pluronic 123 was dispersed in 15 g of water and 60 g of 2 M HCl solution while stirring and 4.25 g of TEOS was added into the homogeneous solution. This mixture was continuously stirred at 40 °C for 24 h. Finally, the mixture was crystallized in a Teflon-lined autoclave for 2 days at 100 °C. After crystallization the product was centrifuged, filtered, washed with deionized water, and dried in air at room temperature. The solid was calcined in air to decompose the triblock copolymer at 550 °C for 24 h. A white powder SBA-15 was obtained. This powder was used as the parent material to prepare aluminum-modified SBA-15, via post-synthesis route.

The Al-SBA-15 was prepared by using a post synthesis route of SBA-15 in which 0.5 g of silica SBA-15 was combined with 50 ml of distilled water containing 0.0068 g of $NaAlO_2$ with magnetic stirring for 12 h at room temperature. The obtained solid was filtered, washed with distilled water, and dried at room temperature in air. The Na^+ in post synthesis was removed by ion-exchange with 0.01M NH_4Cl [38].

3.3.3 Zeolite beta and zeolite Y

Zeolite Beta (CP 814E) and zeolite Y (CBV 720), white with odorless dried powder, were supplied by Zeolyst International. Ammonium form in both zeolites is

first converted to acidic form before use. Both zeolites were activated by drying at 500 °C for 6 h.

3.3.4 Ion-exchange resins S100 and S200

The sulfonic acid functionalized styrene-divinyl benzene copolymer, S100 and S200, were supplied by Bayer. Wet S100 with brown gel type beads of 0.58 mm uniform particle size and wet S200 with dark brown gel type beads of 0.60 mm for mean bead size, were washed with deionized water, then with 15%HCl and rinsed with deionized water. The effluent pH was measured until it became more than 4.3. The resin was dried at 110 °C for 12 h.

Amberlyst 15, a strong acid ion-exchange resin, bead size 0.60-0.80 mm, pale grey color, was supplied by Rohm and Hass.

3.4 Catalyst characterization

3.4.1 X-ray powder diffraction (XRD)

XRD patterns of Pr-SO_3H-SBA15, Al-SBA15, zeolite Beta and zeolite Y were acquired on SCINTAG PADX diffractometer using Cu-K_α radiation. The data were recorded from 0 ° to 4 ° (2θ) with a resolution of 0.02 °.

3.4.2 Nitrogen adsorption isotherms

The nitrogen adsorption and desorption isotherms of these catalysts were measured at 77K by using a Belsorp mini-II pore size distribution and surface area analyzer. The samples were dehydrated at 110 °C for 8 h. The specific surface areas, A_{BET}, for Pr-SO_3H-SBA15, Al-SBA15, Zeolite Beta, Zeolite Y and Amberlyst 15 were determined from the linear part of the BET equation at P/P_0 = 0-0.9.

Resin S100 and S200 were determined by using the t-plot method of De Boer. The specific surface area was determined using the standard BET method on the basis of adsorption data. The pore size distributions were calculated from both adsorption and desorption branches of the isotherms using the BJH method and the corrected Kelvin equation.

3.4.3 Acid capacity of catalysts

Acid capacity of heterogeneous catalysts was measured using aqueous solution of 2 M NaCl. In an experiment, 0.05 g of catalyst was added to 15 g of aqueous solution containing the sodium salt. The suspension was allowed to equilibrate and then was titrated by drop addition of 0.01 M NaOH aqueous solution.

3.5 Etherification of glycerin with olefin gases and C_5 to C_8 alkenes

The etherification of glycerin with olefin gases was performed by the following procedure. 1.26 g of glycerin and 0.12 g of catalyst were added into micro reactor. Nitrogen gas was purged for 3 times to eliminate the oxygen from the reactor. Liquefied olefin gas (1.53 g of ethylene, 2.30 g of propylene and 3.06 g of 1-butene) was added into the reactor. The starting pressure of reaction was fixed at 20 bar due to vapor pressure limitation of ethylene gas and liquefied propylene. The pressure of liquefied 1-butene was 8 bar. The reaction pressure of 1-butene etherification was adjusted to 20 bar by using nitrogen gas. The reaction temperature on alkylation was regulated by using temperature adjustment from 90 °C and 100 °C. The stirring frequency in the reaction was controlled at 1,000 rpm. The reaction temperature was restricted at 100 °C due to the maximum operating temperature of sulfonic acid functionalized resins, S100 and S200, which was 120 ^{0}C. The reaction time was started from 8 h and increased every 8 h.

The etherification of glycerin with alkene was performed by the following procedure. 1.26 g of glycerin and 0.12 g of catalyst were added into micro reactor. Nitrogen gas was purged for 3 times to eliminate the oxygen from the reactor. The alkene (3.83 g of 1-pentene, 4.60 g of 1-hexene, 5.37 g of 1-heptene and 6.13 g of 1-octene) was added into the reactor. The reaction pressure of alkene etherification was adjusted to 20 bar by using nitrogen gas. The reaction temperature on alkylation was regulated by using temperature adjustment from 90 °C and 100 °C. The stirring frequency in the reaction was controlled at 1,000 rpm. The reaction time was started from 8 h and increased every 8 h.

The reaction performance was monitored by using glycerin conversion from GCMS results.

3.6 Characterization of glycerin and alkyl alycerol ethers by FTIR

Functional group characterization of etherification products was identified by using FTIR. The IR spectrum of standard glycerin is shown in Figure 3.2.

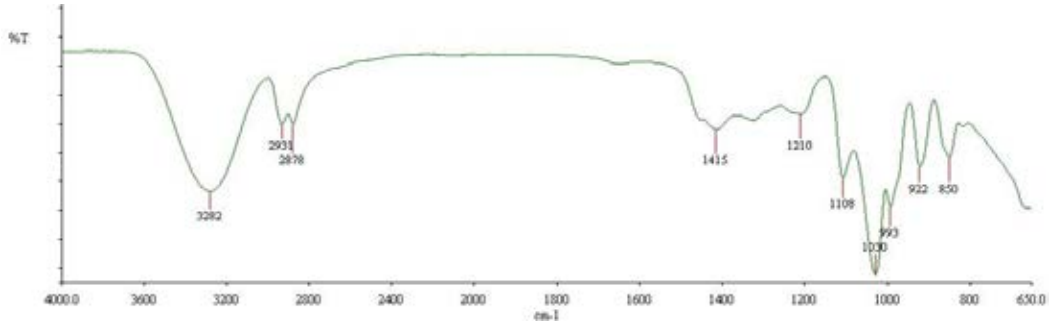

Figure 3.2 FTIR spectrum of standard glycerin.

3.7 Characterization of glycerin and alkyl glycerol ethers by GCMS

The quantitative determination of the glycerin and alkyl glycerol ethers was characterized by gas chromatography. The column temperature was increased at temperature program rate until the sample was completely eluted from the column. The eluted components were detected by a mass spectrometric detector and recorded on computer system. The peak area could be measured by data analysis software. The individual structure was identified by mass spectrometric software. The percentage of each hydrocarbon was calculated by mormalized area of the GCMS peaks.

3.7.1 Operating condition of GC

1. Carrier gas — Helium
2. Make up flow — 25 ml/min
3. Spit ratio — 50 : 1
4. Back pressure — 1.2 psi
5. Column temperature — Initial temperature 45 ^{o}C holding time 5 min, temperature program rate 20 ^{o}C / min, final temperature 220 ^{o}C with holding time 10 min
6. Injector temperature — 240 ^{o}C
7. Detector temperature — 240 ^{o}C

8.	Sample preparation	The products from etherification reaction were prepared before introduction into GCMS by diluting 0.5 g of product with methanol to 10 ml [39].
9.	Injection volume	1.0 μl
10.	Calculation	Area normalization

3.7.2 Operating condition of MSD

1.	Temperature	230 ^{o}C
2.	Mass range	10 to 800 amu (atomic mass unit)
3.	Threshold	150
4.	Detector off	3.75 min
5.	Detector on	4.35 min

Mass spectrum of standard glycerin is shown in Figure 3.3.

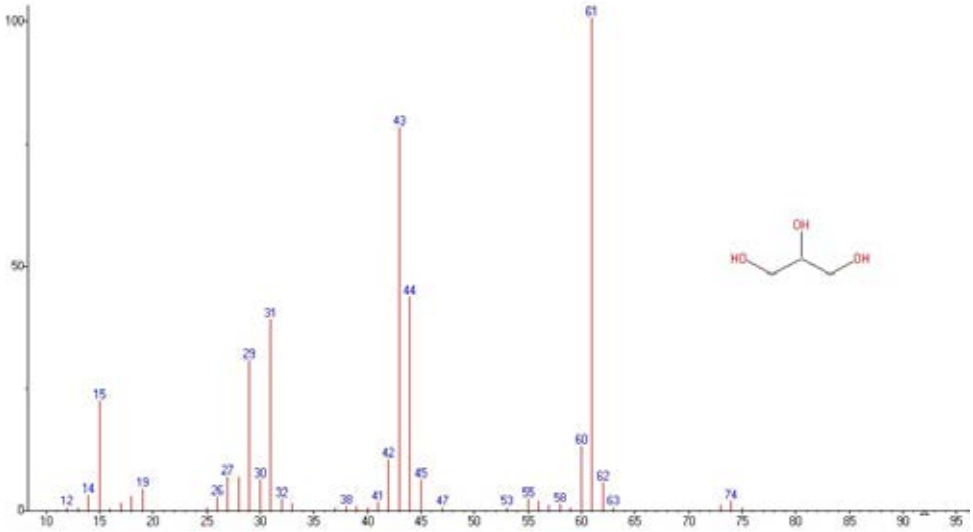

Figure 3.3 Mass spectrum of standard glycerin.

3.8 Pour point procedure

Pour points of mixed PGE and TPGE in blended palm biodiesels were determined by following ASTM D97. The pour point is defined as the temperature at which the fuel can no longer be poured due to gel formation. The temperature at least 9 ^{o}C above the expected pour point was observed of the sample when immersed into an -18 ^{o}C cooling bath. The sample was transferred to -33 ^{o}C cooling bath when it

was not ceased to flow in -18 ^{o}C cooling bath after held the sample in a horizontal position for 5 seconds. The temperature was read for every 3 ^{o}C decrease until it totally ceased to flow, when the sample was held for 5 seconds in horizontal position [10].

3.9 Cloud point procedure

Cloud points of mixed PGE and TPGE in blended palm biodiesels were performed by following procedure of ASTM D2500. The cloud point is defined as the temperature at which a cloud of wax crystal first appears in a liquid when it is cooled under controlled conditions during a standard test. The cooling procedure was performed as same described in ASTM D97. The sample was examined at intervals of 1 ^{o}C until the smallest observable cluster occurred. The cloud point was reported to the nearest 1 ^{o}C [8].

3.10 Cetane index procedure

ASTM D976, the calculated cetane index represents a means for estimating the ASTM cetane number of distillate fuels from API gravity and middle-boiling point. The calculated cetane index is computed from the formula. The calculated cetane index is used for cetane number estimation where a test engine is not available for determination. The approximating cetane number is convenience when the quantity of fuel is not enough for an engine rating. The index is also useful as a cetane number initial check before the cetane number of a fuel will be performed for exact value [40].

The calculated cetane index (CI) is determined from the following equation:

$$CI = -420.34 + 0.016\,G^2 + 0.192\,G \log M + 65.01\,(\log M)^2 - 0.0001809\,M^2 \quad \text{Equation 3.1}$$

$$CI = 454.74 - 1641.416\,D + 774.74\,D^2 - 0.554\,B + 97.803\,(\log B)^2 \quad \text{Equation 3.2}$$

Where : G is API gravity, determined by test method D1298,

M is middle-boiling temperature, °F, determined by test method D86,

D is density at 15 °C, g/ml, determined by test method D1298, and

B is middle-boiling temperature, °C, determined by test method D86

Cetane indices of diesel and palm biodiesel with 10% of oxygenated-compound additives were measured by following this procedure.

3.11 Density, relative density, or API gravity procedure

ASTM D1298, determination of density, specific gravity and API gravity, the sample is introduced to a specified temperature and a test portion is transferred to a hydrometer cylinder that has the same temperature. The hydrometer, also at a similar specified temperature, is lowered into the test portion and allowed to settle. The hydrometer scale is read and the temperature of the test portion is taken after equilibrium temperature is reached. The hydrometer cylinder is placed in a constant temperature bath to avoid excessive temperature variation during the test. Apply any hydrometer correction to the observed reading and record the corrected hydrometer scale reading to the nearest 0.1 kg/m^3 in density, 0.0001 g/ml, kg/l or relative density, or 0.1 °API [41]. Convert the corrected hydrometer scale reading to density, relative density or API gravity using the appropriate parts of the Petroleum Measurement Tables in Guide D1250 according to the nature of the materials under test [42]. Densities of diesel and palm biodiesel in 10% of oxygenated-compound additives for calculated cetane index were determined by following ASTM D1298.

3.12 Distillation of petroleum products procedure

ASTM D86, distillation of petroleum products, based on its composition, vapor pressure, expected initial boiling point (IBP) or expected final boiling point (FBP), or combination. The sample is placed in one of five groups. Apparatus arrangement, condenser temperature, and other operational variables are defined by the group in which the sample falls. A 100 ml of the sample is distilled under conditions for the group of the sample. The distillation is performed unit at ambient pressure under conditions that are designed to provide approximately one theoretical plate fractionation. Observations of temperature readings and volumes of condensate are made, depending on the needs of the user of the data. The volume of the residue and the losses are also recorded. At the conclusion of the distillation, the observed vapor temperatures can be corrected for barometric pressure and the data are examined for conformance to procedural requirements, such as distillation rates.

The test is repeated if any specified condition has not been met. Test results are commonly expressed as percent evaporated or percent recovered versus corresponding temperature, either in a table or graphically, as a plot of the distillation curve [43]. Distillations of diesel and palm biodiesel by adding 10% of oxygenated-compound additives for calculated cetane index were performed by following ASTM D1298.

3.13 Octane number procedure

The standard test methods for research octane number (RON) and motor octane number (MON) of spark ignition engine fuel are ASTM D2699 [44] and ASTM D2700 [45], respectively. The fuel was tested using a single cylinder, four-stroke cycle, variable compression ratio and carbureted engine. Engine speed was adjusted at 600 ± 6 rpm for ASTM D2699 or at 900 ± 9 rpm for ASTM D2700. The fuel knock intensity was compared to primary reference fuel. The primary reference fuels, for knock testing, volumetrically-proportioned-mixtures of isooctane with n-heptane defined the octane number scale. Isooctane and n-heptane were assigned as octane number 100 and 0, respectively. The octane number of the primary reference fuel that matched the knock intensity of the mixed PGE and TPGE in gasoline established the RON and MON.

CHAPTER IV
RESULTS & DISCUSSION

4.1 Characteristics of catalysts

The textural properties of the acidic catalysts in this work are summarized in Table 4.1. The increasing in acid strength, ion-exchange resins > mesostructured silicas > zeolites, was reported in the table. The results of the catalyst's acidity showed that the Amberlyst-15 gave the highest acidity among the strong acid ion-exchange resins. The Pr-SO_3H-SBA-15 exhibited the moderate acid strength. But Al-SBA-15 had the lowest acidity value in this research. The BET surface area (A_{BET}), pore volume and pore size of catalysts in this research were calculated from nitrogen adsorption-desorption experiment that are shown in Table 4.1. The BET surface area was found to be zeolites > mesostructured silicas > ion-exchange resins. Both micro pore zeolites, Z-Beta and Z-Y, exhibited high surface area as 571 and 791 m^2/g, respectively. The pore volume and pore size of Pr-SO_3H-SBA-15, Al-SBA-15, Z-Beta, Z-Y and Amberlyst-15 were obtained from the BET method. The pore volume and pore size of resin S100 and S200 were observed from the t-plot method. The t-plot was determined for non-porous material. The results of the pore volume and pore size increased in the order: mesostructured silicas > micro-pore zeolites > ion-exchange resins. The Pr-SO_3H-SBA-15 gave the largest pore volume. The Amberlyst-15 showed the highest pore size.

As seen in the Table 4.1, strong acid ion-exchange resin Amberlyst-15 had the highest acidity and pore size with quite low surface area. The mesostructured silicas, Al-SBA-15 and Pr-SBA-15, had rather high pore size, moderate surface area but weak acidity. The sulfonic acid functionalized styrene-divinyl benzene copolymers, S100 and S200, had strong acidity with lowest surface area non porous material. The micro pore zeolites, Z-Beta and Z-Y, had the highest surface area, weak acidity with moderate pore size.

Table 4.1 Properties of catalysts.

Catalyst	Acidity (mmol/g)	A_{BET} (m^2/g)	Pore vol. (cm^3/g)	Pore size (nm)
Al-SBA-15	0.12	426	0.759	7.13
Pr-SO_3H-SBA-15	1.34	429	0.767	7.19
Amberlyst-15	3.70	40	0.075	7.45
Resin S100	3.00	2	0.001	2.01
Resin S200	3.53	2	0.001	2.01
Zeolite beta	0.45	571	0.487	3.41
Zeolite Y	0.34	791	0.486	2.41

The properties of catalysts in this research were compared with reference catalysts as follows. The surface area of Al-SBA-15 (426 m^2/g) was corresponded to the surface area of reference Al-SBA-15 (428 m^2/g) [18]. Reference Pr-SO_3H-SBA-15 had acidity 1.21 mmol/g and A_{BET} 666 m^2/g [14]. The synthesized Pr-SO_3H-SBA-15 gave the same acidity but low surface area when compared with reference Pr-SO_3H-SBA-15. Amberlyst-15 in this research had acidity and A_{BET} lower than reference Amberlyst-15. Reference Amberlyst-15 showed acidity 4.7 mmol/g with A_{BET} 53 m^2/g [34]. Reference zeolite beta gave acidity and A_{BET} higher than zeolite beta in this research. Reference zeolite beta had acidity 1.03 mmol/g, A_{BET} 681 m^2/g [34]. Reference zeolite Y showed acidity 0.56 mmol/g and A_{BET} 697 m^2/g [34]. Zeolite Y in this research gave low acidity but high surface area when compared with reference zeolite Y.

4.1.1 X-ray powder diffraction (XRD)

Figures 4.1, 4.2, 4.3 and 4.4 showed XRD patterns of Pr-SO_3H-SBA15, Al-SBA15, Zeolite Beta and Zeolite Y, respectively. Pr-SO_3H-SBA-15 and Al-SBA-15 showed (100) reflection with a prominent peak at 0.9° 2θ, (110) and (200) reflections with two low peaks at 1.5° and 1.8° 2θ, respectively. These patterns related to the pattern of SBA-15, which revealed the formation of hexagonal arrangement of channels with mesoporous structures [17].

XRD pattern of Zeolite Beta in Figure 4.3 showed two peaks at 7.0° and 22.0° 2θ. Figure 4.4 showed XRD pattern of Zeolite Y with a prominent peak at 6.0° 2θ. The XRD powder patterns of Zeolite Beta and Zeolite Y were corresponded to the XRD powder patterns in the Structure Commission of the International Zeolite Association (IZA-SC).

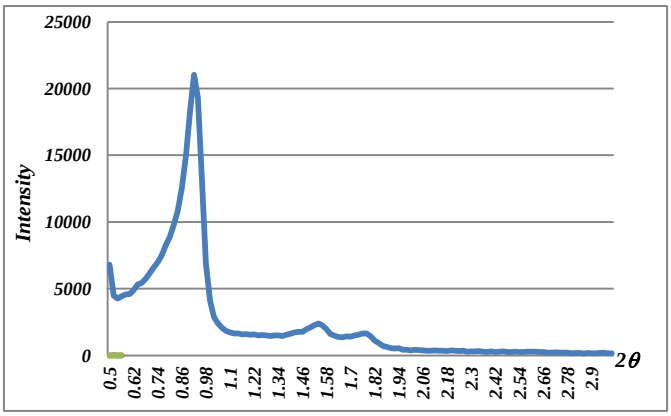

Figure 4.1 XRD pattern of Pr-SO_3H-SBA-15.

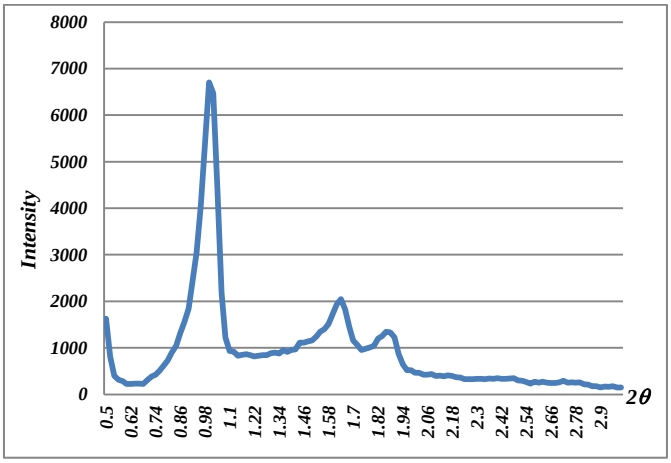

Figure 4.2 XRD pattern of Al-SBA-15.

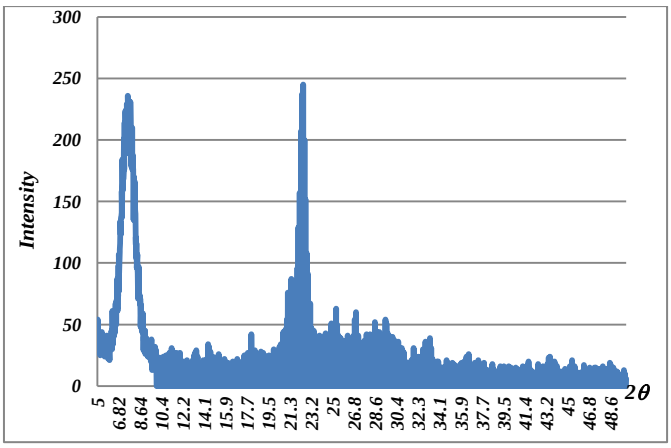

Figure 4.3 XRD pattern of zeolite beta.

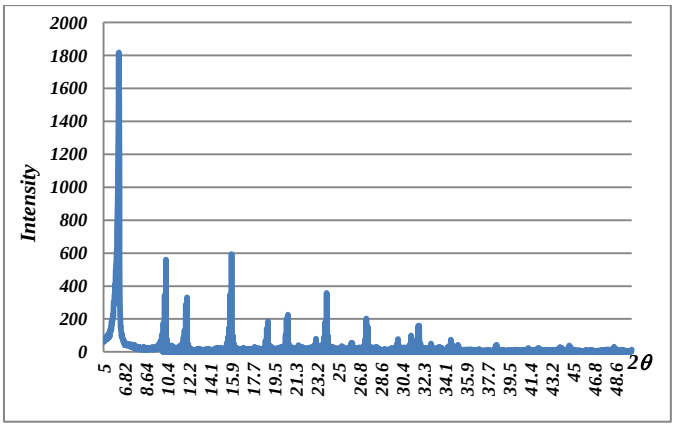

Figure 4.4 XRD pattern of zeolite Y.

4.1.2 Nitrogen adsorption

The BJH plot in Figure 4.5 evidenced that Amberlyst-15 was non porous material. It related to the reversible type II isotherm. The beginning is multilayer adsorption. The almost linear middle section of the isotherm is indicated the complete monolayer coverage [46]. Figure 4.6 indicated that ion-exchange resins S100 and S200 were non porous materials. It was similar to the reversible type III isotherm. The physisorption isotherm was convex to the p/p_0 axis over its entire range [46]. Zeolite-Beta and Zeolite-Y contained micro pores. It related to the reversible type I isotherm. Type I isotherm is concave to the p/p_0 axis [46]. Al-SBA-15 and Pr-SO_3H-SBA-15 materials showed mesoporous structure. It was similar to the irreversible type IV adsorption isotherm. Characteristic feature of the type IV isotherm is H1 hysteresis loop, which is associated with capillary condensation [46].

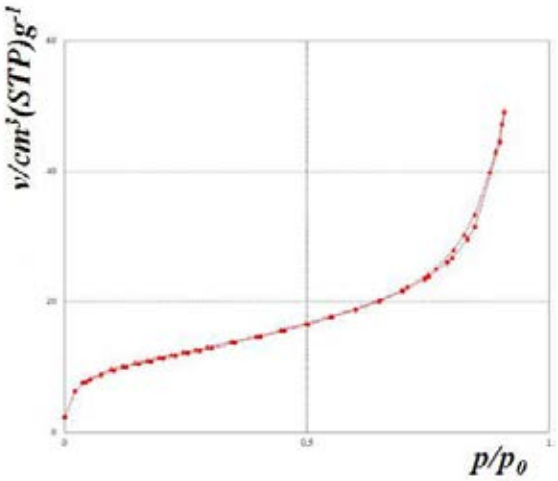

Figure 4.5 BJH plot of Amberlyst-15.

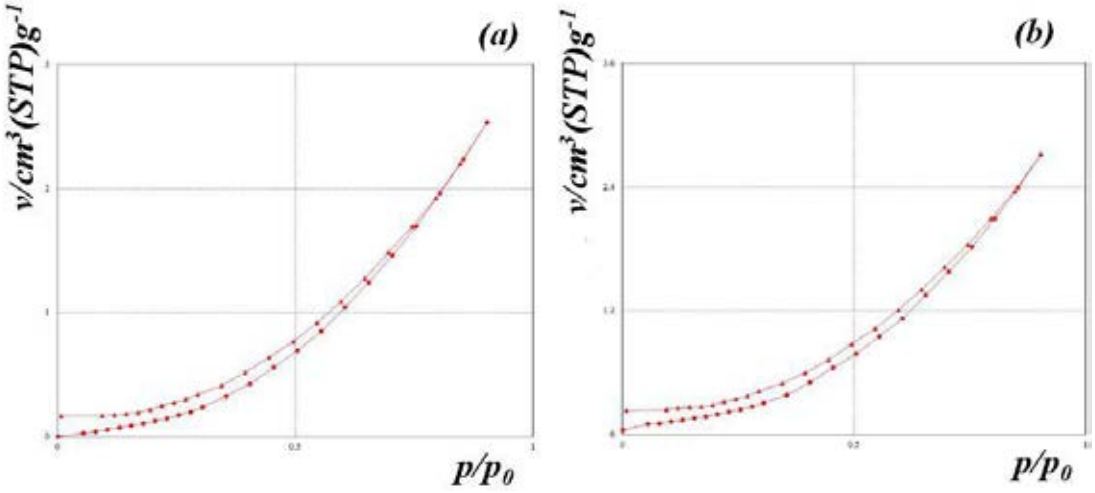

Figure 4.6 BJH plot of resins (a) S100 and (b) S200.

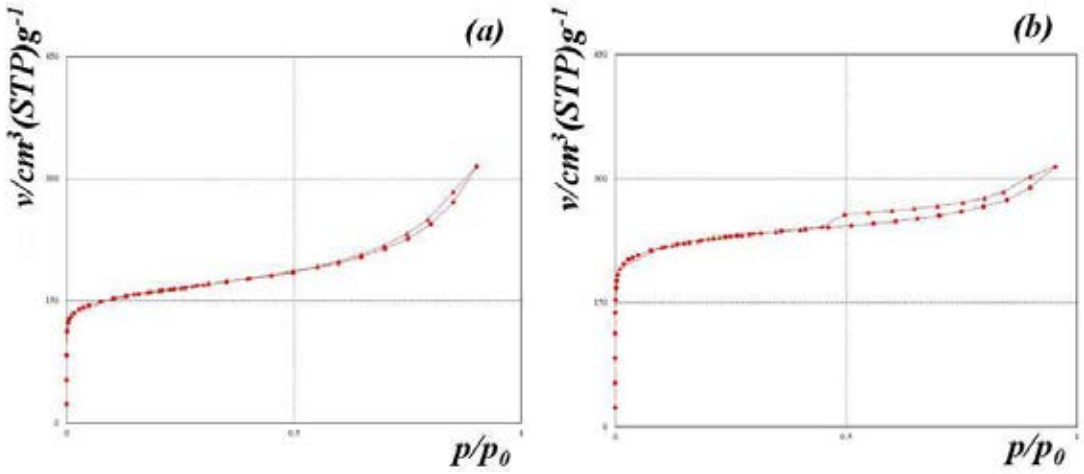

Figure 4.7 BJH plot of zeolites (a) zeolite beta and (b) zeolite Y.

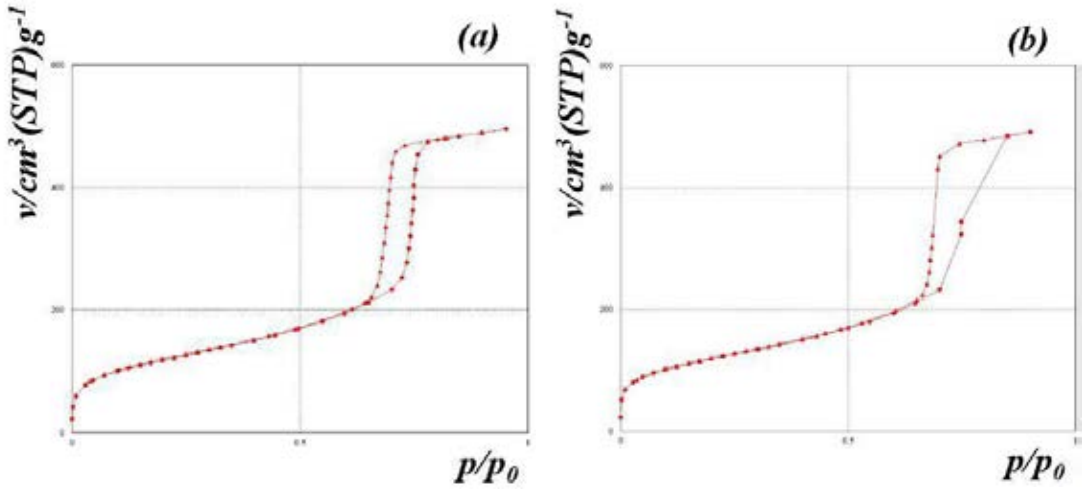

Figure 4.8 BJH plot of mesopores (a) Pr-SO_3H-SBA-15 and (b) Al-SBA-15.

4.2 Performance of catalysts

4.2.1 Etherification of glycerin with olefin gases and C_5 to C_8 alkenes

Figure 4.9 shows the glycerin conversion in the reaction of glycerin etherification with alkenes over acidic catalysts at temperature 90 °C within 8 h of reaction time. The result showed that only propylene gave 6.21% of glycerin conversion over Amberlyst-15. There were no response with other olefins and alkenes over all of acidic catalysts. Therefore, the adjustment in reaction temperature was increased within 8 h reaction time for monitoring the glycerin conversion. The result is shown in Figure 4.10 that glycerin conversion of propylene alkylation rose up

rapidly to 59.54% of at temperature 100 °C within 8 h reaction time. In the same manner, the butylation of glycerin over Amberlyst-15 had 24.76% conversion. These reaction conditions established that propylation of glycerin over Amberlyst-15 showed the best performance of etherification reaction when compared with other olefin gases and C_5 to C_8 alkenes over all of acidic catalysts. The enhancement of the etherification response was carried out by increasing the reaction time continuously in every 8 h from 16 to 72 h and maintained the reaction temperature at 100 °C.

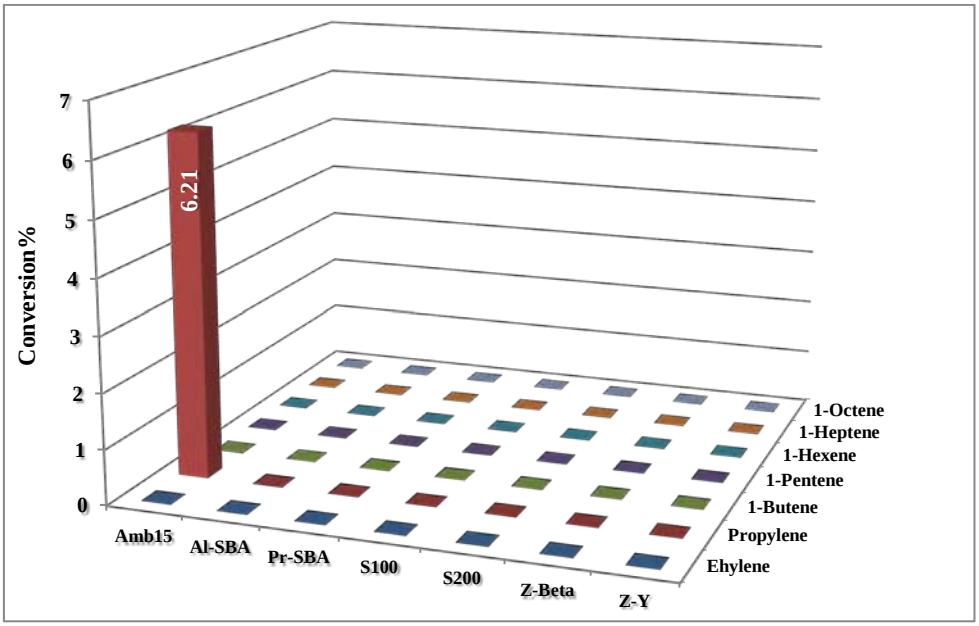

Figure 4.9 Glycerin conversion of etherification between glycerin and alkenes on acidic catalysts, glycerin/alkene = 1/4, catalyst/glycerin = 10 wt %, temperature 90 °C, reaction time 8 h.

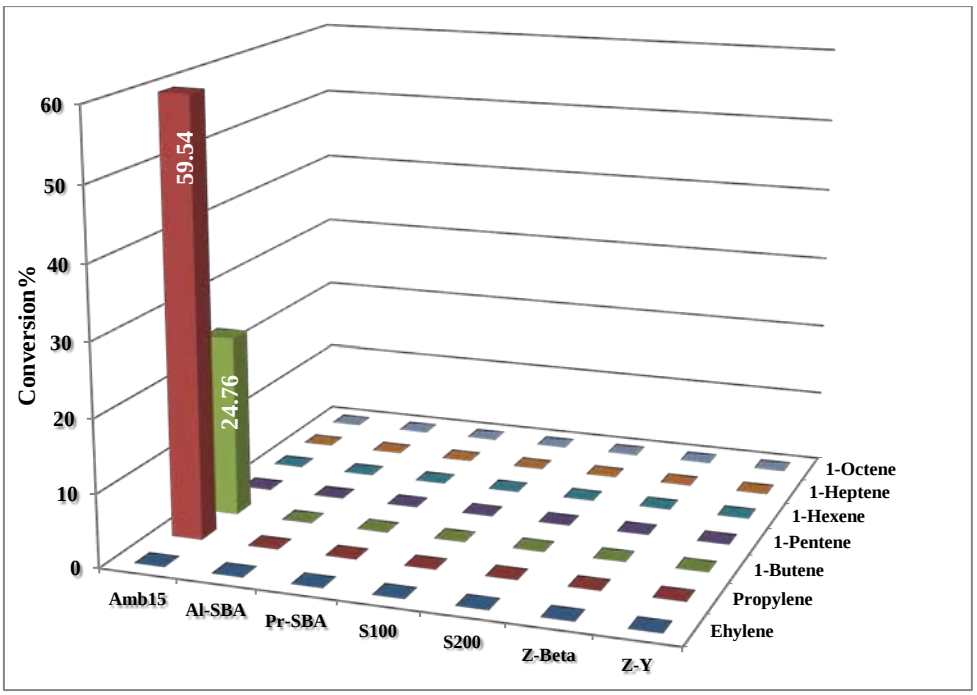

Figure 4.10 Glycerin conversion of etherification between glycerin and alkenes on acidic catalysts, glycerin/alkene = 1/4, catalyst/glycerin = 10 wt %, temperature 100 °C, reaction time 8 h.

4.2.2 Etherification of glycerin with propylene

It was found in Table 4.2 that the etherification of propylene over Amberlyst-15 at 100 °C glycerin conversion was 100% after 24 h of reaction time. At the same operating condition as Amberlyst-15, ion exchange resins S100 and S200 gave low catalyst activity than Amberlyst-15. It was evidenced that after 72 h reaction time resins S100 and S200 did not reach complete conversion of glycerin. The mesostructured silicas, Al-SBA-15 and Pr-SO_3H-SBA-15, and micro pore zeolites, Z-Beta and Z-Y, showed no reaction response on propylation of glycerin.

It could be noted that glycerin etherification with propylene, the hydroxyl group of glycerin molecule was protonated in the presence of acidic condition which mad glycerin molecule to be electron acceptor. In this experiment, the best electron donor group was propylene. Conversely, ethylene and C_5 to C_8 alkenes showed no reaction response. In addition, the catalyst properties such as acidity and pore size indicated influence on performance of the reaction. The results indicated that strong acidity (3.70 mmol/g) and mesopore size (7.7 nm) of Amberlyst-15 gave the highest

activity in propylation of glycerin. The resins S100 and S200 with strong acidity (3.00 and 3.53 mmol/g, respectively) but non porous type, had low response in propylation of glycerin.

Table 4.2 Glycerin conversion (%) of etherification between glycerin and propylene on acidic catalysts, glycerin/propylene = 1/4, catalyst/glycerin = 10 wt%, temperature 100 °C.

Time (h)	Amb-15	Al-SBA	Pr-SBA	S100	S200	Z-Beta	Z-Y
16	77.06	0	0	5.77	17.53	0	0
24	100	0	0	17.36	21.74	0	0
32	100	0	0	41.68	50.52	0	0
40	100	0	0	42.14	56.27	0	0
48	100	0	0	57.11	58.43	0	0
56	100	0	0	57.54	60.82	0	0
64	100	0	0	58.95	69.92	0	0
72	100	0	0	69.92	72.43	0	0

4.2.3 Etherification of glycerin with 1-butene

1-Butene was used in the reaction under the same operating condition as propylene in alkylation reaction. Table 4.3 showed the butylation results between 1-butene and glycerin over acidic catalysts at 100 °C under reaction time from 16 to 72 h. The Amberlyst-15 gave reaction performance of 1-butene alkylation better than resin S200. The 100% conversion was obtained after 64 h over Amberlyst-15 and reached only 38.99% conversion after 72 h over resin S200. The acid resin S100, mesostructured silicas Al-SBA-15 and Pr-SO_3H-SBA-15, and micropore zeolites Z-Beta and Z-Y, showed no reaction response on butylation between 1-butene and glycerin.

It was evidenced that the 1-butene alkylation had performance lower than propylene alkylation. Propylene was activated by high acidity and porosity of Amberlyst-15 better than 1-butene. It meaned that 1-butene gave lower activity for electron donor group than propylene in this reaction condition. The butylation of glycerin over S100 resin was not activated because this resin had no pore and low acidity, when compared with S200 resin. S200 resin, high acidity with no pore, gave low glycerin conversion. It could be noted that high acidity and porosity of catalyst were necessary for butylation of glycerin.

Table 4.3 Glycerin conversion (%) of etherification between glycerin and 1-butene on acidic catalysts, glycerin/1-butene = 1/4, catalyst/glycerin = 10 wt%, temperature 100 °C.

Time (h)	Amb-15	Al-SBA	Pr-SBA	S100	S200	Z-Beta	Z-Y
16	46.87	0	0	0	9.62	0	0
24	58.83	0	0	0	15.57	0	0
32	71.51	0	0	0	18.78	0	0
40	78.71	0	0	0	21.58	0	0
48	80.45	0	0	0	22.72	0	0
56	85.21	0	0	0	24.32	0	0
64	100	0	0	0	25.57	0	0
72	100	0	0	0	38.99	0	0

The results from glycerin etherification with olefin gases and alkenes over acidic heterogeneous catalysts at temperature 100 °C indicated that the strong acid ion-exchange resin Amberlyst-15 had highest activity on propylene and 1-butene.

4.3 Characterization of etherification products by using FTIR

In order to determine the functional group of etherification products, the identification of FTIR results must be used. The characterization by using FTIR, the products from the etherification of glycerin with propylene over strong acid ion-exchange resin Amberlyst-15 at 100 °C after reaction time 24 and 48 h were used. The products from the etherification of glycerin with butene-1 over Amberlyst-15 at 100 °C after reaction time 72 h were used for FTIR determination.

The IR spectrum of tri-propyl glycerol ether (1,2,3-tri-isopropoxypropane) is shown in Figure 4.11. This spectrum showed CH aliphatic functional group at wave number 2971 cm^{-1}. It was evidenced that CH_2 group in the aliphatic structure because a peak at 1467 cm^{-1} was also detected. The peak at wave number 1368 cm^{-1} showed isopropyl group [$-CH(CH_3)_2$] in the chemical structure due to two bands in this peak. The peak area of isopropyl group was higher than the peak area of CH_2 group, it means that tri-isopropyl groups were expected in structure of this product. The wave number at 1125 cm^{-1} in the spectrum indicated C-O group. It appeared that there had no OH group in this product structure due to the absence of wave number 3500 to 3250. It cloud be expected that the FTIR result from the etherification of glycerin with

propylene over Amberlyst-15 at 100 °C after 48 h reaction time, consisted of tri-isopropyl ether in the glycerin backbone.

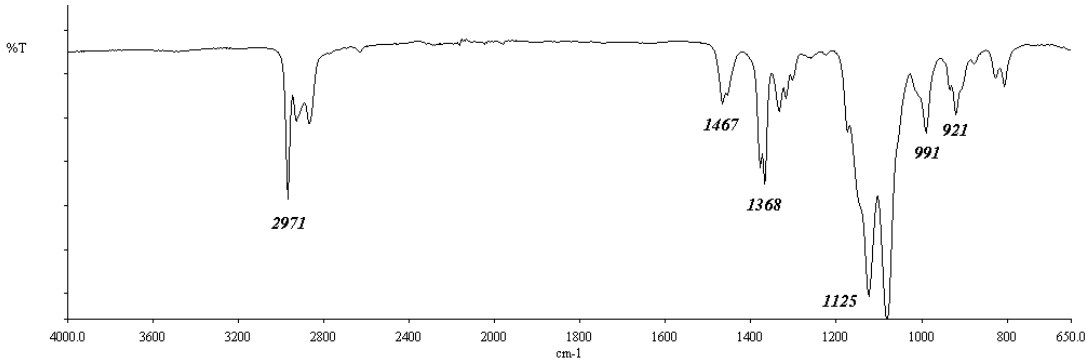

Figure 4.11 FTIR spectrum of tri-propyl glycerol ether.

Figure 4.12 shows the FTIR spectrum of propyl glycerol ethers. This spectrum gave the similar pattern to spectrum of tri-isopropyl ether. It indicated functional groups of CH aliphatic, CH_2 with CH_3 of isopropyl group, and C-O group. It was evidenced that there was mono-propyl glycerol ether or di-propyl glycerol ether or their mixture in the product from the etherification of glycerin with propylene over Amberlyst-15 at 100 °C after 24 h reaction time.

Figure 4.13 shows the FTIR spectrum of product from butylation of glycerin. The spectrum showed OH functional group at 3386 cm^{-1}. The CH aliphatic group was detected at 2967 cm^{-1}. The CH_2 and CH_3 groups in this aliphatic structure appeared at 1463 and 1374 cm^{-1}, respectively. A peak at 1083 cm^{-1} was determined to be C-O group. It was observed that mono- or di-butyl glycerol ethers were major compositions in glycerin etherification product, due to the presence of OH group did not appear in the structure.

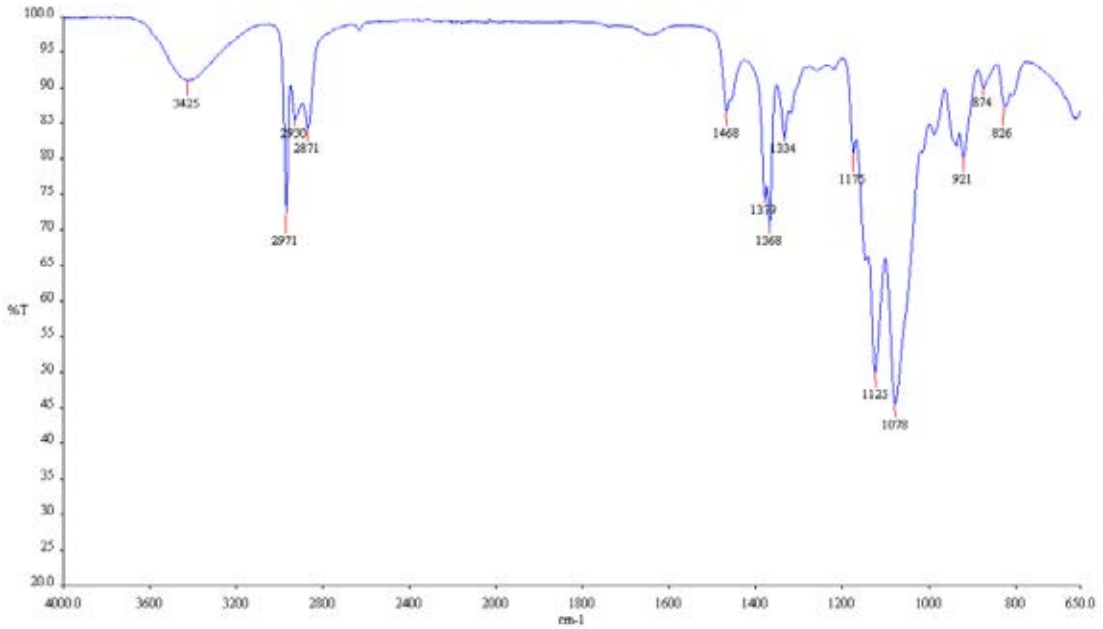

Figure 4.12 FTIR spectrum of propyl glycerol ethers.

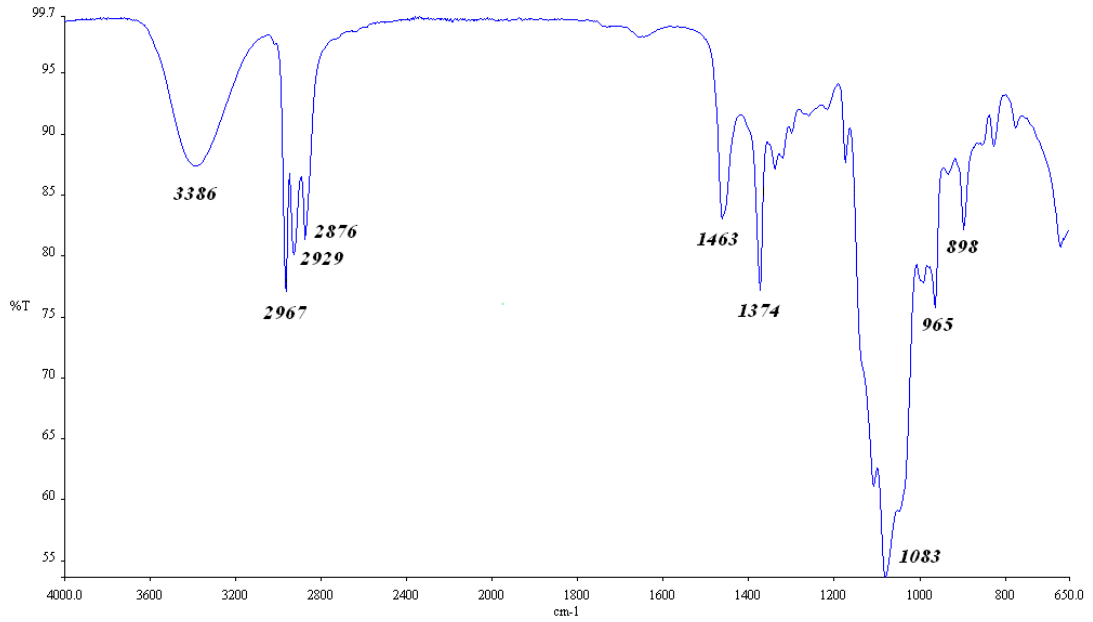

Figure 4.13 FTIR spectrum of butyl glycerol ethers.

4.4 Characterization of etherification products by using GCMS

The samples from the etherification of glycerin with propylene and butene-1 over resin Amberlyst-15 at 100 °C after 24 h reaction time were characterized by using GCMS. Three peaks in chromatogram of propyl glycerol ethers were acquired in mass spectrum by using enhanced data analysis program. Figure 4.14 A shows mass spectrum of 1-mono propyl glycerol ether (3-isopropoxypropane-1,2-diol) with molecular weight 134. It might be reasoned that this spectrum showed $HOCH_2CH(OH)CH_2OC^+HCH_3$ at peak M-15 (m/z = 119), $HOC^+HCH_2OCH(CH_3)_2$ at peak M-31 (m/z = 103) and $^+CH_2OCH(CH_3)_2$ at peak M-61 (m/z = 73). The mass spectrum of 1,3-di propyl glycerol ether (1,3-diisopropoxypropan-2-ol) with molecular weight 176, was indicated in Figure 4.14 B. This mass spectrum showed the fragment of $(CH_3)_2CHOCH_2CH(OH)CH_2OC^+HCH_3$ at peak M-15 (m/z = 161), the fragment of $(CH_3)_2CHOCH_2CH(OH)CH_2O^+$ at peak M-43 (m/z = 133) and $(CH_3)_2CHOCH_2C^+HOH$ at peak M-73 (m/z = 103). The mass spectrum in Figure 4.14 C showed the isomer of di propyl glycerol ether. It was 1,2-di propyl glycerol ether (2,3-diisopropoxypropan-1-ol) with same molecular weight (m/z = 176). It had the fragment of $HOCH_2CH(OC^+HCH_3)CH_2OH$ at peak M-57 (m/z = 119). The fragment $HOCH_2C^+HOCH(CH_3)_2$ was appeared at peak M-73 (m/z = 103). This mass spectrum had the fragment of $C^+HCH_2OCH(CH_3)_2$ at peak M-91 (m/z = 85). Figure 4.14 D shows mass spectrum of 1,2,3-tri propyl glycerol ether (MW 218). It was clear that high abundance of fragments was observed at peaks of $^+CH(CH_3)_2$ (m/z = 43), $HOCH_2C^+HOH$ (m/z = 61), $^+CHCH_2OCH(CH_3)_2$ (m/z = 85) and $^-OCH_2CH(O^-)CH_2OC^+H$ (m/z = 103).

There were five components of butyl glycerol ethers in etherification products between glycerin and butene-1 over Amberlyst-15, which are shown in Figures 4.15 A to 4.15 E. The mass spectrum of 1-mono butyl glycerol ether (3-(sec-butoxy)propane-1,2-diol), MW 148, was indicated in Figure 4.15 A. It was evidenced that there had the fragment of $HOCH_2CH(OH)CH_2OC^+HCH_3$ at peak M-29 (m/z = 119), $H_2C^+OCH(CH_3)C_2H_5$ fragment at peak M-61 (m/z = 87) and $HOCH_2CH(OH)C^+H_2$ fragment at peak M-73 (m/z = 75).

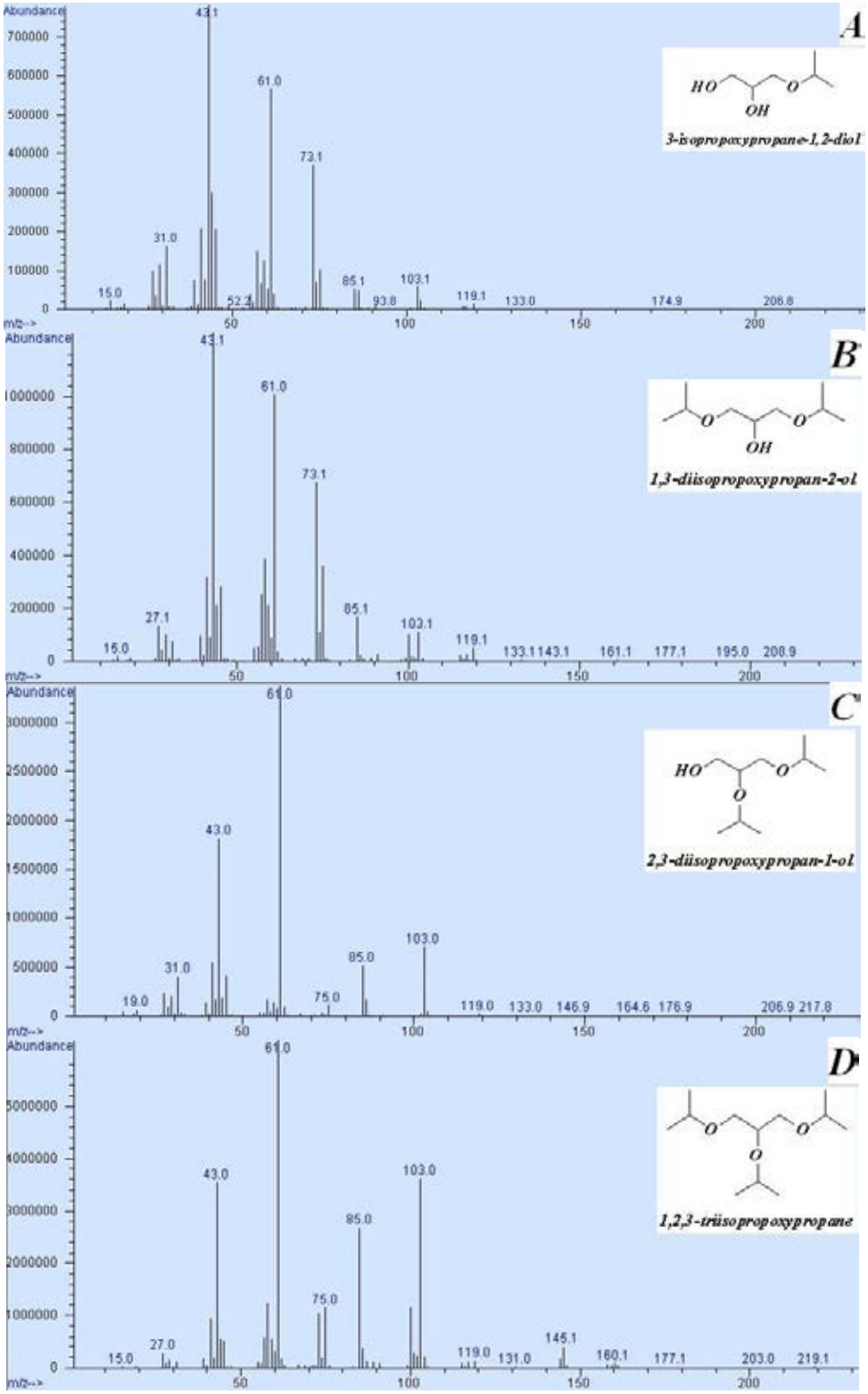

Figure 4.14 Mass spectrum of propyl glycerol ethers.

The chemical structure of 1-mono butyl glycerol ether in Figure 4.15 B was 2-(sec-butoxy)propane-1,3-diol. It had the mass spectrum and molecular weight similar to those of (3-(sec-butoxy)propane-1,2-diol). There were $HOCH_2CH(OH)CH_2OC^+HCH_3$ fragment at peak M-29 (m/z = 119), $HOCH_2C^+HOCH(CH_3)(C_2H_5)$ fragment at peak M-31 (m/z = 117), $(C^+H_2)_2CHOCH(CH_3)(C^+H_2)$ fragment at peak (M-17 - M-17 - M-15) m/z = 99, and $HOCH_2CH(OH)C^+H_2$ fragment at peak M-73 (m/z = 75).

The mass spectrum in Figure 4.15 C had fragments of dioxan derivative. The dioxan derivative was formed through dehydration between 1-mono butyl glycerol ether (3-(sec-butoxy)propane-1,2-diol) with glycerin. The expected-chemical-structure of dioxan derivative was (5-(sec-butoxymethyl)-1,4-dioxan-2-yl) methanol, MW 204. The peak M-29 (m/z = 175) was $HOCH_2(C_4H_6O_2)CH_2OC^+HCH_3$ fragment. The $CH_2(C_4H_6O_2)CH_2OC^+HCH_3$ fragment gave peak at (M-29 - M-18) (m/z = 157). The $HOCH_2CH(OH)CH_2OC^+HCH_3$ fragment gave peak at (M-29 - M-18 - M-38) (m/z = 119). The peak at (M-31 - M-74) (m/z = 99) was $(C_4O_2H_6)C^+H$ fragment.

Di-butyl glycerol ethers had mass spectrum shown in Figures 4.15 D and 4.15 E. It was clear that there were two isomers of di-butyl glycerol ether, as indicated in Figures 4.15 D and 4.15 E. Their chemical structures were 1,3-di-sec-butoxypropan-2-ol and 2,3-di-sec-butoxypropan-1-ol. They had the same molecular weight at 204. The fragment of $CH_2C(CH_3)OCH_2CH(OH)CH_2OCH(CH_3)C^+H_2$ appeared at peak (M-15 - M-15 - M-1) (m/z = 173). The high abundance of fragments $HOCH_2CH(OH)CH_2OC^+HCH_3$ was observed at peaks of (M-56 - M-29) (m/z = 119), and fragment of $(C_4H_9)OCH_2C^+H(OH)$ was observed at peaks of (M-87) (m/z = 117). There were $C^+HCH_2O(C_4H_9)$ fragment at peak of M-105 (m/z = 99) and $HOCH_2CH(OH)C^+H_2$ fragment at peak (M-73 - M-56) (m/z =75).

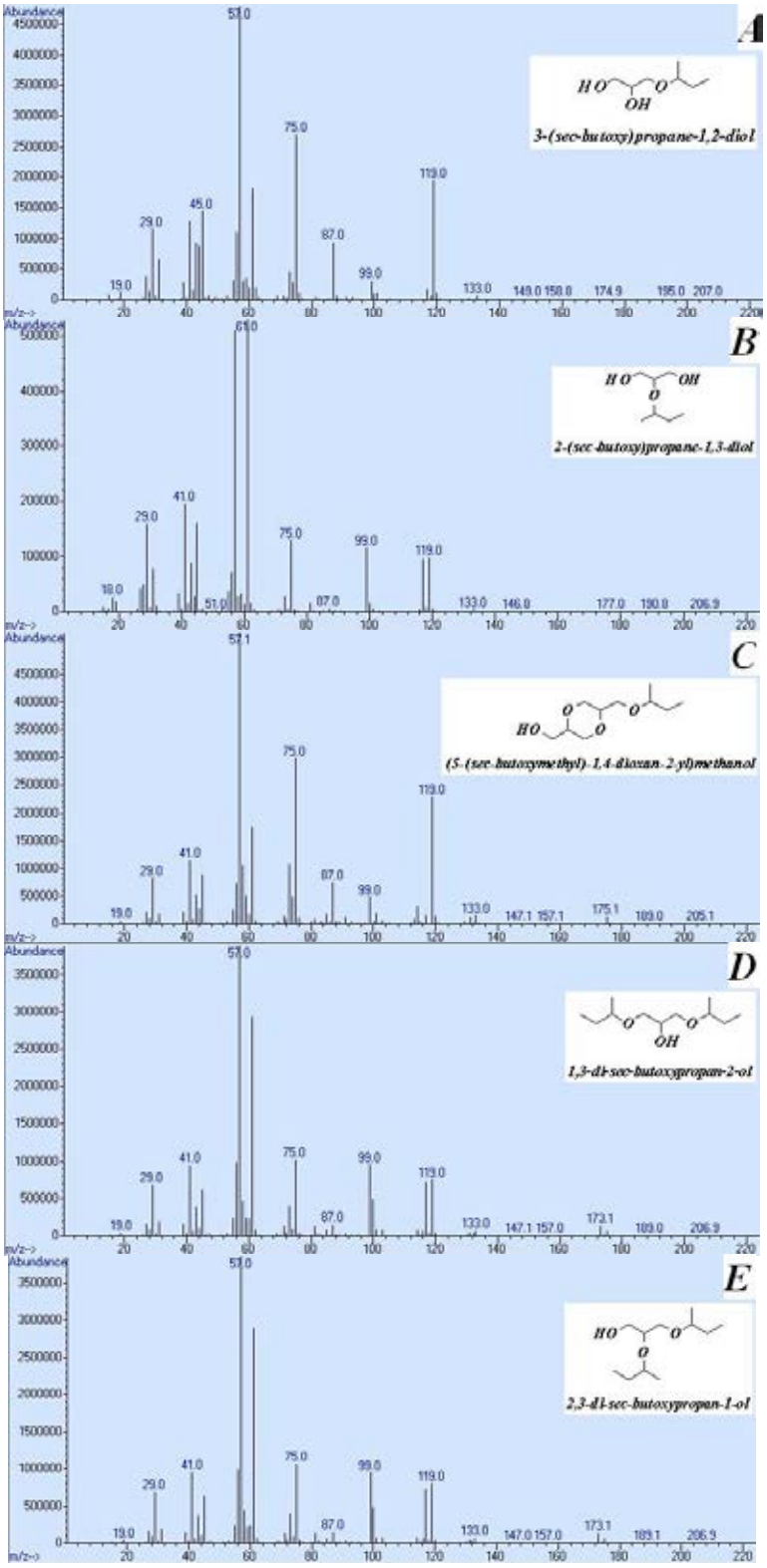

Figure 4.15 Mass spectrum of butyl glycerol ethers.

4.5 Reaction pathways

GC chromatograms of propyl- and butyl-glycerol ethers are shown in Figures 4.16 and 4.17, respectively. All of the compositions for both ethers were verified for their chemical structure by using the results from MSD. The products from propylation of glycerin over Amberlyst-15 at temperature 100 °C within 8 h reaction time were 3-MPGE, two isomers of DPGE (1,3-DPGE and 2,3-DPGE) and TPGE, which are shown in Figure 4.16 A. The GC chromatogram in Figure 4.16 B showed the sequence of propyl-glycerol ethers from etherification between glycerin and propylene over Amberlyst-15 at temperature 100 °C within 24 h reaction time. Figure 4.16 C showed TPGE from propylation of glycerin with propylene over Amberlyst-15 at temperature 100 °C within 48 h reaction time.

The products from the butylation of glycerin with 1-butene were two isomers of mono-butyl glycerol ether (3-MBGE and 2-MBGE), dioxan derivative and two isomers of di-butyl glycerol ether (1,3-DBGE and 2,3-DBGE) as shown in Figure 4.17.

The reaction pathways of ethers through alkylation of glycerin were monitored by using percentages of components from every condition. The components in chromatogram were measured the peak area responses. Then, all of the responses were calculated to concentration in percentage unit by using normalization method. The percentages of components in products were used for monitoring the product distribution. The product distribution of etherification between glycerin and propylene over Amberlyst-15, S200 and S100 are shown in Tables 4.4, 4.5 and 4.6, respectively. Tables 4.7 and 4.8 show the product distribution of butylation of glycerin over Amberlyst-15 and S200, respectively.

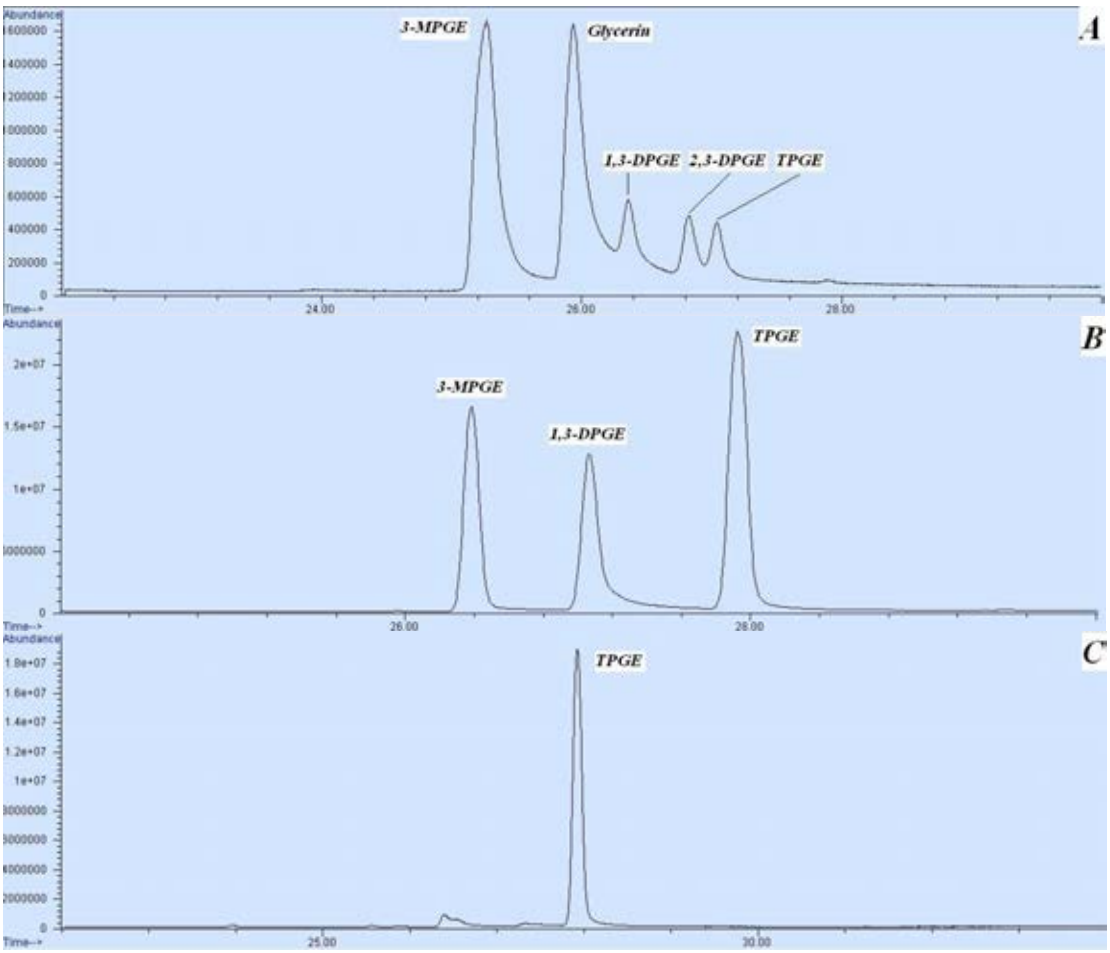

Figure 4.16 Chromatogram of propyl glycerol ethers.

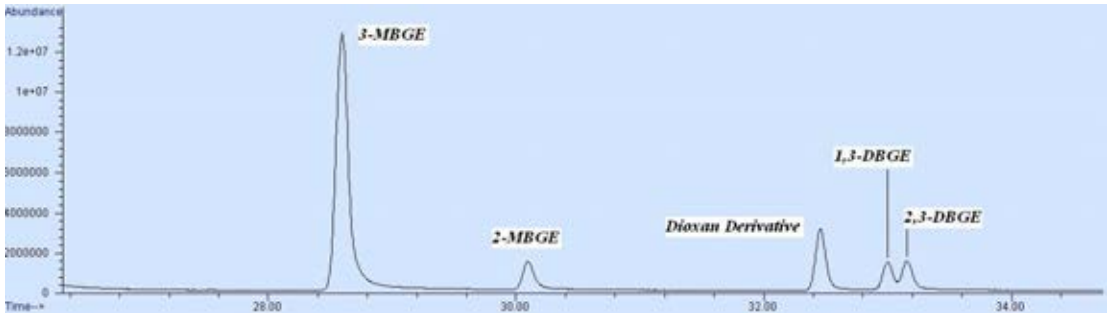

Figure 4.17 Chromatogram of butyl glycerol ethers.

It appeared in Table 4.4 that glycerin was decreased rapidly within 24 h. The product MPGE (mono-propyl glycerol ether) was maximized at 16 h reaction time, then it had decreased gradually within 48 h. The percentage of DPGE (di-propyl glycerol ether) had risen slightly over 8 h. It reached the highest level at 24 h and then it had disappeared after 48 h. The percentage of TPGE (tri-propyl glycerol ether) had increased significantly. It reached a complete formation at 48 h. The products from etherification between glycerin and propylene on resin S200 is shown in Table 4.5. The reaction rate was gone up slowly that 72.43% conversion was obtained after 72 h reaction time. The MPGE was the main product in this reaction while the DPGE was the lowest composition. The product distribution of propylation of glycerin over resin S100 is shown in Table 4.6. It gave the same result as products which obtained over resin S200. The reactions over resin S100 & S200 had not reach complete reaction within 72 h. It was confirmed that propylation preferred to form MPGE. The MPGE was hardly reacted to obtain DPGE. The DPGE was further reacted with alkenes to form TPGE. In Table 4.5 the concentration of MPGE was increased continuously from 32-56 h reaction time then it decreased considerably at 64 h, because MPGE was consumed to form DPGE and TPGE. The concentration of TPGE was decreased from reaction temperature at 40-56 h and 64-72 h. It could be note that the concentration of MPGE was increased.

Table 4.4 Product distribution of etherification between glycerin and propylene on Amberlyst-15, glycerin/propylene = 1/4, catalyst/glycerin = 10 wt %.

Etherification product	**Condition (°C/h)**						
	90/8	**100/8**	**100/16**	**100/24**	**100/32**	**100/40**	**100/48**
	Distribution of etherification product (%)						
TPGE	0	9.25	25.28	54.17	67.25	74.60	100
DPGE	0	6.40	4.83	20.84	9.92	5.57	0
MPGE	6.21	43.89	46.95	24.99	22.83	19.82	0
Glycerin	93.79	40.46	22.94	0	0	0	0

Table 4.5 Product distribution of etherification between glycerin and propylene on S200, glycerin/propylene = 1/4, catalyst/glycerin = 10 wt %.

Etherification product	Condition (°C/h)									
	90/8	100/8	100/16	100/24	100/32	100/40	100/48	100/56	100/64	100/72
	Distribution of etherification product (%)									
TPGE	0	0	0	1.06	8.63	17.11	14.75	13.15	21.77	14.75
DPGE	0	0	2.34	6.25	7.50	0.91	0.88	0.81	2.88	6.07
MPGE	0	0	15.19	14.43	34.12	38.25	42.80	46.86	45.27	51.61
Glycerin	100	100	82.47	78.26	49.75	43.73	41.57	39.18	30.08	27.57

Table 4.6 Product distribution of etherification between glycerin and propylene on S100, glycerin/propylene = 1/4, catalyst/glycerin = 10 wt %.

Etherification product	Condition (°C/h)									
	90/8	100/8	100/16	100/24	100/32	100/40	100/48	100/56	100/64	100/72
	Distribution of etherification product (%)									
TPGE	0	0	0	0	9.42	10.97	14.03	16.18	15.56	21.77
DPGE	0	0	0	4.65	1.07	0.43	0.73	1.05	4.87	2.88
MPGE	0	0	5.77	12.71	31.19	30.74	42.35	40.31	38.52	45.27
Glycerin	100	100	94.23	82.64	58.32	57.86	42.89	42.46	41.05	30.08

The strong acid resins were very active catalysts for etherification reaction with isobutylene. The reaction achieved 100% of glycerol conversion with 92% selectivity to di- and tri-ethers over Amberlyst-39 after 8 h reaction time at 60 ºC. At the same reaction condition Amberlyst-15 gave 86% selectivity to di- and tri-ethers [34]. This isobutylation of glycerin used lower reaction time and temperature when compared with etherification between glycerin and propylene on strong acid resins. The propylation of glycerin gave a sole product of tri propyl glycerol ether.

The results from the etherification between glycerin and 1-butene over resin Amberlyst-15 which is shown in Table 4.7 reached 100% conversion after 64 h reaction time. It was evidenced that there was 3-MBGE as the main product. Table 4.8 shows the butylation of glycerin etherification on resin S200. The rate of reaction was grown slowly that gave only 38.99% conversion after 72 h of reaction time. This reaction condition, gave 3-MBGE as the main product. There had side reaction between 3-MBGE and glycerin to form dioxan derivative through dehydration reaction. The identification of chemical structures from MSD results could be

confirmed that dioxan derivative was obtained (5-(sec-butoxymethyl)-1,4-dioxan-2-yl) methanol. The dioxan derivative reached 9.71% over Amberlyst-15 resin and 1.48% over S200 resin under 72 h of reaction time. The DBGE was also detected in butylation of glycerin. There were two isomers of di-butyl glycerol ether, 1,3-DBGE and 2,3-DBGE, that obtained with same concentration for each isomer in every reaction condition. It was confirmed that tri-butyl glycerol ether was not obtained in the etherification between glycerin and 1-butene.

Table 4.7 Product distribution of etherification between glycerin and 1-butene on Amberlyst-15, glycerin/1-butene = 1/4, catalyst/glycerin = 10 wt %.

Etherification product	**Condition (°C/h)**									
	90/8	**100/8**	**100/16**	**100/24**	**100/32**	**100/40**	**100/48**	**100/56**	**100/64**	**100/72**
	Distribution of etherification product (%)									
2,3-DBGE	0	0	1.37	0.89	2.01	3.47	5.52	5.30	5.83	5.65
1,3-DBGE	0	0	1.27	0.81	1.81	3.10	4.54	5.03	5.30	5.24
Dioxan Derivative	0	0	3.60	1.46	2.65	5.53	10.55	9.01	9.86	9.71
2-MBGE	0	3.23	3.86	7.28	11.06	8.09	5.52	9.43	8.59	7.80
3-MBGE	0	21.53	36.77	48.39	53.98	58.52	54.32	56.44	70.42	71.60
Glycerin	100	75.24	53.13	41.17	28.49	21.29	19.55	14.79	0	0

Table 4.8 Product distribution of etherification between glycerin and 1-butene on S200, glycerin/1-butene = 1/4, catalyst/glycerin = 10 wt %.

Etherification product	**Condition (°C/h)**									
	90/8	**100/8**	**100/16**	**100/24**	**100/32**	**100/40**	**100/48**	**100/56**	**100/64**	**100/72**
	Distribution of etherification product (%)									
2,3-DBGE	0	0	0	0	0	0.13	0.14	0.13	0.20	0.72
1,3-DBGE	0	0	0	0	0	0.15	0.15	0.13	0.14	0.55
Dioxan Derivative	0	0	0	0	0	0.38	0.38	0.39	0.45	1.48
2-MBGE	0	0	1.94	2.19	2.62	2.88	2.99	2.82	3.00	4.35
3-MBGE	0	0	7.68	13.38	16.16	18.04	19.06	20.85	21.78	31.89
Glycerin	100	100	90.38	84.43	81.22	78.42	77.28	75.68	74.43	61.01

The etherification between glycerin and isobutylene on Amberlyst-15 at temperature 75 °C after 8 h reaction time gave 99% of glycerin conversion with 90% selectivity to DTBG and TTBG [14]. The etherification between glycerin and 1-butene on Amberlyst-15 used reaction time and temperature higher than isobutylation of glycerin. The main product of 1-butylation of glycerin was MBGE 79%.

It was reported that zeolites Y and beta gave lower selectivity than ion-exchange resins in tert-butylation of glycerin. The conversion of glycerin at 60 °C over zeolite beta was 100% and yield of DTBG was 80% after 8 h., but no TTBG was formed. The glycerin etherification with isobutylene on zeolite Y at the same condition gave 69% selectivity to DTBG and TTBG with 94% of glycerin conversion [34]. The glycerin etherification with 1-butene was not catalyzed on zeolites Y and beta in this research. It means that 1-butene required activation energy for reaction higher than isobutylene.

These experiment results identified the reaction factors that affected on the etherification between glycerin and olefin gases over the strong acid ion-exchange resin, Amberlyst-15, and the sulfonic acid functionalized styrene-divinyl benzene copolymers, S100 and S200.

Firstly, electrophilic addition to olefins, the reaction took place at the carbon-carbon double bond in the form of Markovnikov's rule. An electrophile in this reaction was hydrogen ion from functionalized sulfonic acid catalyst. This step left a secondary (2°) carbocation intermediate, isopropyl cation from propylene and isobutyl cation from 1-butene. Isopropyl and isobutyl cations were more stable than propyl and butyl cations, primary (1°) carbocation intermediates, respectively. These 2° carbocation intermediates reacted with an unshared pair of electron of the oxygen atom of glycerin to give PGE or BGE.

Secondly, the propylene gave the lowest of reaction time and the lowest side-reaction, when compared with the reaction of 1-butene. The isobutyl cation had methyl and ethyl groups that bonded to the charge-bearing carbon. The isopropyl cation had two methyl groups that bonded to the charge-bearing carbon. It means that isobutyl cation was more stable than isopropyl cation. But, in the reaction of glycerin etherification isopropyl cation was more reactive than isobutyl cation. Glycerin had unshared pair of electrons of three OH groups. These three OH groups were steric

hindrance for alkene etherification. It could be noted that size of isopropyl cation was able to access to the reaction site, OH group of glycerin, better than size of isobutyl cation.

Finally, the acidity of catalyst indicated the performance of these etherification reactions. The strong acid catalysts, i.e. Amberlyst-15, S200 and S100, activated the propylation and butylation for glycerin etherification reaction better than the reaction from the weak acid catalysts, i.e. Al-SBA-15, Pr-SO_3H-SBA-15, Zeolite Beta and Zeolite Y. Amberlyst-15 gave the best performance in glycerin etherification with alkenes, when compared with S200 and S100 resins. In this etherification reaction, isopropyl and isobutyl cations were Lewis acid and OH groups of glycerin were Lewis base. It appeared from the properties of catalyst in Table 4.1 that Amberlyst-15 had porosity in the bead. It had surface area, pore size and pore volume higher than S200 and S100 resins. These resins, S200 and S100, were nonporous bead. It could be noted that the porosity in Amberlyst-15 activated the propylation and the butylation for glycerin etherification better than the nonporous, S200 and S100 resins. The catalyst S100 in butylation for glycerin etherification gave no activity. It was evidenced that the low acidity with nonporosity of S100 could not activate the isobutyl cation to access to the reaction site. But in glycerin etherification with propylene the low acidity with nonporous of S100 resin had sufficient activity to access the isopropyl cation to the reaction site.

It could be concluded that the etherification between glycerin with olefin gases was electrophilic addition reaction. The structures of PGE and BGE products were conformed to Markovnikov's rule. The intermediates in this reaction were 2° carbocations, isopropyl and isobutyl cations (Lewis acid). The OH groups of glycerin showed Lewis base. The isopropyl cation was able to access to the reaction site, steric hindrance OH groups of glycerin, better than size of isobutyl cation. Amberlyst-15, S200 and S100 resins activated the propylation and butylation for glycerin etherification. The catalyst with high acidity and porosity gave high performance of etherification. The isopropyl cation in high acidity and porosity gave performance of glycerin etherification better than isobutyl cation in same properties of catalyst.

In addition, there was a possible reaction path way of glycerin propylation and glycerin butylation. In etherification reaction, thermal and acidic conditions would

protonated double bond of propylene and 1-butene to be electron acceptor (Lewis acid). The pi bond of the olefins was broken and that the electron pair was used to form a new covalent bond with the hydrogen ion from functionalized sulfonic acid catalyst. One carbon atom with only six electrons in its valence shell carried a carbocation. The 2° carbocation of propylene was the stable intermediate. It was an unstable intermediate. The OH groups of glycerin molecule would be the electron donor group (Lewis base). It means that –OH end group of glycerin reacted rapidly with protonated propylene (isopropyl cation) to form the new carbon-oxygen bond. It appeared from this study that MPGE was formed at first stage in the reaction phase. This isopropyl cation intermediate then completed its valence shell by forming a new covalent bond with an unshared pair of electrons of the oxygen atom of remained –OH end group and remained –OH middle group to obtain 1,3-DPGE and 2,3-DPGE, respectively. The protonated propylene was preferentially reacted with MPGE at –OH end group to form 1,3-DPGE. Then the DPGE was continuously reacted with isopropyl cation to form TPGE. Similarly, in the reaction of isopropyl cation intermediate with DPGE, the –OH group of DPGE reacted rapidly with protonated propylene to form the carbon-oxygen covalent bond of TPGE. The TPGE was increased dramatically over strong acid catalyst, Amberlyst-15. The possible reaction path way of etherification between glycerin and propylene over acidic catalyst, Amberlyst-15, is shown in Figure 4.18.

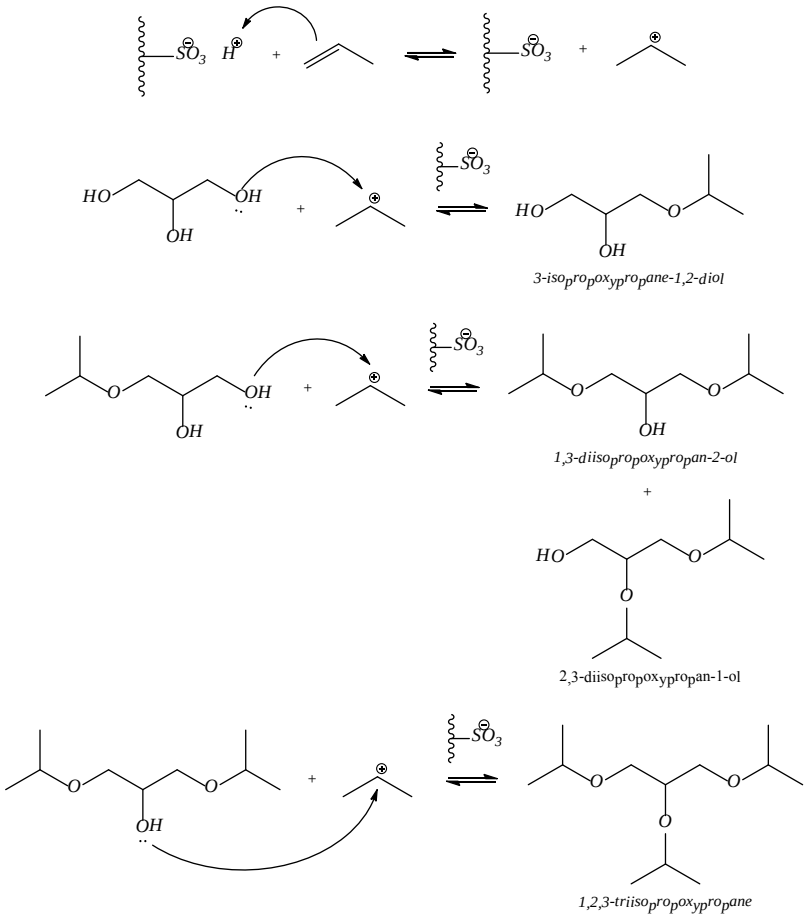

Figure 4.18 Reaction pathway of etherification between glycerin and propylene on Amberlyst-15.

The possible reaction path ways of etherification between glycerin and 1-butene over acid mesoporous catalyst, Amberlyst-15, are shown in Figures 4.19 to 4.21. Like propylene, 1-butene was protonated by acidic catalyst at double bond to be electron acceptor (isobutyl cation). The 2° carbocation of 1-butene was the stable intermediate. The –OH groups, electron donor of glycerin molecule, reacted with protonated 1-butene to form 3-MBGE and 2-MBGE. According to the results from Table 4.7 indicated that 3-MBGE (3-(sec-butoxy)propane-1,2-diol) was the main product. It is found that –OH groups at the end of glycerin backbone have more convenient for reaction with protonated 1-butene than –OH group at the middle position.

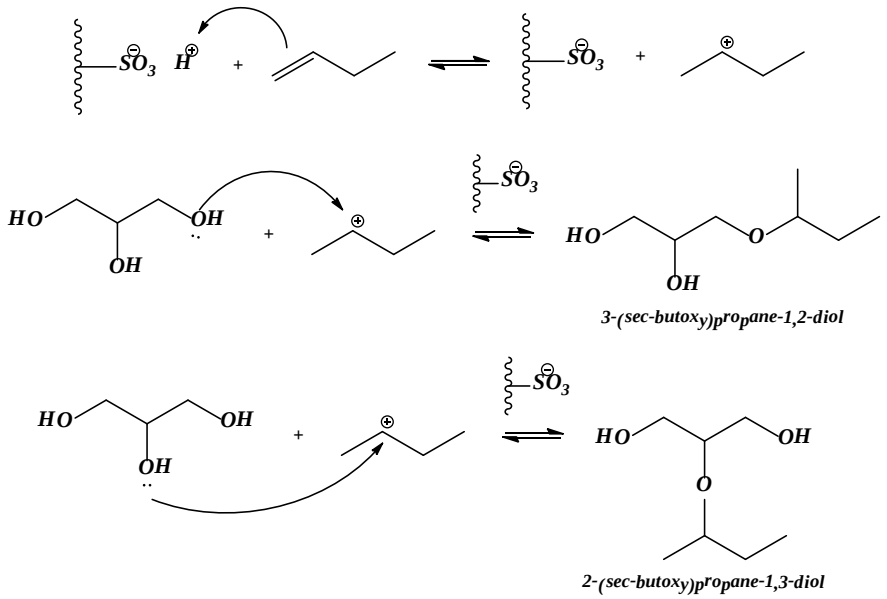

Figure 4.19 Reaction pathway of etherification between glycerin and 1-butene on Amberlyst-15 to form 3-MBGE and 2-MBGE.

The results in Table 4.7 indicated that the dioxan derivative was presence in the etherification products. It meaned that both remained –OH groups of 3-MBGE were protonated by acidic catalyst. The 2° oxonium ion of 3-MBGE was the stable intermediate. Then, 2° oxonium ion reacted with 1° –OH group of free glycerin through dehydration reaction. The intermediate product was 3-((1-(sec-butoxy)-3-hydroxypropan-2-yl)oxy)propane-1,2-diol. Addition of proton from acidic catalyst to the 2° of this intermediate product formed the 2° oxonium ion of 3-((1-(sec-butoxy)-3-hydroxypropan-2-yl)oxy)propane-1,2-diol. This oxonium ion reacted with 1° –OH group, in this intermediate product, through dehydration reaction. This side reaction formed dioxan derivative, (5-(sec-butoxymethyl)-1,4-dioxan-2-yl) methanol. The possible reaction path way of dehydration between 3-MBGE and free glycerin is shown in Figure 4.20.

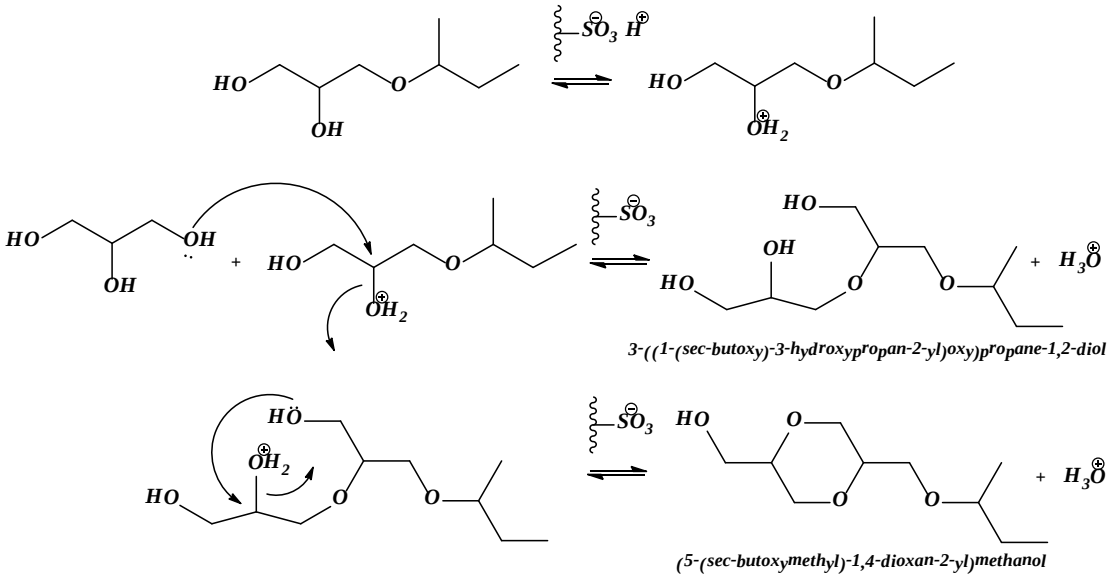

Figure 4.20 Reaction pathway of etherification between glycerin and 1-butene on Amberlyst-15 to form dioxan derivative.

Not only 3-MBGE was the main product, but also 2-MBGE was found in the butylation of glycerin. The results in Table 4.7 indicate that two isomers of DBGE, i.e. 1,3-DBGE and 2,3-DBGE, were detected in etherification product. It could be note that proton transferred from isobutyl cation to unshared pair electrons of the oxygen of –OH group of 3-MBGE or 2-MBGE to form C-O covalent bond in 1,3-DBGE or 2,3-DBGE. In Figure 4.21 the isobutyl cation reacted with 1° –OH group of 3-MBGE to obtain 1,3-DBGE. The 2,3-DBGE was obtained from reaction between isobutyl cation with 2° –OH group of 3-MBGE or 1° –OH group of 2-MBGE, as shown in Figure 4.21. This experiment was observed that tri butyl glycerol ether was not obtained in product. It means that isobutyl cation need high activation energy, reaction temperature or acidity of catalyst, to react with 1,3-DBGE and 2,3-DBGE.

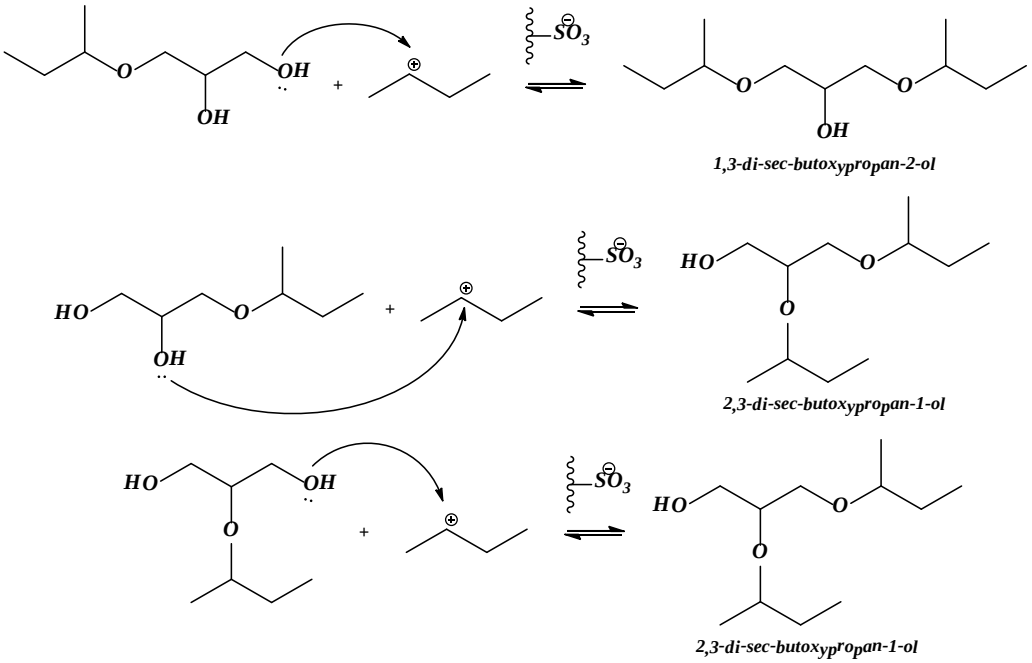

Figure 4.21 Reaction pathway of etherification between 3-MBGE and 2-MBGE with 1-butene on Amberlyst-15 to form 1,3-DBGE and 2,3-DBGE.

4.6 Influence of mixed-propyl glycerol ethers and tri-propyl glycerol ether on cold flow performance of palm biodiesels

It should be noted that the pour point of B100 from vegetable oils is depended on the amount of saturated fatty acids. The saturated fatty acids at 8% in canola biodiesel, 15% in soybean biodiesel and 50% in palm biodiesel, give pour point at -3 °C, 3 °C and 11 °C, respectively [2]. Generally, the palm biodiesel contain 50% of saturated fatty acids (palmitic acid and stearic acid), 40% of monounsaturated fatty acid (oleic acid) and 10% of polyunsaturated fatty acid (linoleic acid). They form the cluster of hydrocarbon crystals in the blended fuels and begin to build up a gel layer that is visually observed as the blended fuels are cooled.

In order to obtain the efficiency of cold flow improvement of mixed-propyl glycerol ether and tri-propyl glycerol ether, the cold flow performances of their blending with palm biodiesels and palm biodiesel blended with diesel were evaluated. The mixed-propyl glycerol ether consisted of MPGE, DPGE and TPGE at 24.99%, 20.84% and 54.17%, respectively. This cold flow depressant was obtained from the etherification between glycerin and propylene on Amberlyst-15 at 100 °C over 24 h.

The tri-propyl glycerol ether was prepared from the glycerin etherification with propylene on Amberlyst-15 at 100 °C over 48 h. These two cold flow improvers were tested at concentrations of 0.05, 0.10, 0.50, 1.00, 5.00, 10.00 and 20.00% successively for each of B2, B5, B80, B90 and B100 blended palm biodiesels. In this paper, the cold flow properties, cloud point and pour point, were investigated. The obtained data were plotted in Figures 4.22 to 4.25. The line curves showed that the increasing concentrations of additives increased the performances of cold flow properties. These two additives were oxygenated compounds with weak polarity, which gave the best solubility in blended palm biodiesels. They achieved improvement in the cold flow properties of blended palm biodiesels. In addition to data in Table 4.9, which summarized from the line curves in Figure 4.22 to 4.25, gave the range of cold flow temperatures of propyl glycerol ethers in blended palm biodiesels It was evidenced that mixed propyl glycerol ether could reduce cloud point and pour point of blended palm biodiesels in range of 1-3 °C by adding the additives at the lowest concentration of 0.10%. The pour points were reduced in range of 3-5 °C, 4-6 °C and 5-10 °C when the mixed propyl glycerol ethers at 1.0, 10.0 and 20%, respectively. Tri-propyl glycerol ether could reduce the cold flow temperatures of blended palm biodiesels in range of 1-4 °C at 1.0% of blended concentration. The pour points were reduced in range of 3-6 °C and 5-9 °C by adding the tri-propyl glycerol ether at 10 and 20%, respectively.

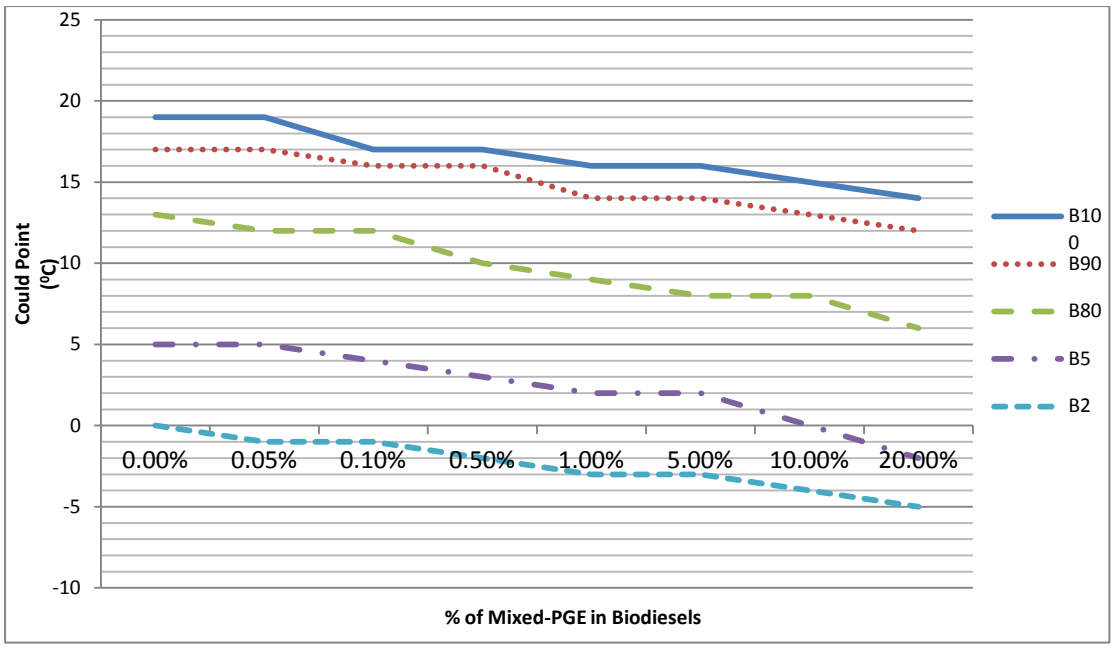

Figure 4.22 Could point of mixed-propyl glycerol ethers in blended palm biodiesels.

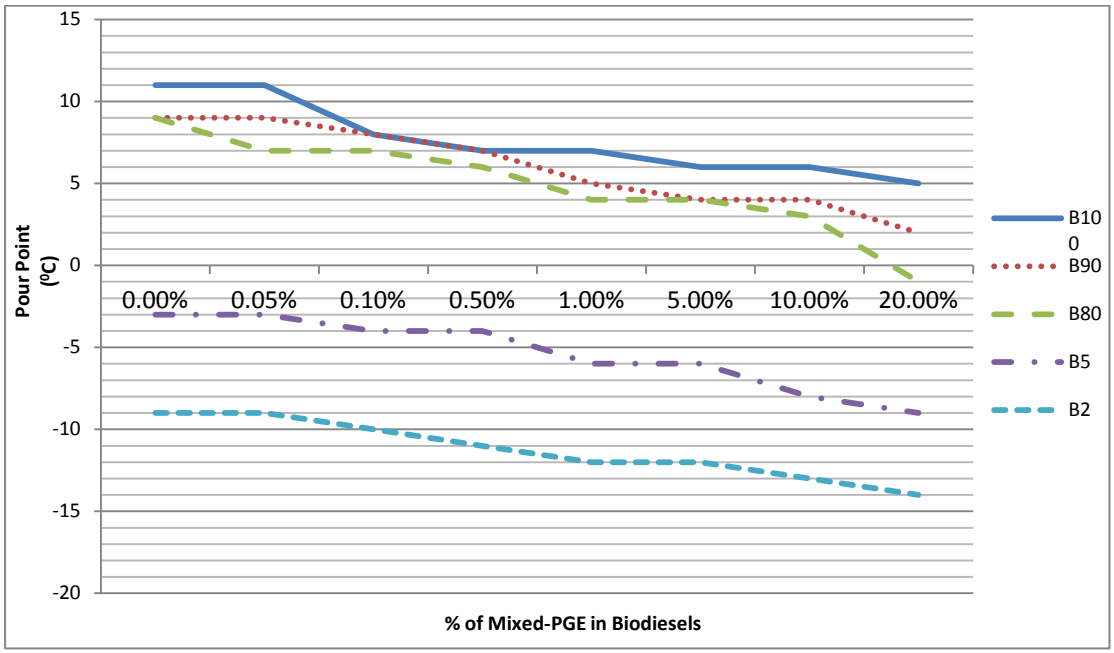

Figure 4.23 Pour point of mixed-propyl glycerol ethers in blended palm biodiesels.

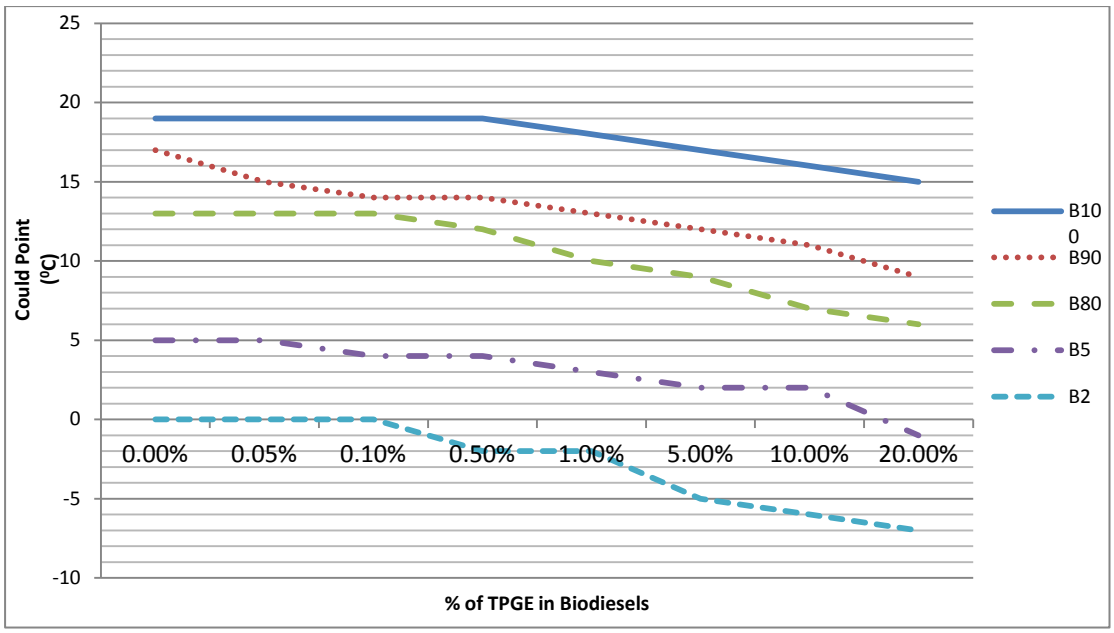

Figure 4.24 Could point of tri-propyl glycerol ether in blended palm biodiesels.

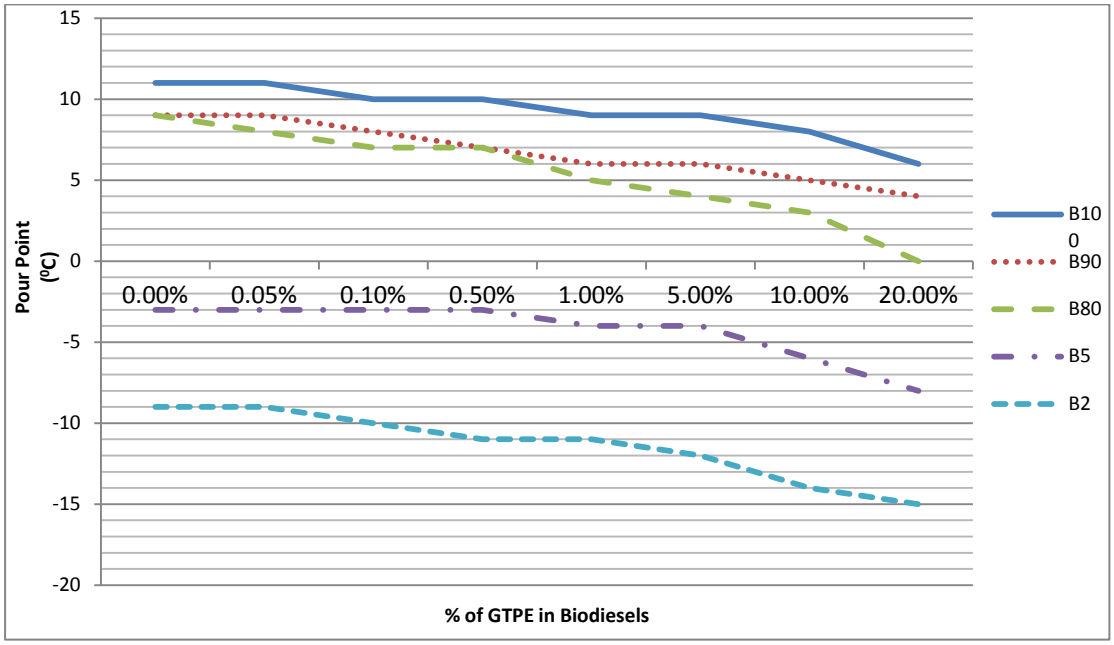

Figure 4.25 Pour point of tri-propyl glycerol ether in blended palm biodiesels.

Table 4.9 Cold flow properties of propyl glycerol ethers in blended palm biodiesels.

% of PGE in Biodiesel	Δ Cloud point (°C)		Δ Pour point (°C)	
	Mixed PGE	TPGE	Mixed PGE	TPGE
0.05	0-1	0-2	0-2	0-1
0.1	1-2	0-3	1-3	0-2
0.5	1-3	0-3	1-4	0-2
1.0	3-4	1-4	3-5	1-4
5.0	3-5	2-5	3-5	1-5
10	4-5	3-6	4-6	3-6
20	5-7	4-8	5-10	5-9

The cold flow performance in this report evidenced that these prepared ethers as cold flow dispersants could decrease and disperse the saturated hydrocarbon wax crystals. The mixed propyl glycerol ether gave the cold flow performances over blended palm biodiesels slightly better than the tri-propyl glycerol ether. The presence of MPGE and DPGE in ether decreased the cold flow temperatures of blended palm biodiesels when compared with the performance of only tri-propyl glycerol ether. This palm biodiesel contained 50% of palmitic and stearic acid methyl esters. Hydrocarbon chain, palmitate and stearate, in palm biodiesel showed hydrophobic region. Methyl ester group in palm biodiesel showed hydrophilic region. The MPGE had 2 groups of –OH that gave more polar than DPGE (with a –OH group). The TPGE with no –OH group showed the lowest polarity when compared with MPGE and DPGE. It should be noted that polarity of cold flow depressant and wax crystal size were affected on cold flow temperatures of palm biodiesel and their blend with diesel. The cold flow temperatures were reduced when the crystal size of saturated fatty acids was decreased. The crystal size of saturated fatty acids was decreased when the polarity of cold flow additive was increased. The results in Table 4.9 indicate that the polar PGE contacted with polar methyl ester group to arrange the cluster size of hydrocarbon crystals when the palm biodiesel was cooled. The MPGE and DPGE (with high polarity) in mixed propyl glycerol ethers could reduce the cluster size of palmitate and stearate crystals, and could reduce the cold flow temperatures better than TPGE (with low polarity).

Whereas, BGE showed no performance in cold flow property over blended palm biodiesels because BGE could not dissolved in blended palm biodiesels. The butyl glycerol ether was prepared from the glycerin etherification with 1-butene on Amberlyst-15 at 100 °C over 72 h. This cold flow depressant consisted of 3-MBGE, dioxane derivative, 2-MBGE, 2,3-DBGE, 1,3-DBGE at 71.60%, 9.71%, 7.80%, 5.65% and 5.24%, respectively. The 3-MBGE was the main product in BGE which had high polarity by 2 –OH groups. It was evidenced that it could not dissolve well in non-polar hydrocarbons in diesel.

There were study process for producing biodiesel fuel with reduced viscosity and a cloud point below 32 °F [33]. Researcher reported that the mixture of di- and tri-tertiary butyl ethers from glycerol etherification with isobutylene, at 80 °C, 320 psig, 4% of catalyst loading with residence time of 2 hr, was added into the soybean biodiesel to improve its cloud point. The reduction in 5 °C of cloud point was reported when 12% of the mixture of di- and tri-tertiary butyl ethers was added into soybean biodiesel. It was observed from this research that the mixed propyl glycerol ether from glycerol etherification with propylene reduced cloud point and pour point of blended palm biodiesels in range 4-5 °C and 4-6 °C, respectively, by adding the additive at the concentration of 10%. The TPGE from glycerol etherification with propylene reduced cloud point and pour point of blended palm biodiesels in range 3-6 °C by adding the additive at the concentration of 10%.

4.7 Influence of mixed-propyl glycerol ethers and tri-propyl glycerol ether on cetane index and octane number of palm biodiesels

The cetane index of diesel and palm biodiesel was measured by adding 10% of oxygenated-compound additives, i.e. ethanol, MTBE, mixed PGE and TPGE, are shown in Table 4.10.

Table 4.10 Cetane index of diesel and palm biodiesel by adding 10% of oxygenated-compound additives.

Fuel	Cetane index	Fuel	Cetane index
Diesel	55.0	B100	67.5
Diesel + Ethanol	54.9	B100 + Ethanol	69.0
Diesel + MTBE	56.4	B100 + MTBE	70.2
Diesel + Mixed PGE	52.0	B100 + Mixed PGE	66.2
Diesel + TPGE	49.3	B100 + TPGE	67.1

Diesel with higher cetane index had shorter ignition delay periods than diesel with lower cetane index. There were hundreds of components in this diesel fuel that had a different cetane index. The overall cetane index of this diesel was the average cetane index of all the components. Generally, diesel engines operate well with a cetane index from 40 to 55.

The additive, butyl glycerol mixture (60 to 70% by weight of 1,3-di-t-alkyl glycerol, 5 to 15 wt % of 1,2-di-t-alkyl glycerol and 15 to 30 wt % of 1,2,3-tri-t-alkyl glycerol) was blended 5 volume % into diesel fuel (31% aromatic content, 400 ppm sulfur and 43 cetane number) that gave cetane number at 44 [37]. The results in Table 4.10 indicated that mixed PGE and TPGE reduced 3.0 and 5.7 cetane indices of diesel, respectively. Mixed PGE and TPGE reduced 1.3 and 0.4 cetane indices of B100, respectively. It was found that palm biodiesel had cetane index higher than diesel. It means that biodiesel consisted of un-branched chain molecules of FAME which ignited faster than mixed branched with un-branched chain molecules of diesel. It is clear that MTBE with high carbon/oxygen ratio 6/1 gave cetane index higher than cetane index of TPGE (C/O ratio 5/1) and cetane index of mixed PGE (C/O ratio less than 4/1).

Table 4.11 Octane number of gasoline by adding 10% of oxygenated-compound additives.

Fuel	**RON**	**MON**
Gasoline	81.1	91.0
Gasoline + Ethanol	84.4	94.4
Gasoline + MTBE	85.4	96.5
Gasoline + Mixed PGE	81.6	94.0
Gasoline + TPGE	82.1	93.6

In contrast, fuels with low cetane index but high octane number, are ideal for gasoline engines. Higher octane number of gasoline correlates to higher activation energy of engine. The oxygenated compound helps gasoline to burn more completely. The octane number of gasoline in this research was measured by adding 10% of oxygenated-compound additives, i.e. ethanol, MTBE, mixed PGE and TPGE, are shown in Table 4.11. The results indicated that mixed PGE and TPGE increased 0.5 and 1.0 of RON (research octane number) in gasoline, respectively. Mixed PGE and TPGE increased 3.0 and 2.6 of MON (motor octane number) in gasoline, respectively. MTBE in gasoline increased 4.3 of RON and 5.5 of MON. Ethanol in gasoline increased 3.3 of RON and 3.4 of MON. Mixed PGE and TPGE gave lower octane number than MTBE and ethanol. It should be concluded that new oxygen-containing compounds, mixed PGE and TPGE, from glycerin etherification with propylene could be used as fuel supplement because they increased the numerical rating of knock resistance and raised the oxygen content in gasoline for complete combustion.

CHAPTER V
CONCLUSION

The etherification of glycerin with olefin gases, i.e. ethylene, propylene and 1-butene, or C_5 to C_8 alkenes, i.e. 1-pentene, 1-hexene, 1-heptene and 1-octene, over acidic heterogeneous catalysts, i.e. strong acid ion-exchange resins (Amberlyst-15, S100 and S200), mesostructured silicas (Al-SBA-15 and Pr-SO_3H-SBA-15) and micro-pore zeolites (Z-Beta and Z-Y), was studied. The results from glycerin etherification with olefin gases and alkenes over acidic heterogeneous catalysts at temperature 100 °C indicated that Amberlyst-15 had the highest activity on propylene and 1-butene. Acidity and pore size of catalyst indicated influence on performance of the reaction. Strong acidity (3.70 mmol/g) and mesopore size (7.7 nm) of Amberlyst-15 gave the highest activity in propylation and butylation of glycerin. S200 resin with strong acidity (3.53 mmol/g) with non porous type showed low response in glycerin etherification with propylene and 1-butene. S100 resin with strong acidity (3.00 mmol/g) with non porous type gave the lowest response in glycerin propylation and gave no reaction of glycerin butylation. In this reaction condition, high acidity and porosity of catalyst activated propylene better than 1-butene. Weak acidity with high pore size of Al-SBA-15, Pr-SO_3H-SBA-15, Z-Beta and Z-Y gave no response on glycerin etherification with propylene and 1-butene. The products from the propylation of glycerin were mono-propyl glycerol ether (3-MPGE), two isomers of di-propyl glycerol ether (1,3-DPGE and 2,3-DPGE) and tri-propyl glycerol ether. The products from the glycerin etherification with 1-butene were two isomers of mono-butyl glycerol ether (3-MBGE and 2-MBGE), dioxan derivative and two isomers of di-butyl glycerol ether (1,3-DBGE and 2,3-DBGE). The TPGE reached a complete formation through propylene alkylation of MPGE and DPGE, over Amberlyst-15 after 48 h reaction time. The etherification between glycerin with propylene and 1-butene was electrophilic addition reaction. The intermediates were 2° carbocations of isopropyl and isobutyl cations (Lewis acid). The Lewis base was OH group of glycerin. The structures of PGE and BGE products were conformed to Markovnikov's rule.

The mixed propyl glycerol ethers (MPGE 24.99%, DPGE 20.84% and TPGE 54.17%) reduced cloud point 4-5 °C and pour point 4-6 °C of blended palm biodiesels with 10% of mixed PGE. The TPGE reduced 3-6 °C of cloud point and pour point of blended palm biodiesels with 10% of TPGE. The polar group of PGE contacted with the polar group of methyl ester to reduce the cluster size of palmitate and stearate crystals, and could reduce the cold flow temperatures when the blended palm biodiesel was cooled. The mixed butyl glycerol ethers (3-MBGE 71.60%, dioxane derivative 9.71%, 2-MBGE 7.80%, 2,3-DBGE 5.65% and 1,3-DBGE 5.24%) showed no performance in cold flow property over blended palm biodiesels. Due to MBGE, high polarity by 2 –OH groups, could not dissolve well in non-polar hydrocarbons in diesel. Mixed PGE and TPGE reduced 3.0 and 5.7 cetane indices of diesel, and reduced 1.3 and 0.4 cetane indices of B100, respectively. Mixed PGE and TPGE increased 0.5 and 1.0 of RON in gasoline, and increased 3.0 and 2.6 of MON in gasoline, respectively. Mixed PGE and TPGE, from glycerin etherification with propylene could be used as fuel supplement because they increased the numerical rating of knock resistance and raised the oxygen content in gasoline for complete combustion.

Suggestions for future works

1) Tri-butyl glycerol ether from etherification reaction between 1-butene and glycerin should be investigated further with heteropolyacid doped on SBA-15.
2) The etherification of glycerin with 1-pentene should be performed with heteropolyacid doped on SBA-15, higher acid capacity of catalyst, under higher pressure and higher temperature.
3) The mixed propyl glycerol ethers, i.e. MPGE, DPGE and TPGE, should be investigated as gasoline booster.

REFERENCES

[1] Knothe, G. Historical perspectives on vegetable oil-based diesel fuels. *Inform.* 12 (2001): 1103-1107.

[2] McCormick, R. L. *Biodiesel Handling and Use Guidelines*. Third Edition. US Department of Energy: 2006.

[3] William, H.B. Lipids. *Introduction to Organic Chemistry*. USA: Saunders College Publishing, 1997.

[4] American Society for Testing and Materials; Standard specification for biodiesel fuel blend stock (B100) for middle distillate fuels, ASTM D6751; *ASTM*. 05.04. West Conshohocken, PA: 2006.

[5] American Society for Testing and Materials; Standard test method for cetane number of diesel fuel oil, ASTM D613; *ASTM*. 05.05. West Conshohocken, PA: 2001.

[6] American Society for Testing and Materials; Standard test method for flash-point by Pensky-Martens closed cup tester, ASTM D93; *ASTM*. 05.01. West Conshohocken, PA: 2000.

[7] American Society for Testing and Materials; Standard test methods for evaluating lubricity of diesel fuels by the scuffing load ball-on-cylinder lubricity evaluator (SLBOCLE), ASTM D6078; *ASTM*. 05.04. West Conshohocken, PA: 2000.

[8] American Society for Testing and Materials; Standard test methods for cloud point of petroleum products, ASTM D2500; *ASTM*. 05.01. West Conshohocken, PA: 2005.

[9] American Society for Testing and Materials; Standard test methods for filterability of diesel fuels by low-temperature flow test (LTFT), ASTM D4539; *ASTM*. 05.02. West Conshohocken, PA: 2003.

[10] American Society for Testing and Materials; Standard test methods for pour point of petroleum products, ASTM D97; *ASTM*. 05.01. West Conshohocken, PA: 2006.

[11] Perry, R. H., Green, D. W., and Maloney, J. O. H. *Perry's Chemical Engineers' Handbook*. Seventh Edition. McGraw-Hill, 1997.

[12] Lide, D. R. *CRC. Handbook of Data on Organic Compounds*. Third Edition. Boca Raton, FL: CRC Press, 1994.

[13] Norhasyimi, R., Rahmat, A., Zuhairi, A., and Abdul, M. R. Recent progress on innovative and potential technologies for glycerol transformation into fuel additives. *Renewable and Sustainable Energy Reviews*. 14 (2010): 987–1000.

[14] Melero, J. A., et al. Acid-catalyzed etherification of bio-glycerol and isobutylene over sulfonic mesostructured silicas. *Applied Catalysis A: General*. 346 (2008): 44-51.

[15] Harland, C. E. Ion exchange theory and practice. *The Royal Society of Chemistry*. Cambridge, UK: 1994.

[16] Katiyar, A., Yadav, S., Panagiotis, G., Neville, S., and Pinto, G. Synthesis of ordered large pore SBA-15 spherical particles for adsorption of biomolecules. *Journal of Chromatography.*1122 (2006): 13–20.

[17] Zhao, D., et al. Triblock copolymer syntheses of mesoporous silica with periodic 50 to 300 angstrom pores. *Science*. 279 (1998): 548-552.

[18] Luan, Z., Hartmann, M., Zhao, D., Zhou, W., and Kevan, L. Alumination and ion exchange of mesoporous SBA-15 molecular sieves. *Chemistry of Materials*. 11 (1999): 1621-1627.

[19] Margolese, D., Melero, J. A., Christiansen, S. C., Chmelka, B. F., and Strucky, G. D. Direct syntheses of ordered SBA-15 mesoporous silica containing sulfonic acid groups. *Chemistry of Materials*. 12 (2000): 2448-2459.

[20] Melero, J. A., Stucky, G. D., Grieken, R. V., and Morales, G. Direct syntheses of ordered SBA-15 mesoporous materials containing arenesulfonic acid groups. *Journal of Materials Chemistry*. 12 (2002): 1664–1670.

[21] Melero, J. A., Fernando B. L., Morales, G., Iglesias, J., and Rebeca, S. V. Biodiesel production from crude palm oil using sulfonic acid-modified mesostructured catalysts. *Chemical Engineering Journal.* 161 (2010): 323–331.

[22] Melero, J. A., Grieken, R. V., and Morales, G. Advances in the Synthsis and catalytic applications of organosulfonic-functionalized mesostructured materials. *Chemical Reviews*. 106 (2006): 3790-3812.

[23] Newsam, J. M., Treacy, M. M. J., Koetsier W. T., and De Gruyter, C. B. Structural characterization of zeolite beta. *Proceedings of the Royal Society of London, Series A, Mathematical and Physical Sciences*. 420 (1988): 375-405.

[24] Higgins, J. B., et al. The framework topology of zeolite beta. *Zeolites*. 8 (1988): 446-452.

[25] Johnson G. M., Lee, Y. J., Tripathi, A., and Parise, J. B. Structural studies of hydrated germanium X type zeolite via rietveld analysis of synchrotron powder X-ray diffraction data. *Microporous and Mesoporous Materials.* 31 (1999): 195-204.

[26] Baur, W.H. On the cation and water positions in faujasite. *American Mineralogist*. 49 (1964): 697-704.

[27] Scherzer, J. Octane-enhancing, zeolitic FCC catalysts : scientific and technical aspects. *Catalysis Reviews*. 31 (1989): 215.

[28] Hriljac J. A., Eddy, M. M., Cheetham, A. K., Donohue, J. A., and Ray, G. J. Powder neutron diffraction and ^{29}Si MAS NMR studies of siliceous zeolite-Y. *Journal of Solid State Chemistry.* 106 (1993): 66-72.

[29] Occelli, M. L., et al. Gallioaluminosilicate molecular sieves with the faujasite structure. *Journal of Catalysis*. 192 (2000): 119-127.

[30] Adamson, A. W. The BET and related isotherms. *Physical Chemistry of Surfaces.* Fifth Edition. John Wiley and Sons Inc., 1990.

[31] Lippens, B. C., and deBoer, J. H. Studies on pore systems in catalysis V. the t-plot method. *Journal of Catalysis*. 4 (1965): 319.

[32] Lowell, S., Shields, J. E., Thomas, M. A., and Thommes M. BJH method. *Characterization of Porous Solids and Powders: Surface Area, Pore Size and Density*. Dordrecht, Netherland: Springer, 2006.

[33] Klepacova, K., Mravec, D., Kaszonyi, A., and Bajus, M. Etherification of glycerol and ethylene glycol by isobutylene. *Applied Catalysis A: General*. 328 (2007): 1–13.

[34] Klepacova, K., Mravec, D., and Bajus, M. tert-Butylation of glycerol catalysed by ion-exchange resins. *Applied Catalysis A: General*. 294 (2005): 141–147.

[35] Xiao, L., Mao, J., Zhou, J., Guo, X., and Zhang, S. Enhanced performance of HY zeolites by acid wash for glycerol etherification with isobutene. *Applied Catalysis A: General*. 393 (2011): 88–95.

[36] Noureddini, H. Process for producing biodiesel fuel with reduced viscosity and a cloud point below thirty-two (32) degrees Fahrenheit. *United States Patent: 6,015,440*. 2000.

[37] Kesling, Jr., Haven S. K., Lawrence J., Liotta, Jr., and Frank J. Diesel fuel modification for reduced exhaust emissions. *United States Patent: 5,308,365*. 1994.

[38] Zhaohua, L., Hartmann, M., Zhao, D., Zhou, D., and Kevan, L. Alumination and ion exchange of mesoporous SBA-15 molecular sieve. *Chemistry of Materials*. 11 (1999): 1621-1627.

[39] Glycerine monograph. *The United States Pharmacopeial Convention, revision Bulletin.* (May 2009).

[40] American Society for Testing and Materials; Standard test methods for calculated cetane index of distillate fuels, ASTM D976; *ASTM*. 05.01. West Conshohocken, PA: 2002.

[41] American Society for Testing and Materials; Standard test methods for density, relative density (specific gravity), or API gravity of crude petroleum and liquid petroleum products by hydrometer method, ASTM D1298; *ASTM*. 05.01. West Conshohocken, PA: 2002.

[42] American Society for Testing and Materials; Standard guide for petroleum measurement tables, ASTM D1250; *ASTM*. 05.01. West Conshohocken, PA: 2002.

[43] American Society for Testing and Materials; Standard test method for distillation of petroleum products at atmospheric pressure, ASTM D86; *ASTM*. 05.01. West Conshohocken, PA: 2002.

[44] American Society for Testing and Materials; Standard test method for research octane number of spark-ignition engine fuel, ASTM D2699; *ASTM*. 05.05. West Conshohocken, PA: 2002.

[45] American Society for Testing and Materials; Standard test method for motor octane number of spark-ignition engine fuel, ASTM D2700; *ASTM*. 05.05. West Conshohocken, PA: 2002.

[46] Sing, K. S. W., et al. Reporting physisorption data for gas/solid systems with special reference to the determination of surface area and porosity. *International Union of Pure and Applied Chemistry*. 57 (1985): 603-619.

APPENDICES

APPENDIX A

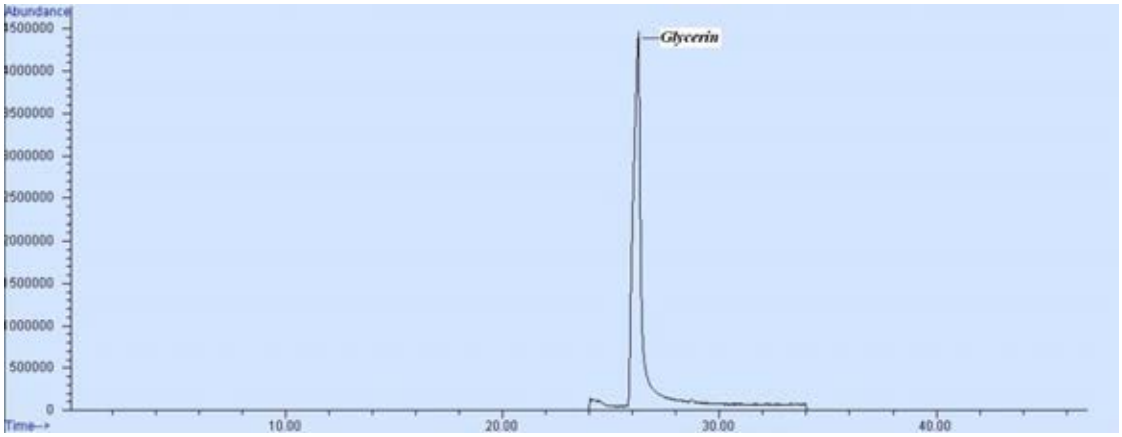

Figure A1 GC chromatogram of pure glycerin.

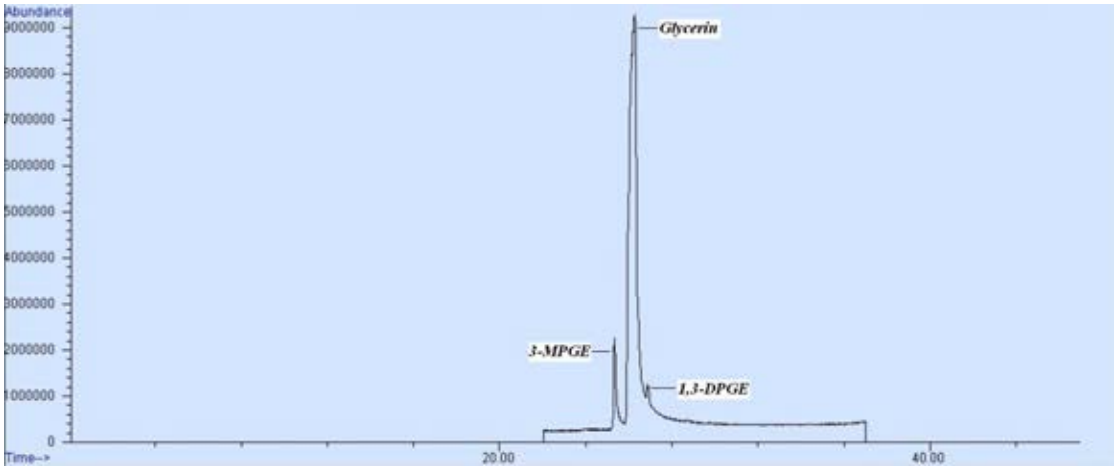

Figure A2 GC chromatogram of etherification between glycerin and propylene over Amberlyst-15, temperature 90 °C and time 8 h.

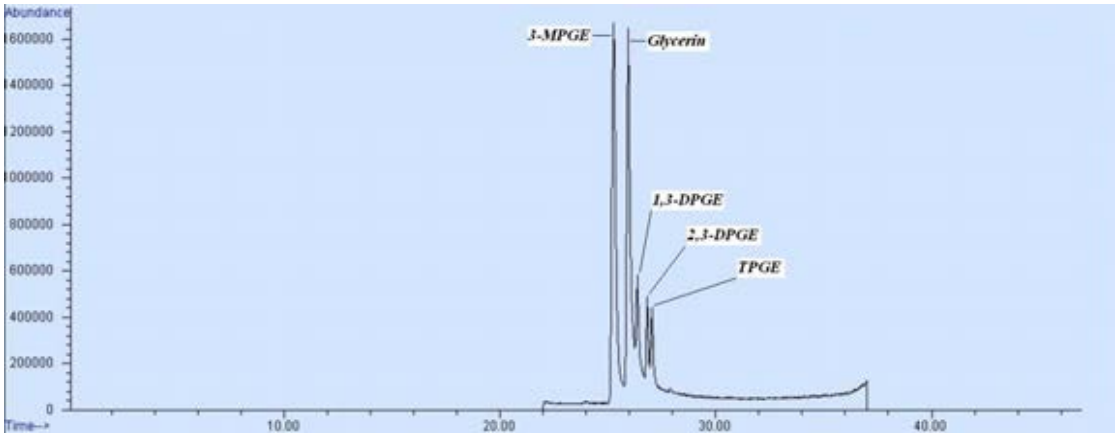

Figure A3 GC chromatogram of etherification between glycerin and propylene over Amberlyst-15, temperature 100 °C and time 8 h.

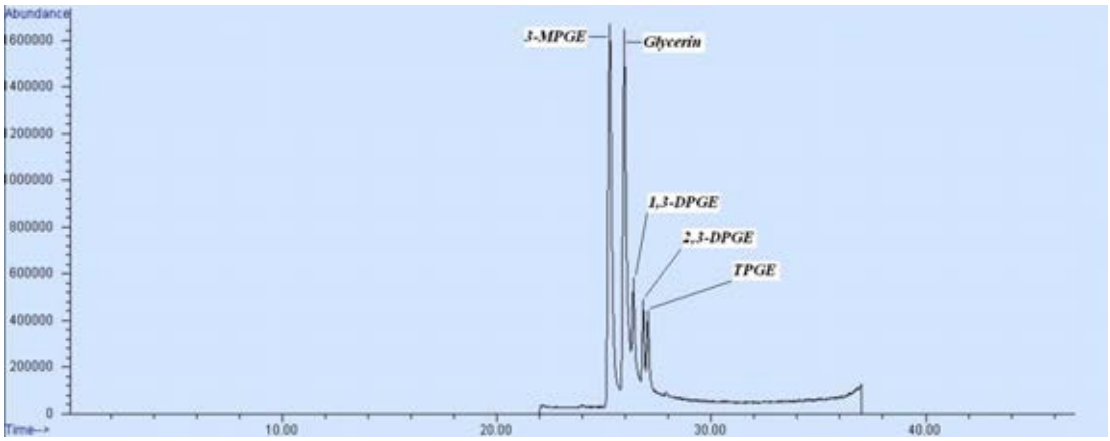

Figure A4 GC chromatogram of etherification between glycerin and propylene over Amberlyst-15, temperature 100 °C and time 16 h.

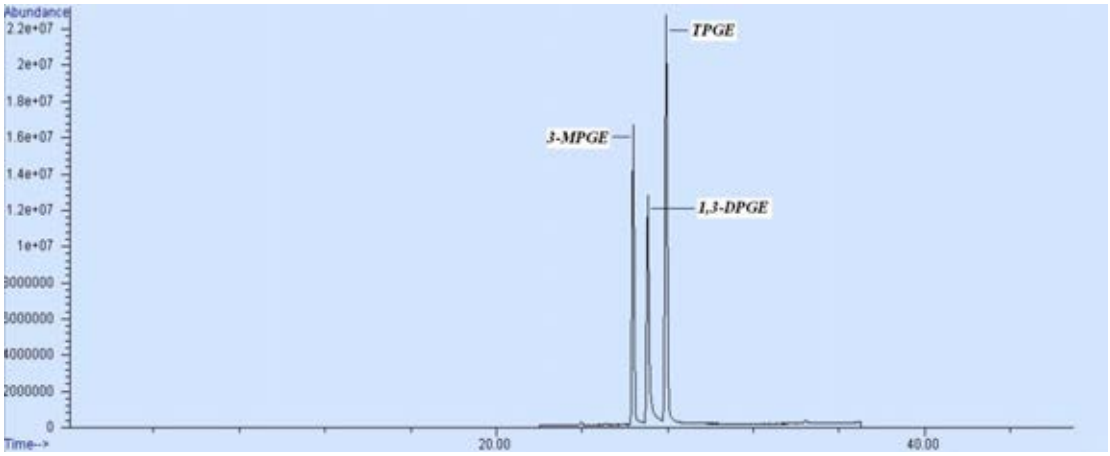

Figure A5 GC chromatogram of etherification between glycerin and propylene over Amberlyst-15, temperature 100 °C and time 24 h.

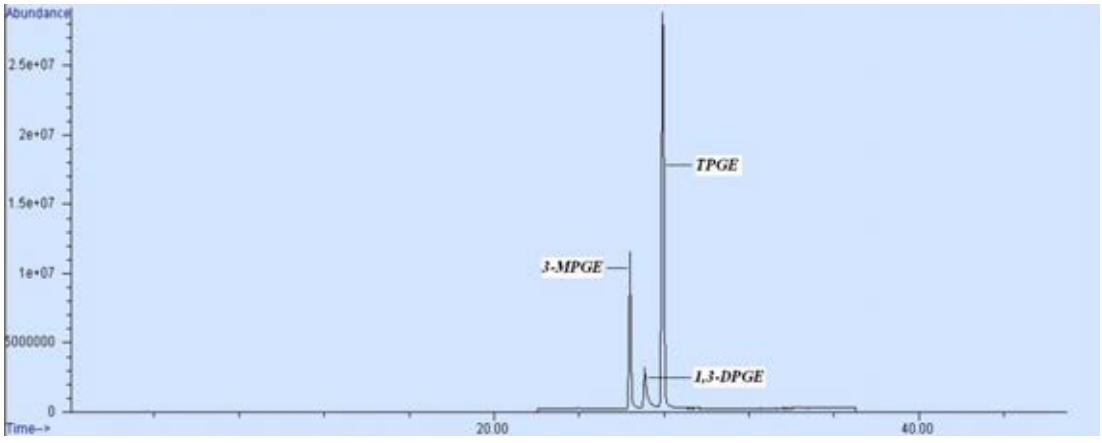

Figure A6 GC chromatogram of etherification between glycerin and propylene over Amberlyst-15, temperature 100 °C and time 32 h.

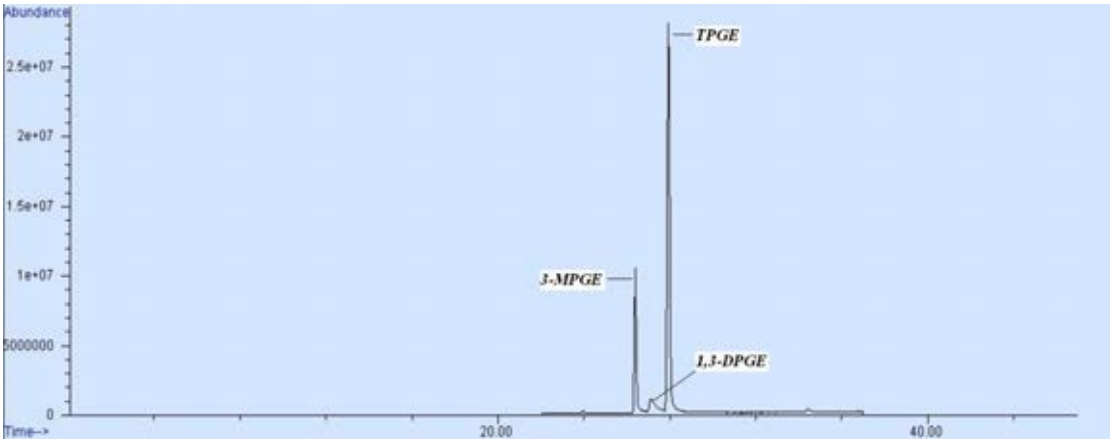

Figure A7 GC chromatogram of etherification between glycerin and propylene over Amberlyst-15, temperature 100 °C and time 40 h.

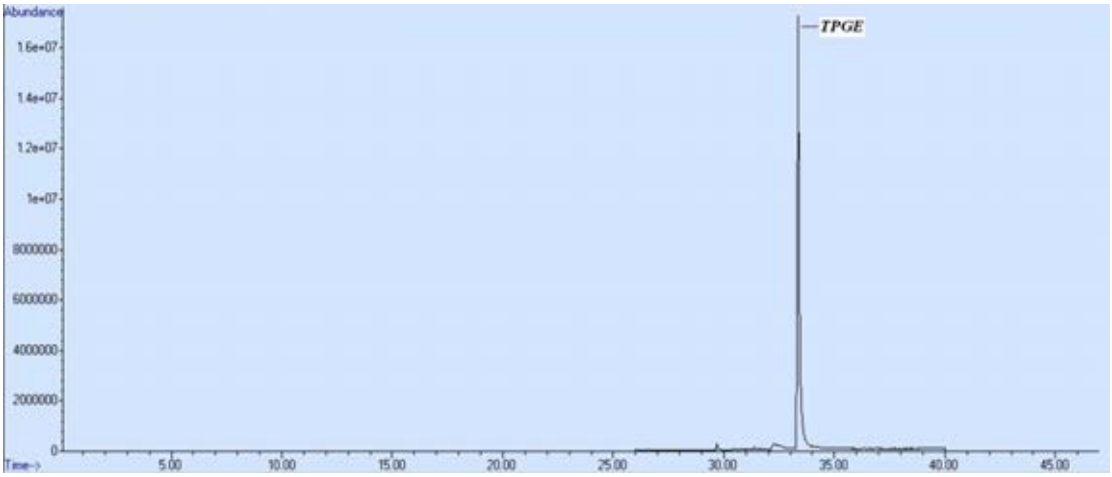

Figure A8 GC chromatogram of etherification between glycerin and propylene over Amberlyst-15, temperature 100 °C and time 48 h.

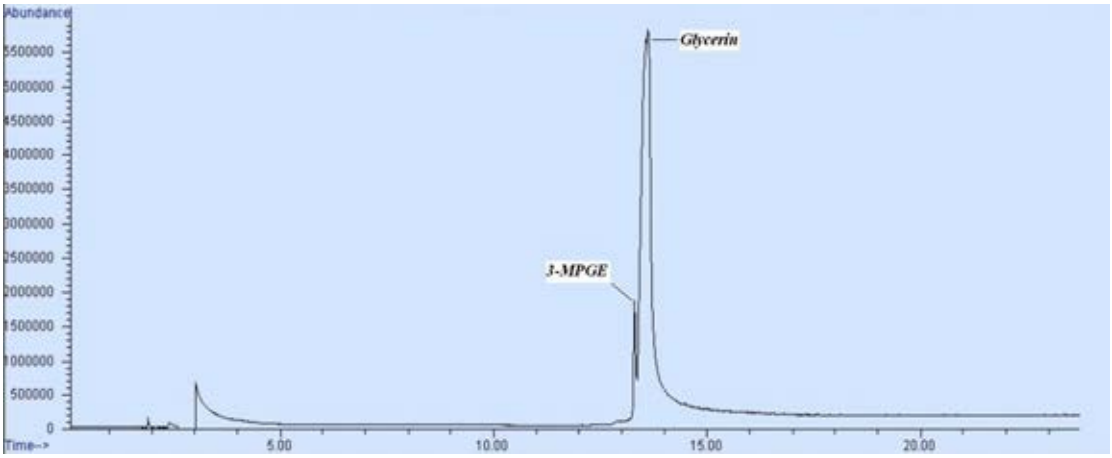

Figure A9 GC chromatogram of etherification between glycerin and propylene over S100 resin, temperature 100 °C and time 16 h.

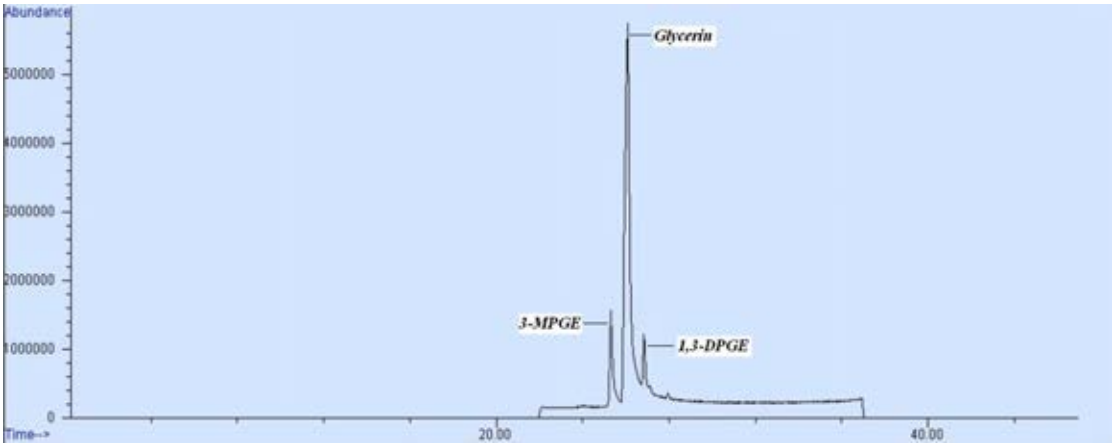

Figure A10 GC chromatogram of etherification between glycerin and propylene over S100 resin, temperature 100 °C and time 24 h.

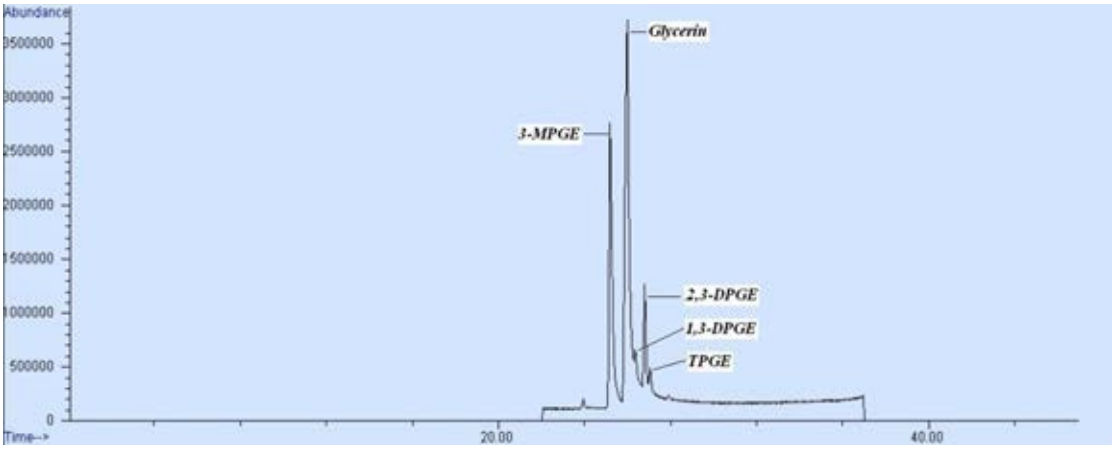

Figure A11 GC chromatogram of etherification between glycerin and propylene over S100 resin, temperature 100 °C and time 32 h.

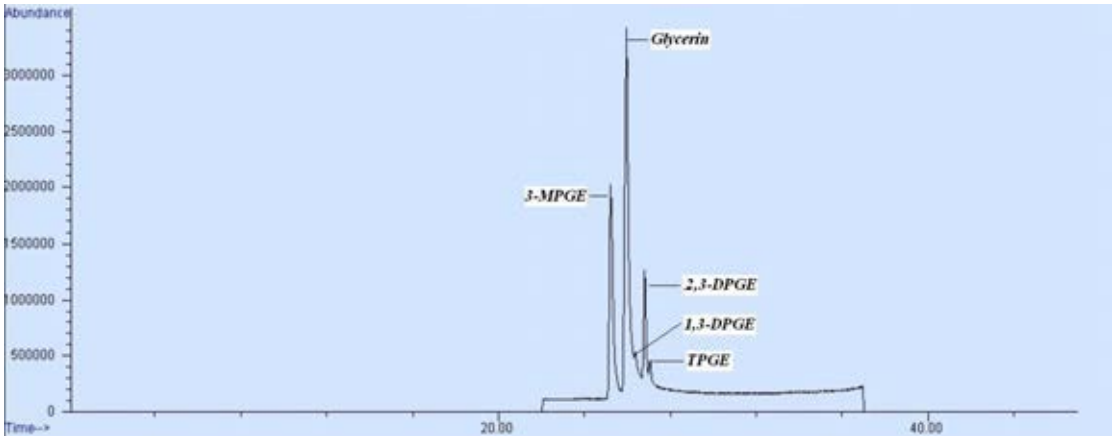

Figure A12 GC chromatogram of etherification between glycerin and propylene over S100 resin, temperature 100 °C and time 40 h.

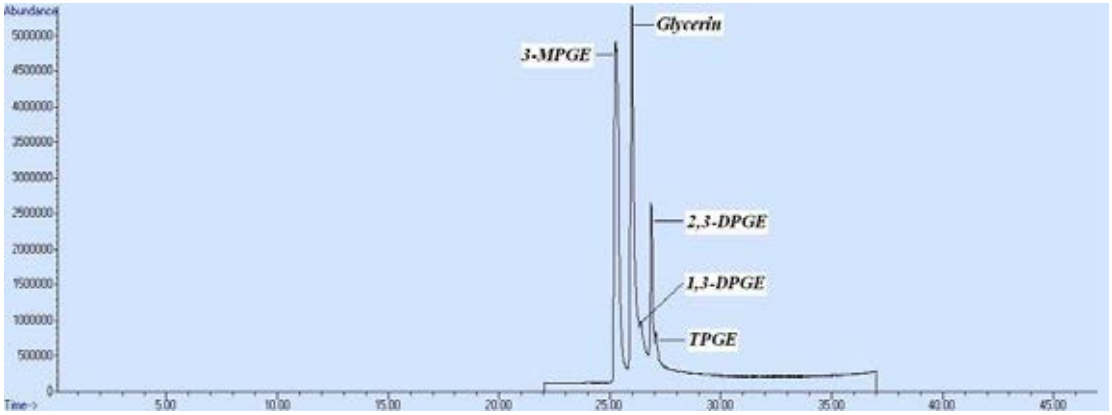

Figure A13 GC chromatogram of etherification between glycerin and propylene over S100 resin, temperature 100 °C, and time 48 h.

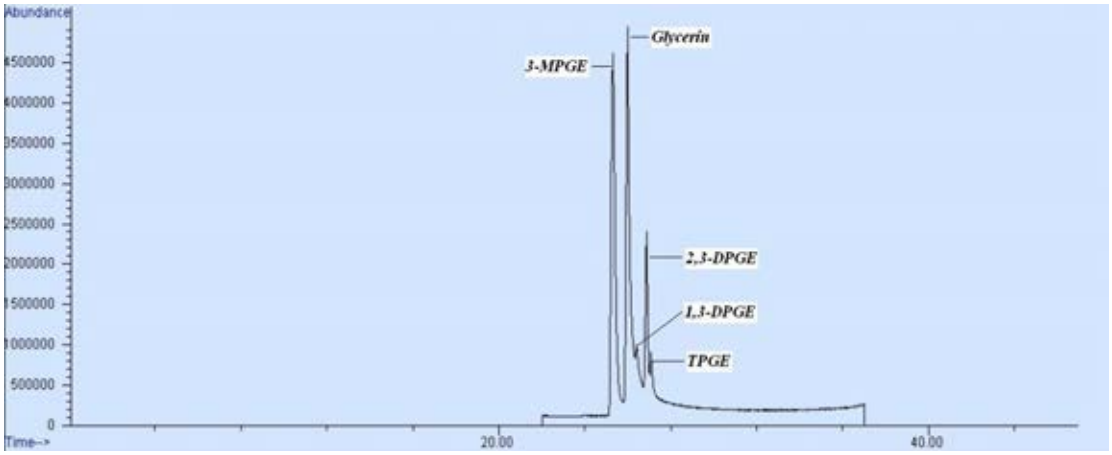

Figure A14 GC chromatogram of etherification between glycerin and propylene over S100 resin, temperature 100 °C and time 56 h.

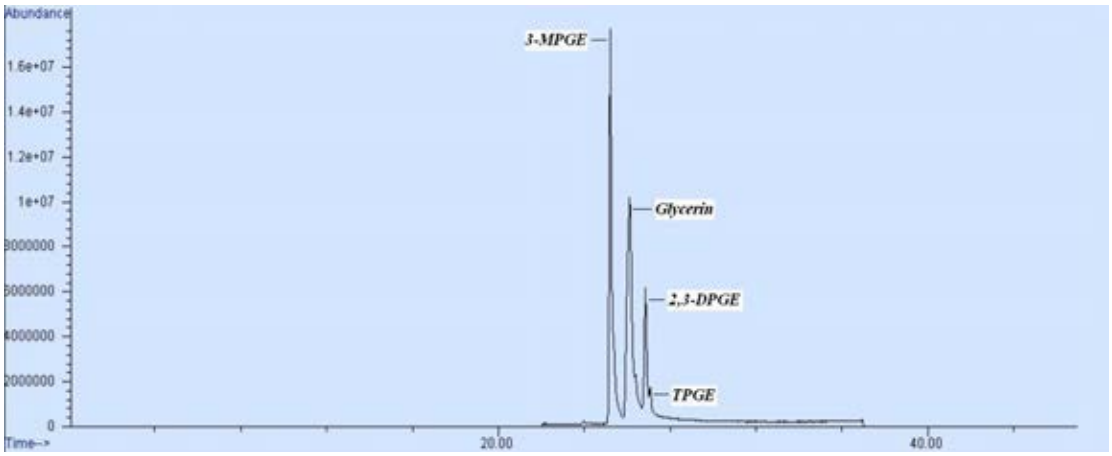

Figure A15 GC chromatogram of etherification between glycerin and propylene over S100 resin, temperature 100 °C and time 64 h.

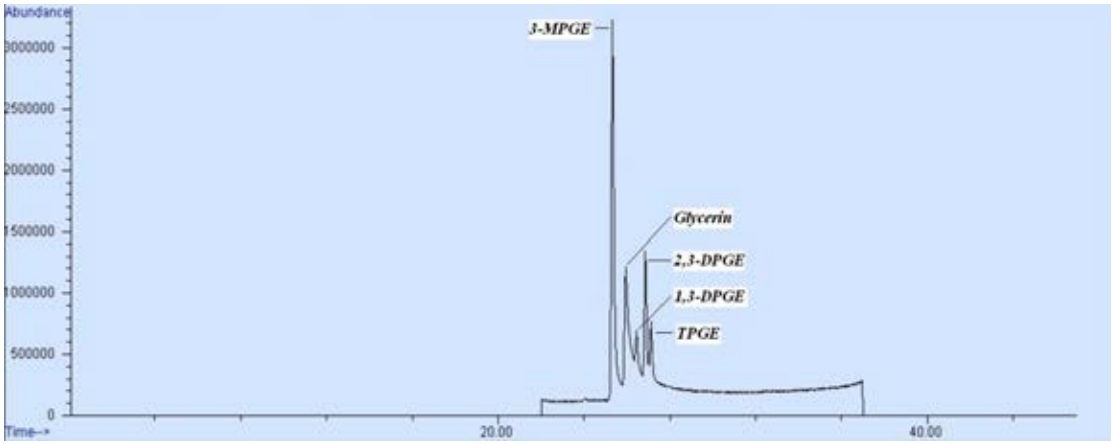

Figure A16 GC chromatogram of etherification between glycerin and propylene over S100 resin, temperature 100 °C and time 72 h.

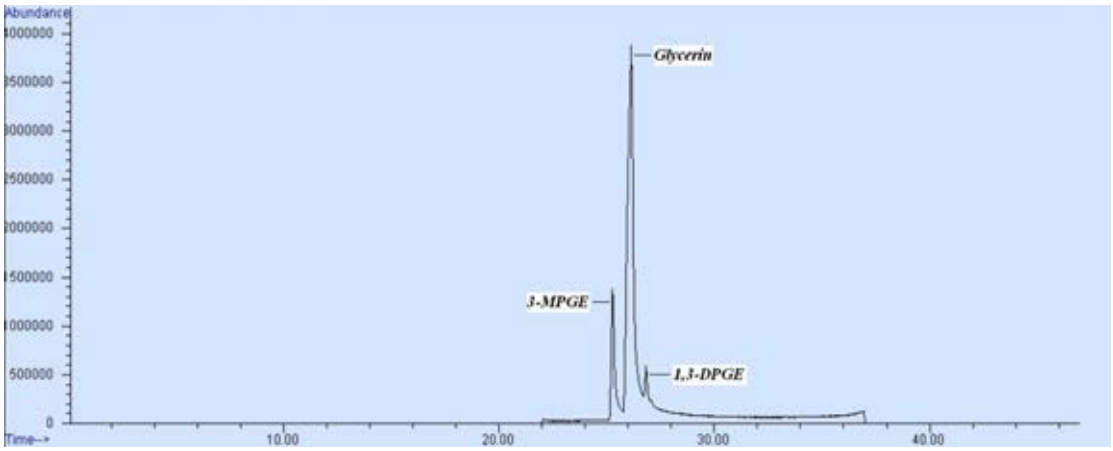

Figure A17 GC chromatogram of etherification between glycerin and propylene over S200 resin, temperature 100 °C and time 16 h.

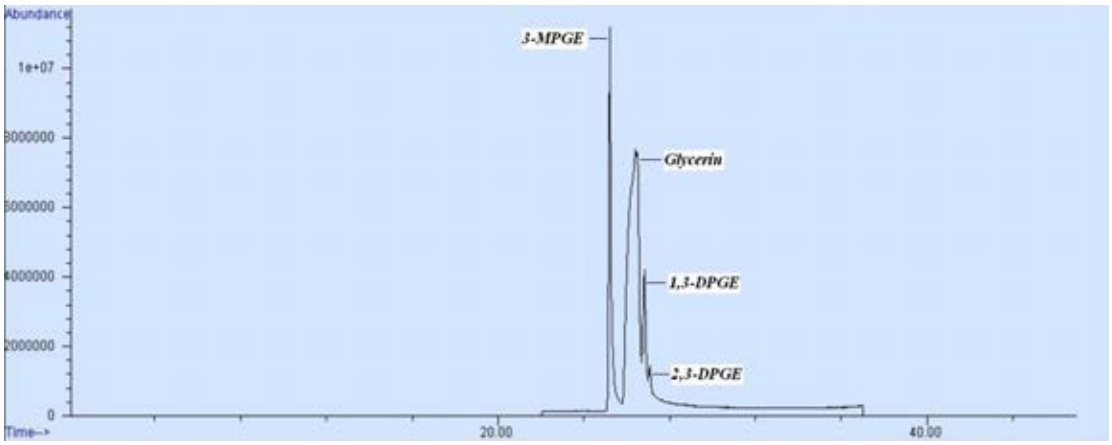

Figure A18 GC chromatogram of etherification between glycerin and propylene over S200 resin, temperature 100 °C and time 24 h.

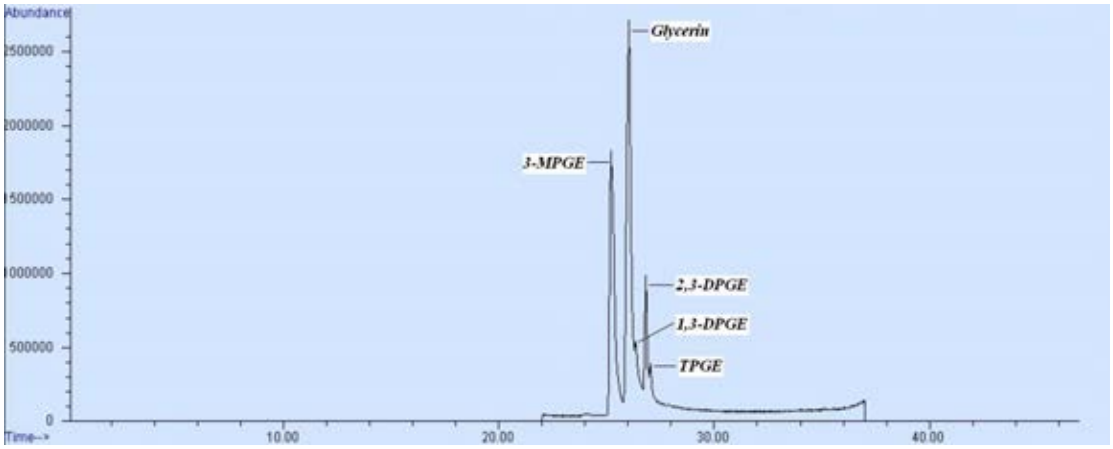

Figure A19 GC chromatogram of etherification between glycerin and propylene over S200 resin, temperature 100 °C and time 32 h.

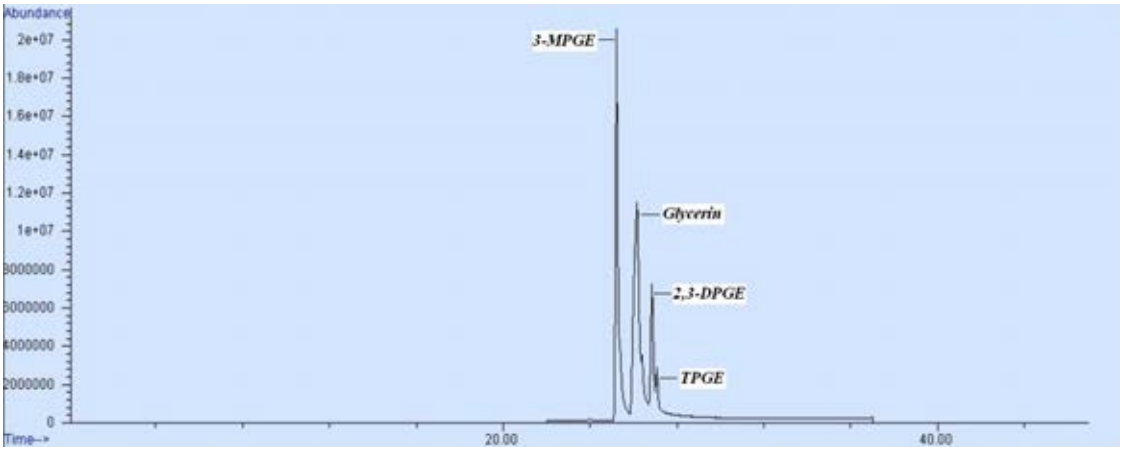

Figure A20 GC chromatogram of etherification between glycerin and propylene over S200 resin, temperature 100 °C and time 40 h.

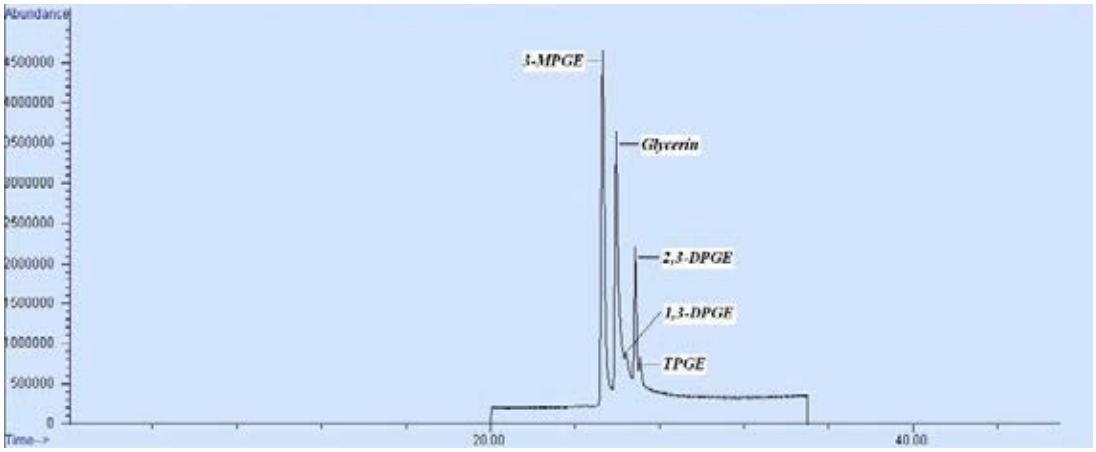

Figure A21 GC chromatogram of etherification between glycerin and propylene over S200 resin, temperature 100 °C and time 48 h.

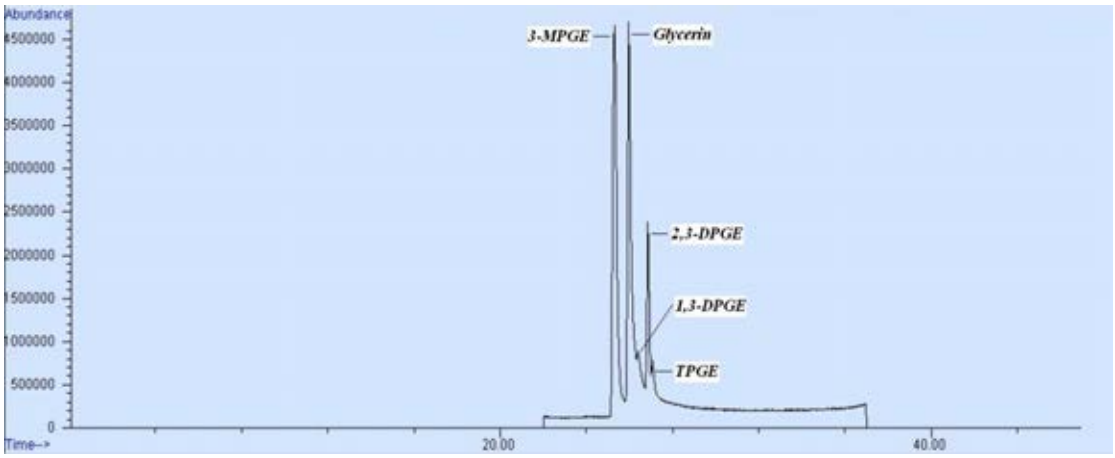

Figure A22 GC chromatogram of etherification between glycerin and propylene over S200 resin, temperature 100 °C and time 56 h.

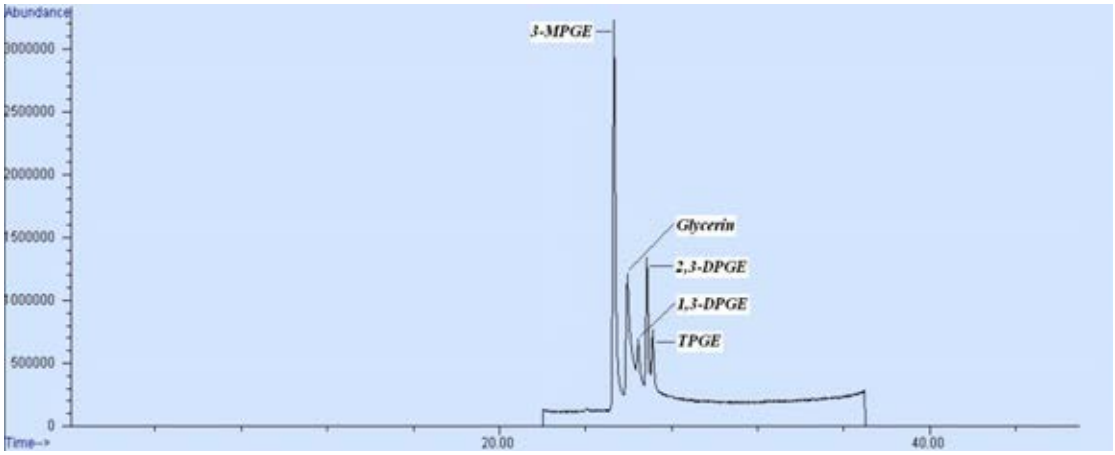

Figure A23 GC chromatogram of etherification between glycerin and propylene over S200 resin, temperature 100 °C and time 64 h.

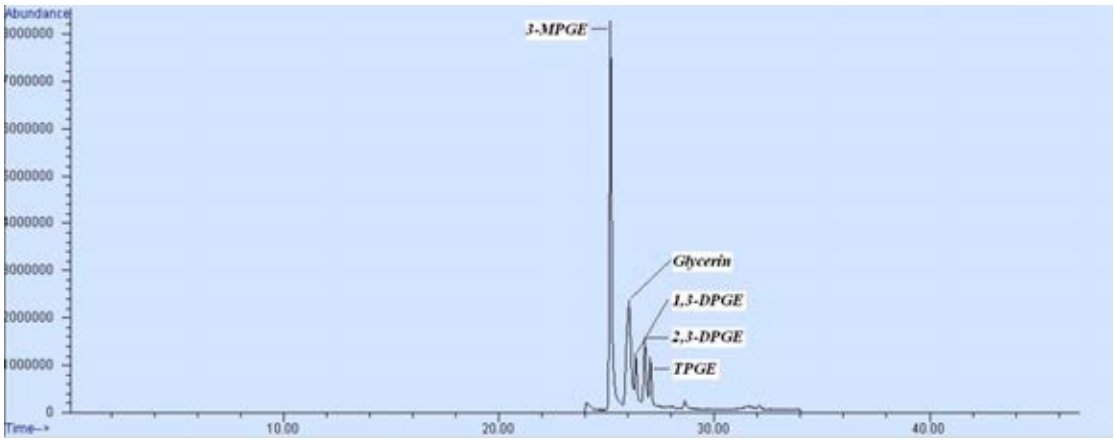

Figure A24 GC chromatogram of etherification between glycerin and propylene over S200 resin, temperature 100 °C and time 72 h.

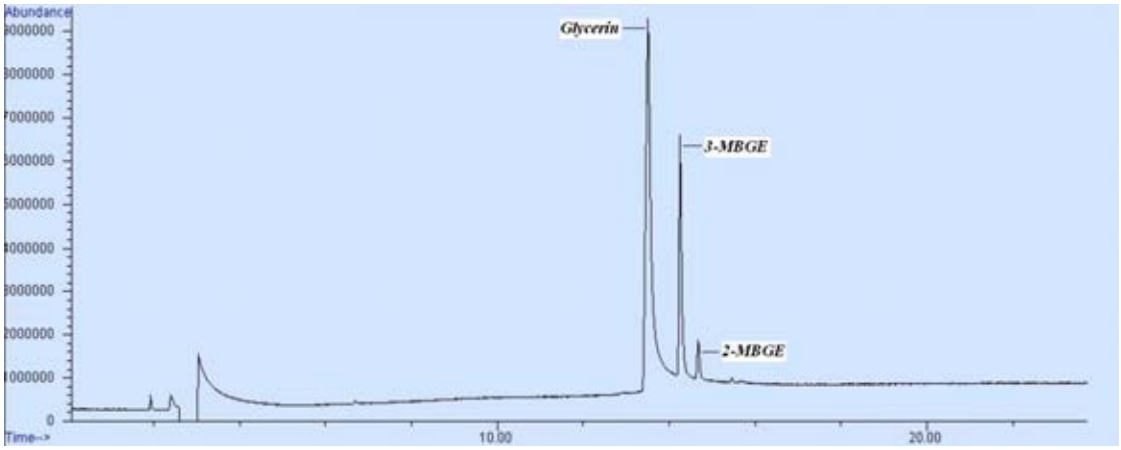

Figure A25 GC chromatogram of etherification between glycerin and 1-butene over Amberlyst-15, temperature 100 °C and time 8 h.

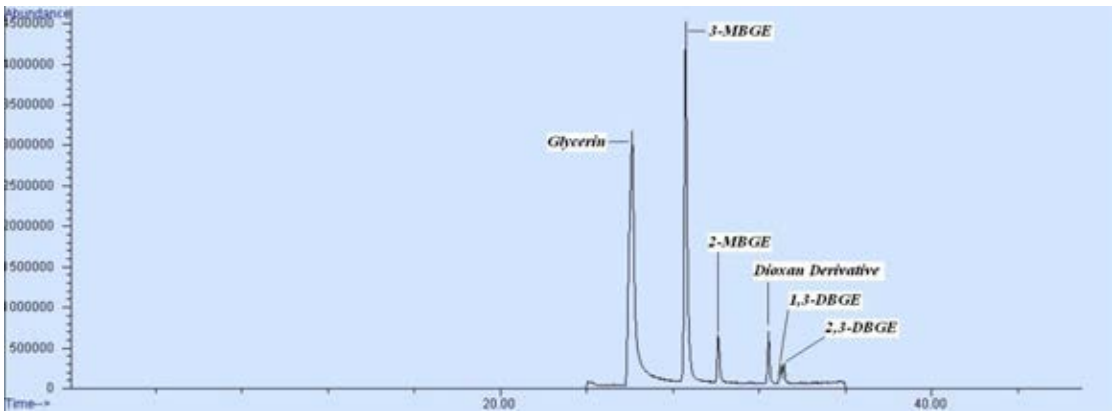

Figure A26 GC chromatogram of etherification between glycerin and 1-butene over Amberlyst-15, temperature 100 °C and time 16 h.

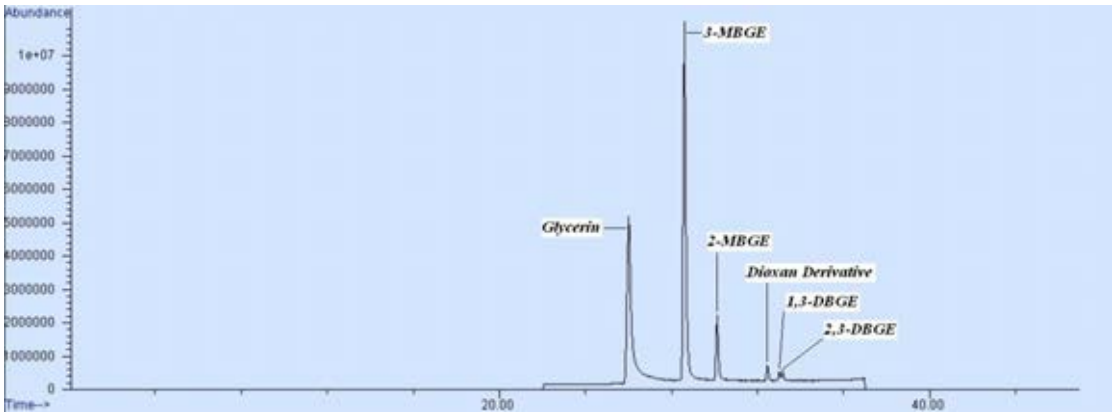

Figure A27 GC chromatogram of etherification between glycerin and 1-butene over Amberlyst-15, temperature 100 °C and time 24 h.

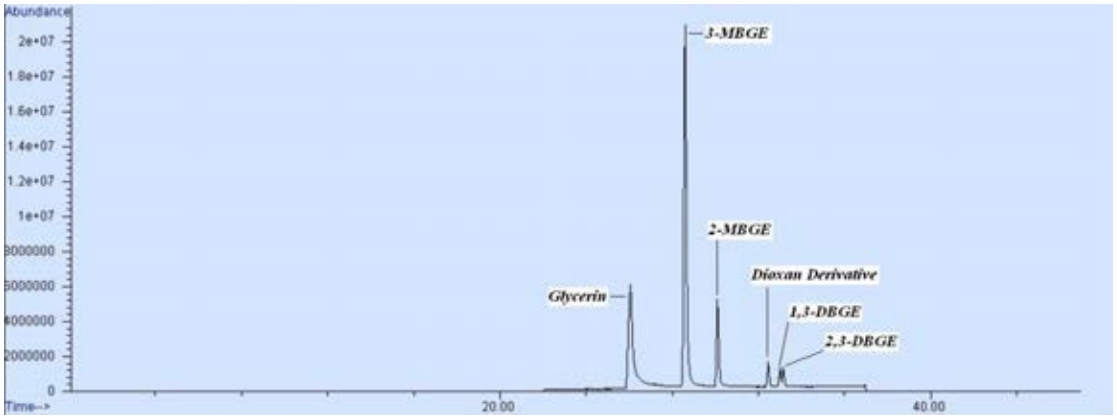

Figure A28 GC chromatogram of etherification between glycerin and 1-butene over Amberlyst-15, temperature 100 °C and time 32 h.

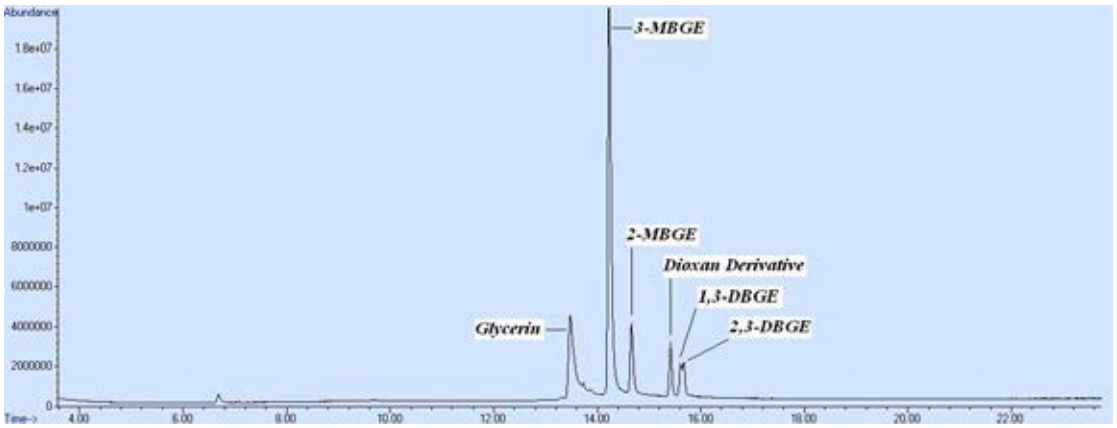

Figure A29 GC chromatogram of etherification between glycerin and 1-butene over Amberlyst-15, temperature 100 °C and time 40 h.

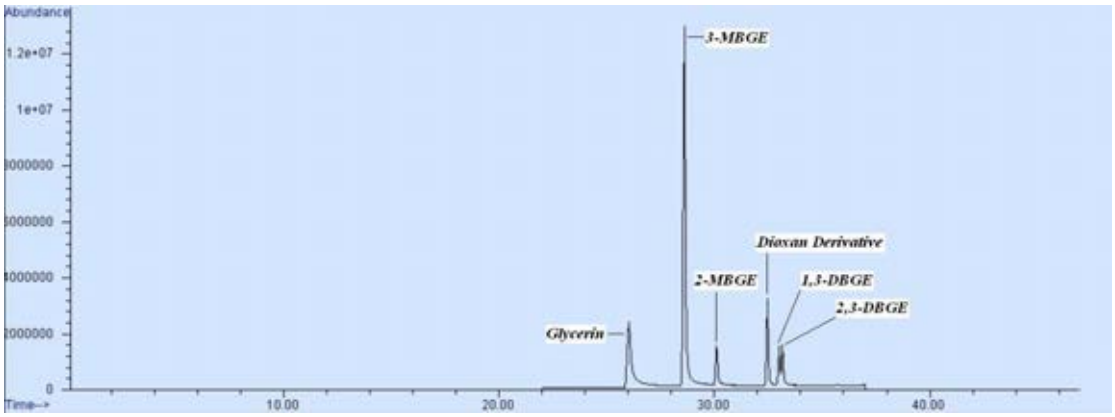

Figure A30 GC chromatogram of etherification between glycerin and 1-butene over Amberlyst-15, temperature 100 °C and time 48 h.

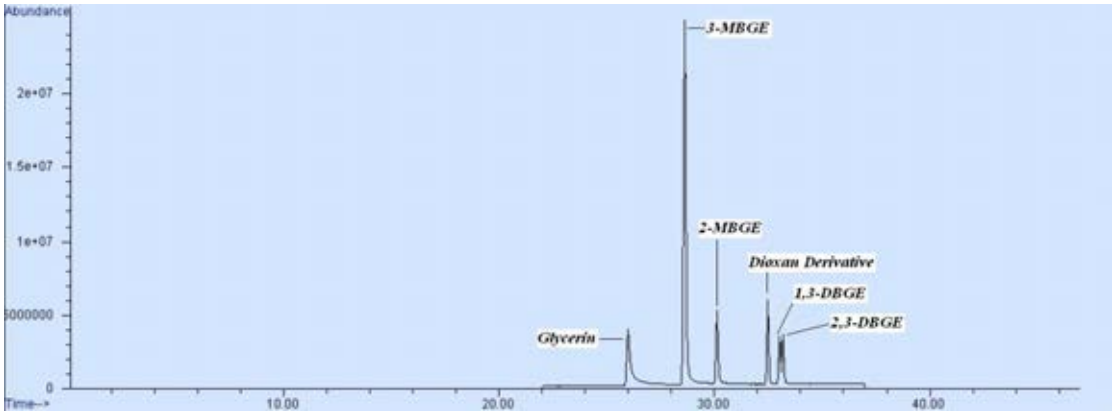

Figure A31 GC chromatogram of etherification between glycerin and 1-butene over Amberlyst-15, temperature 100 °C and time 56 h.

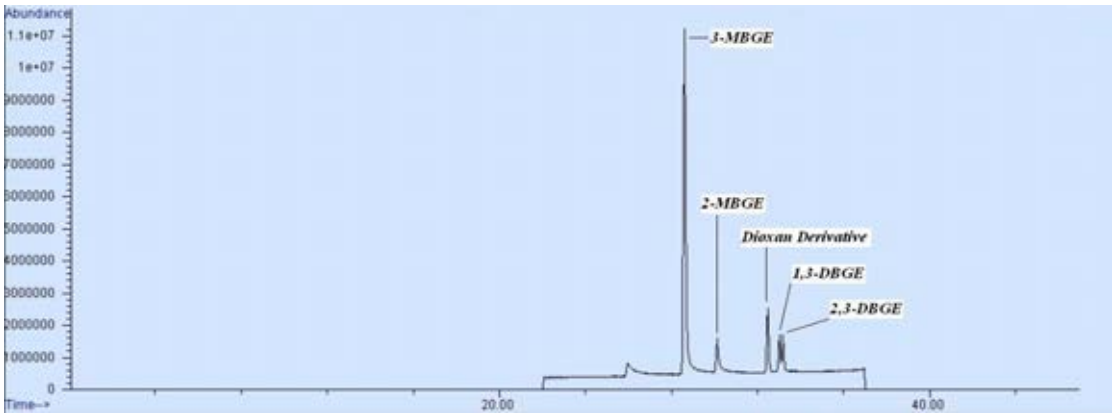

Figure A32 GC chromatogram of etherification between glycerin and 1-butene over Amberlyst-15, temperature 100 °C and time 64 h.

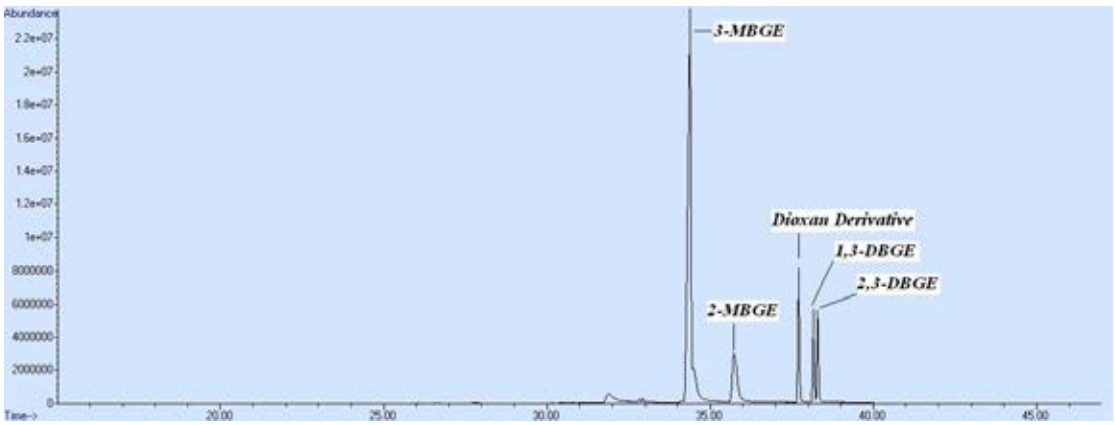

Figure A33 GC chromatogram of etherification between glycerin and 1-butene over Amberlyst-15, temperature 100 °C and time 72 h.

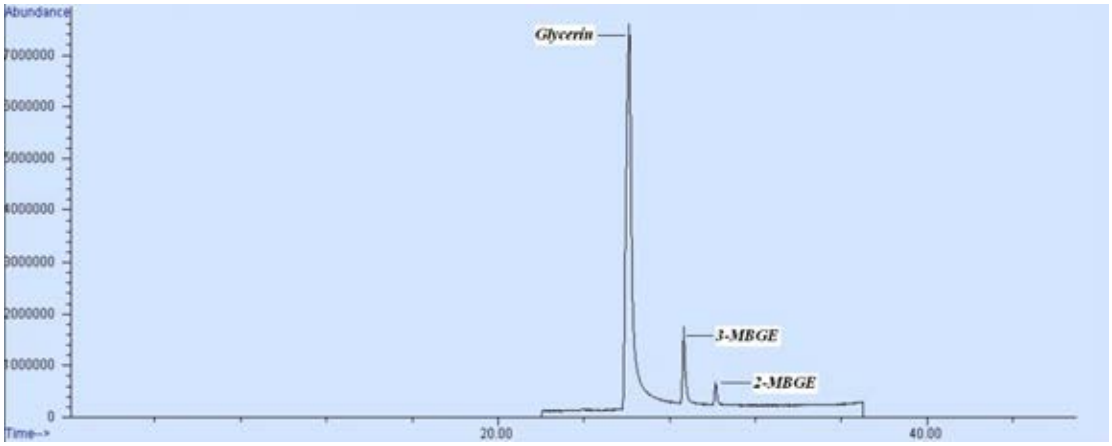

Figure A34 GC chromatogram of etherification between glycerin and 1-butene over S200 resin, temperature 100 °C and time 16 h.

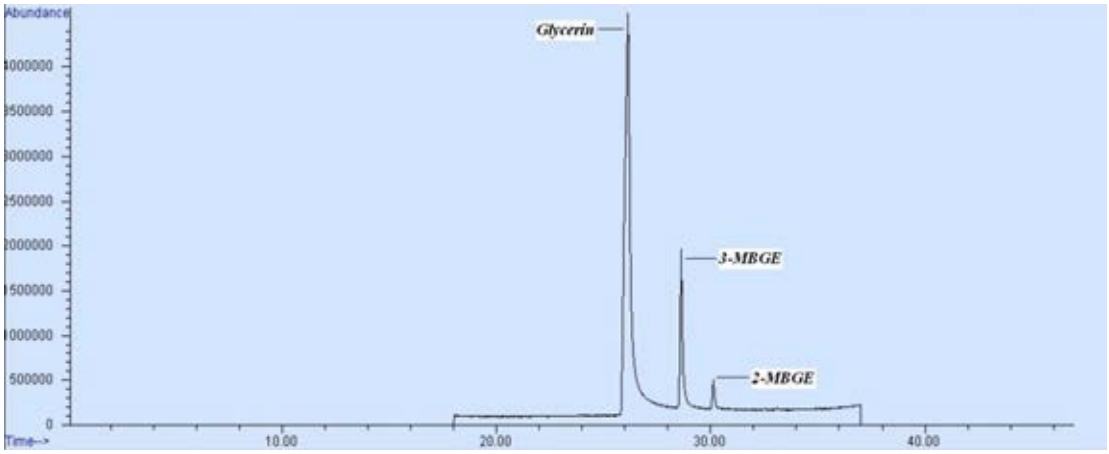

Figure A35 GC chromatogram of etherification between glycerin and 1-butene over S200 resin, temperature 100 °C and time 24 h.

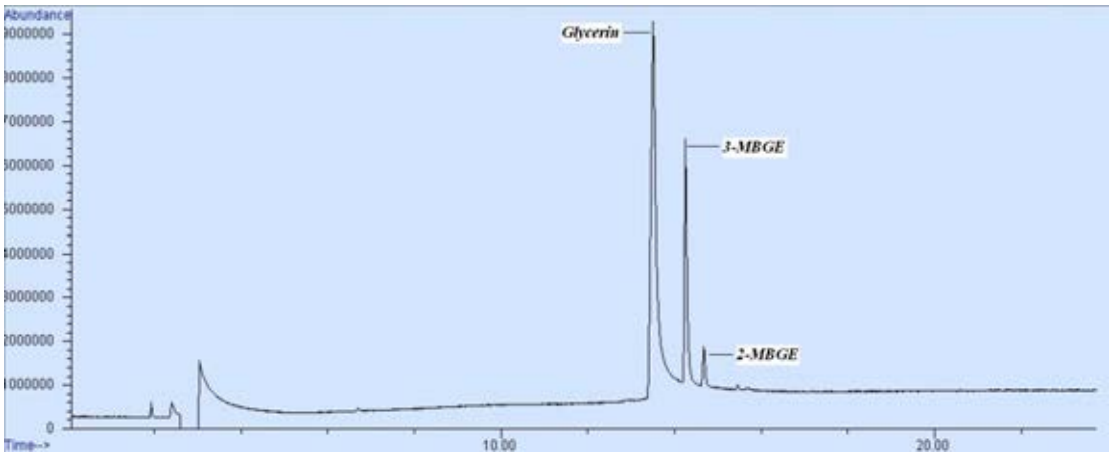

Figure A36 GC chromatogram of etherification between glycerin and 1-butene over S200 resin, temperature 100 °C and time 32 h.

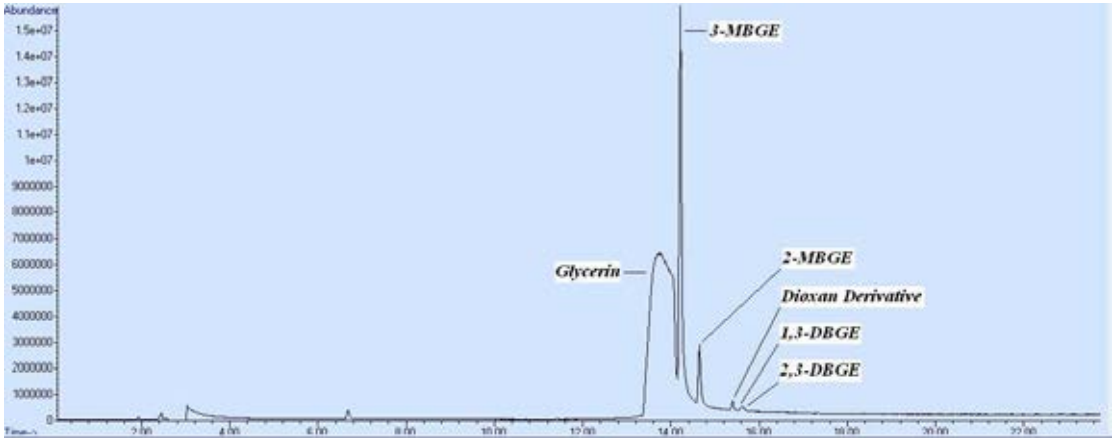

Figure A37 GC chromatogram of etherification between glycerin and 1-butene over S200 resin, temperature 100 °C and time 40 h.

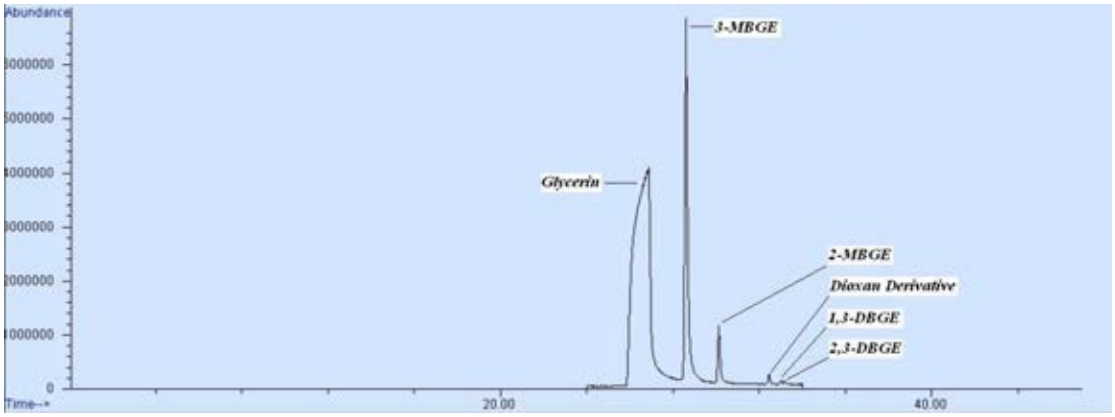

Figure A38 GC chromatogram of etherification between glycerin and 1-butene over S200 resin, temperature 100 °C and time 48 h.

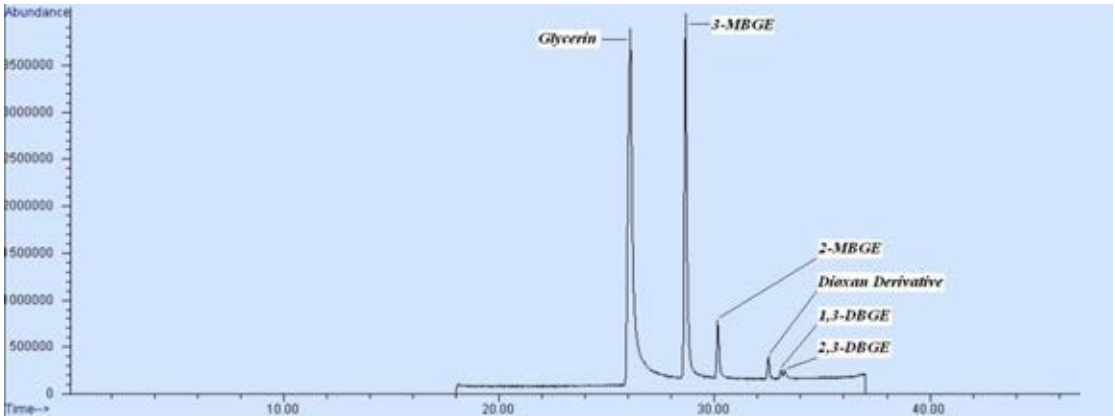

Figure A39 GC chromatogram of etherification between glycerin and 1-butene over S200 resin, temperature 100 °C and time 56 h.

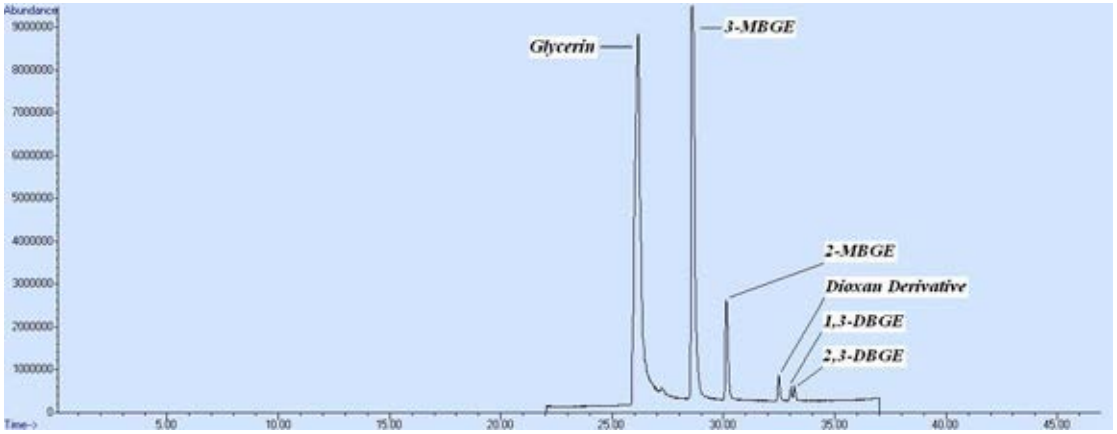

Figure A40 GC chromatogram of etherification between glycerin and 1-butene over S200 resin, temperature 100 °C and time 64 h.

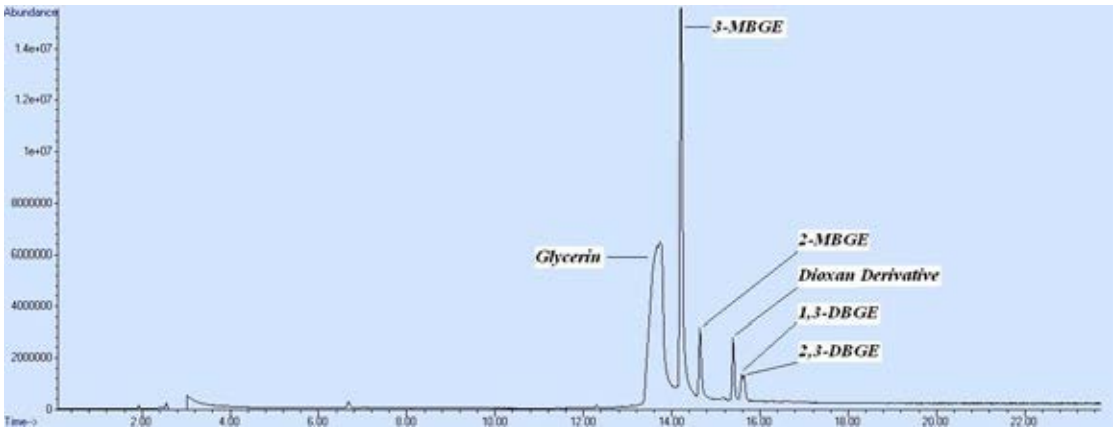

Figure A41 GC chromatogram of etherification between glycerin and 1-butene over S200 resin, temperature 100 °C and time 72 h.

APPENDIX B

Table B1 Analysis result of pure glycerin.

Parameter	Unit	Spec	Result	Method
Glycerin	% wt	99.5 Min	99.78	Ph. Eur. 5
Total impurity	% wt	1.0 Max	0.25	USP 32
Acidity	ml 0.1N NaOH/25g	0.2 Max	<0.2	Ph. Eur.5
Aldehyde	ppm	10 Max	<10	Ph. Eur. 5
Chloride	ppm vol	10 Max	<5	Ph. Eur. 5
Sp. gr. at 25/25 °C	-	1.249 Min	1.2611	USP 32
Density at 20 °C	g/cm^3	1.260-1.263	1.2604	ASTM D 4052-96 (2002) E1
RI at 20°C	-	1.470-1.475	1.4744	Ph. Eur. 5
Fatty acid & ester	ml 0.5N NaOH/25g	1 Max	<1.0	USP 32
Total heavy metal	ppm as Pb	5 Max	<5	Ph. Eur. 5
Ester	ml 0.1N HCl/25g	8 Min	8.9	Ph. Eur. 5
Sulphate ash	% wt	0.01 Max	0.002	Ph. Eur. 5
Residue on ignition	% wt	0.01 Max	<0.001	USP 32
Appearance	-	Clear & Colorless	Clear & Colorless	Ph. Eur. 5
Water content	% wt	0.20 Max	0.0920	ASTM E 203-01

Table B2 Analysis result of palm biodiesel (B100).

Parameter	Unit	Result	Method
Methyl ester	% wt	97.62	DIN EN 14103
Acid value	mg KOH/g	0.30	DIN EN ISO 660-1996
Bound-glycerin	% wt	0.17	DIN EN 14105
CFPP	°C	12	DIN EN 116
Cloud point	°C	19	ASTM D 2500-05
di-Glycerin	% wt	0.08	DIN EN 14105
Flash point	°C	163.0	DIN EN ISO 3679
Free-glycerin	% wt	0.01	DIN EN 14105
Iodine value	g iodine/100g	42.0	ISO 3961-1996
Linolenic acid	% wt	0.34	DIN EN 14103
mono-glyceride	% wt	0.64	DIN EN 14105
Total-glycerin	% wt	0.18	DIN EN 14105
tri-glyceride	% wt	<0.01	DIN EN 14105
Water content	% wt	0.037	ASTM E 203-01

Table B3 Analysis result of diesel.

Parameter	Unit	Spec	Result
API	-	Report	41.43
Sp.Gr.60/60 °F	-	Report	0.8183
Density at 15°C	g/ml	-	0.8179
Appearance	-	Clear	Clear
Total sulfur	ppm wt.	350 max	25.6

Table B4 Properties of catalysts.

Catalyst	Acidity		A_{BET}		Pore vol.		Pore size	
	(mmol/g)	SD	(m^2/g)	SD	(cm^3/g)	SD	(nm)	SD
Al-SBA-15	0.12	0.01	426.085	1.62	0.759	0.01	7.125	0.03
Pr-SBA-15	1.34	0.01	429.440	2.63	0.767	0.01	7.187	0.04
Amb-15	3.70	0.02	40.663	0.22	0.075	0.01	7.451	0.04
S100	3.00	0.03	2.134	0.01	0.001	0.01	2.006	0.01
S200	3.53	0.03	2.278	0.01	0.001	0.01	2.014	0.01
Z-B	0.45	0.01	571.495	2.70	0.487	0.01	3.407	0.05
Z-Y	0.34	0.02	791.660	2.48	0.486	0.01	2.405	0.05

Table B5 Product distribution of etherification between glycerin and propylene over Amberlyst-15.

Condition		%					SD				
°C	h	Conv	Gly	MPGE	DPGE	TPGE	Conv	Gly	MPGE	DPGE	TPGE
90	8	6.21	93.79	6.21	0	0	0.02	0.02	0.03	-	-
100	8	59.54	40.46	43.89	6.40	9.25	1.46	1.46	0.58	0.52	0.36
100	16	77.06	22.94	46.95	4.83	25.28	1.88	1.88	4.52	1.36	1.28
100	24	100	0	24.99	20.84	54.17	-	-	0.14	0.05	0.2
100	32	100	0	22.83	9.92	67.25	-	-	2.39	0.74	3.08
100	40	100	0	19.82	5.57	74.60	-	-	1.76	1.13	2.77
100	48	100	0	0	0	100	-	-	-	-	1.62

Table B6 Product distribution of etherification between glycerin and propylene over S200 resin.

Condition		%					SD				
°C	h	Conv	Gly	MPGE	DPGE	TPGE	Conv	Gly	MPGE	DPGE	TPGE
90	8	0	100	0	0	0	-	-	-	-	-
100	8	0	100	0	0	0	-	-	-	-	-
100	16	17.53	82.47	15.19	2.34	0	0.35	0.35	0.16	0.18	-
100	24	21.74	78.26	14.43	6.25	1.06	0.01	0.01	0.01	0.01	0.01
100	32	50.25	49.75	34.12	7.50	8.63	0.10	0.10	0.15	0.20	0.01
100	40	56.27	43.73	38.25	0.91	17.11	0.02	0.02	1.25	0.09	1.35
100	48	58.43	41.57	42.80	0.88	14.75	0.01	0.01	0.25	0.70	0.45
100	56	60.82	39.18	46.86	0.81	13.15	0.24	0.24	1.22	0.98	0.01
100	64	69.92	30.08	45.27	2.88	21.77	1.38	1.38	2.82	1.53	0.18
100	72	72.43	27.57	51.61	6.07	14.75	0.28	0.28	1.09	0.96	0.15

Table B7 Product distribution of etherification between glycerin and propylene over S100 resin.

Condition		%					SD				
°C	h	Conv	Gly	MPGE	DPGE	TPGE	Conv	Gly	MPGE	DPGE	TPGE
90	8	0	100	0	0	0	-	-	-	-	-
100	8	0	100	0	0	0	-	-	-	-	-
100	16	5.77	94.23	5.77	0	0	0.80	0.80	0.80	-	-
100	24	17.36	82.64	12.71	4.65	0	1.90	1.90	0.63	1.27	-
100	32	41.68	58.32	31.19	1.07	9.42	0.54	0.54	0.10	0.31	0.33
100	40	42.14	57.86	30.74	0.43	10.97	0.18	0.18	0.43	0.34	0.27
100	48	57.11	42.89	42.35	0.73	14.03	0.22	0.22	1.29	1.10	0.03
100	56	57.54	42.46	40.31	1.05	16.18	0.92	0.92	1.17	1.80	1.55
100	64	58.95	41.05	38.52	4.87	15.56	1.20	1.20	2.04	2.45	0.80
100	72	69.92	30.08	45.27	2.88	21.77	0.09	0.09	0.01	1.63	1.73

Table B8 Product distribution of etherification between glycerin and 1-butene over Amberlyst-15.

Condition		%							SD						
°C	h	Conv	Gly	3-MBGE	2-MBGE	Dioxander.	1,3-DBGE	2,3-DBGE	Conv	Gly	3-MBGE	2-MBGE	Dioxander.	2,3-DBGE	1,3-DBGE
90	8	0	100	0	0	0	0	0	-	-	-	-	-	-	-
100	8	24.76	75.24	21.53	3.23	0	0	0	0.01	0.01	0.01	0.01	-	-	-
100	16	46.87	53.13	36.77	3.86	3.60	1.27	1.37	0.28	0.28	0.22	0.05	0.02	0.01	0.01
100	24	58.83	41.17	48.39	7.28	1.46	0.81	0.89	0.32	0.32	0.03	0.06	0.01	0.01	0.02
100	32	71.51	28.49	53.98	11.06	2.65	1.81	2.01	0.28	0.28	0.21	0.04	0.01	0.02	0.02
100	40	78.71	21.29	58.52	8.09	5.53	3.10	3.47	0.08	0.08	0.06	0.01	0.02	0.01	0.02
100	48	80.45	19.55	54.32	5.52	10.55	4.54	5.52	0.77	0.77	0.83	0.02	0.13	0.01	0.17
100	56	85.21	14.79	56.44	9.43	9.01	5.03	5.30	0.25	0.25	0.11	0.05	0.12	0.04	0.04
100	64	100	0	70.42	8.59	9.86	5.30	5.83	-	-	1.05	0.95	0.57	0.25	0.24
100	72	100	0	71.60	7.80	9.71	5.24	5.65	-	-	0.17	0.07	0.11	0.07	0.07

Table B9 Product distribution of etherification between glycerin and 1-butene over S200 resin.

Condition		%							SD						
°C	h	Conv	Gly	3-MBGE	2-MBGE	Dioxander.	1,3-DBGE	2,3-DBGE	Conv	Gly	3-MBGE	2-MBGE	Dioxander.	1,3-DBGE	2,3-DBGE
90	8	0	100	0	0	0	0	0	-	-	-	-	-	-	-
100	8	0	100	0	0	0	0	0	-	-	-	-	-	-	-
100	16	9.62	90.38	7.68	1.94	0	0	0	0.96	0.96	0.35	0.54	-	-	-
100	24	15.57	84.43	13.38	2.19	0	0	0	0.13	0.13	0.05	0.04	-	-	-
100	32	18.78	81.22	16.16	2.62	0	0	0	0.01	0.01	0.01	0.01	-	-	-
100	40	21.58	78.42	18.04	2.88	0.38	0.15	0.13	0.82	0.82	0.23	0.05	0.03	0.01	0.01
100	48	22.72	77.28	19.06	2.99	0.38	0.15	0.14	1.64	1.64	1.81	1.09	1.39	0.84	0.90
100	56	24.32	75.68	20.85	2.82	0.39	0.13	0.13	1.02	1.02	0.71	0.28	0.85	0.43	0.28
100	64	25.57	74.43	21.78	3.00	0.45	0.14	0.20	0.06	0.06	0.60	0.07	0.05	0.49	0.48
100	72	38.99	61.01	31.89	4.35	1.48	0.55	0.72	1.27	1.27	0.91	0.72	0.44	0.53	0.22

Table B10 Could point of mixed-propyl glycerol ethers in blended palm biodiesels.

PGE %	Blended palm biodiesels				
	B100	B90	B80	B5	B2
0	19	17	13	5	0
0.05	19	17	12	5	-1
0.10	17	16	12	4	-1
0.50	17	16	10	3	-2
1.00	16	14	9	2	-3
5.00	16	14	8	2	-3
10.00	15	13	8	0	-4
20.00	14	12	6	-2	-5

Table B11 Pour point of mixed-propyl glycerol ethers in blended palm biodiesels.

PGE %	Blended palm biodiesels				
	B100	B90	B80	B5	B2
0	11	9	9	-3	-9
0.05	11	9	7	-3	-9
0.10	8	8	7	-4	-10
0.50	7	7	6	-4	-11
1.00	7	5	4	-6	-12
5.00	6	4	4	-6	-12
10.00	6	4	3	-8	-13
20.00	5	2	-1	-9	-14

Table B12 Could point of tri-propyl glycerol ethers in blended palm biodiesels.

PGE %	Blended palm biodiesels				
	B100	**B90**	**B80**	**B5**	**B2**
0	19	17	13	5	0
0.05	19	15	13	5	0
0.10	19	14	13	4	0
0.50	19	14	12	4	-2
1.00	18	13	10	3	-2
5.00	17	12	9	2	-5
10.00	16	11	7	2	-6
20.00	15	9	6	-1	-7

Table B13 Pour point of tri-propyl glycerol ethers in blended palm biodiesels.

PGE %	Blended palm biodiesels				
	B100	**B90**	**B80**	**B5**	**B2**
0	11	9	9	-3	-9
0.05	11	9	8	-3	-9
0.10	10	8	7	-3	-10
0.50	10	7	7	-3	-11
1.00	9	6	5	-4	-11
5.00	9	6	4	-4	-12
10.00	8	5	3	-6	-14
20.00	6	4	0	-8	-15

Table B14 Cetane index of diesel by adding 10% of oxygenated-compound additives.

Fuel	**CI**	**Density at 15 °C**		**Middle-boiling**	
		(g/ml)	**SD**	**(°C)**	**SD**
Diesel	55.0	0.8242	0.0003	262.0	2.65
Diesel + Ethanol	54.9	0.8199	0.0002	255.0	2.00
Diesel + MTBE	56.4	0.8165	0.0004	256.0	2.65
Diesel + Mixed PGE	52.0	0.8268	0.0003	253.5	0.87
Diesel + TPGE	49.3	0.8246	0.0007	240.5	1.80

Table B15 Cetane index of biodiesel by adding 10% of oxygenated-compound additives.

Fuel	CI	Density at 15 °C		Middle-boiling	
		(g/ml)	SD	(°C)	SD
B100	67.5	0.8241	0.0004	353	2.00
B100 + Ethanol	69.0	0.8199	0.0005	352.3	0.82
B100 + MTBE	70.2	0.8166	0.0004	351.7	0.26
B100 + Mixed PGE	66.2	0.8273	0.0004	350.7	1.47
B100 + TPGE	67.1	0.8245	0.0002	348.9	1.15

Table B16 Octane number of gasoline by adding 10% of oxygenated-compound additives.

Fuel	Octane number			
	RON	SD	MON	SD
Gasoline	81.1	0.61	91.0	0.30
Gasoline + Ethanol	84.4	0.44	94.4	0.61
Gasoline + MTBE	85.4	0.61	96.5	0.70
Gasoline + Mixed PGE	81.6	0.62	94.0	0.50
Gasoline + TPGE	82.1	0.50	93.6	0.62

VITAE

Mr. Chakrapong Saengarun was born on July 30, 1965 in Bangkok. He received his Master's Degree in the Program of Petrochemistry and Polymer Science, Faculty of Science, Chulalongkorn University, in 2000. He began his Ph.D.'s Degree study in the Program of Petrochemistry, Faculty of Science, Chulalongkorn University, in 2007 and completed the program in 2012.